



TECHNISCHE
UNIVERSITÄT
WIEN
Vienna University of Technology

Unterschrift des Betreuers

DIPLOMARBEIT

Adaptive Radiotherapie des Zervixkarzinoms

Dosimetrischer Einfluss von Organbewegungen

Ausgeführt am
Atominstitut
der Technischen Universität Wien

Unter der Anleitung von
Prof. DI Dr. Dietmar GEORG
Yvette SEPPENWOOLDE, PhD
von der
Abteilung Medizinische Strahlenphysik
Abteilung Radioonkologie
Medizinische Universität Wien

durch
Michaela Daniel, BSc
Hauptplatz 18/12A
2700 Wr.Neustadt

11.Mai 2015

Unterschrift (Student)



TECHNISCHE
UNIVERSITÄT
WIEN
Vienna University of Technology

Signature Supervisor

MASTER THESIS

Adaptive radiotherapy of cervix cancer

—

dosimetric implications of organ variations

at the

Institute of Atomic and Subatomic Physics
of the Technical University Vienna

supervised by

Prof. DI Dr. Dietmar GEORG
Yvette SEPPENWOOLDE, PhD

of the

Division Medical Radiation Physics
Department of Radiation Oncology
Medical University of Vienna

by

Michaela Daniel, BSc
Hauptplatz 18/12A
2700 Wr.Neustadt

12. Mai 2015

Signature Student

Contents

Acknowledgements	1
Abstract	2
Kurzfassung	5
1 Introduction to some Principles of Radiation Therapy	8
1.1 Introduction	8
1.2 Dose	9
1.3 Medical Linear Accelerators	11
1.4 Delivery Methods	13
1.4.1 Three-Dimensional Conformal Radiotherapy (3D-CRT)	13
1.4.2 Static and Dynamic Intensity Modulated Radiotherapy (IMRT)	14
1.4.3 Rotational Intensity Modulated Radiotherapy	15
1.4.4 Flattening Filter Free Beams (FFF Beams)	16
1.5 Oncological Volume Definitions	17
1.6 Treatment Planning Process	19
1.7 Adaptive Radiotherapy	20
1.7.1 General Concept	20
1.7.2 ART for Cervical Cancer Cases	21
1.8 Motivation	23
1.9 Objectives	23
2 Materials and Methods	25
2.1 Patient Cohort	25
2.2 Patient Setup and Preparations for Planning	26
2.2.1 Cone-Beam Computed Tomography	27
2.3 Structures of Interest and Organs at Risk	29
2.4 Monaco [®] Planning System	31
2.4.1 Principles of Pencil Beam Calculation	31
2.4.2 Monte Carlo Dose Calculation Algorithm	33
2.4.3 Cost Functions	36

2.5	Dose Volume Histograms	40
2.6	Planning Strategies	41
2.6.1	Motion Model / "Plan of the Day"-Approach	41
2.6.2	Motion Robust Plan	43
2.6.3	Non-ART Plan	43
2.7	Planning Aims / Prescription	44
2.8	Evaluation and Analyzing Methods	45
2.8.1	Clinical and Technical Requirements to an ART Interpolation Tool .	47
2.9	VMAT Settings, Monaco-Prescription	48
3	Results	50
3.1	Organ Contour Adaptor Tool - OrCA	50
3.1.1	Datastructure	51
3.1.2	Interpolation	51
3.1.3	Smoothing	51
3.2	Non-Adapted vs. Adapted Radiotherapeutic Treatment Planning	53
3.2.1	Non-Movers	53
3.2.1.1	DVH-Values	53
3.2.1.2	DVH-Plots	56
3.2.1.3	Dose Distributions	56
3.2.2	Mover	58
3.2.2.1	DVH-Values	58
3.2.2.2	DVH-Plots	62
3.2.2.3	Dose Distributions	63
3.3	Influence of Decreasing the CTV-PTV-Margin	65
3.3.1	DVHs	65
3.3.2	DVH-Values	65
4	Summary and Discussion	71
4.1	Advantages and Disadvantages of ART	72
4.2	Issues concerning Hollow Organs and Bladder Filling	72
4.3	Dose Calculation of TPS with unchanged ED Distribution	73
4.4	Planning Study versus Future Clinical Workflow	74
4.5	Inferior Results of Patient 12	74
4.6	Extreme Organ Movements of Patient 21	74
4.7	Atypical Movement Patterns	75
4.8	The Dose Summation Issue	76
4.9	Small Margin versus Big Margin	76

5 Conclusion and Outlook	77
Appendix	78
Bibliography	84
List of Abbreviations	91
List of Tables	93
List of Figures	95

Acknowledgements

At this point I would like to devote the following lines to all who contributed to the success of this thesis and my whole course of study.

First of all, I would like to thank my supervisor Prof. DI Dr. Dietmar Georg for giving me the opportunity to compile this master thesis at the department of radiotherapy at the Medical University of Vienna with the team of the Christian Doppler Laboratory. He opened up the topic of adaptive radiotherapy to me, made sure that no organizational issues would occur and supported me with his expertise whenever he could.

I would also like to express my heartfelt gratitude to Yvette Seppenwoolde, PhD, my co-supervisor and advisor. Her support reached from inspiring discussions to patiently answering all my questions and providing highly useful comments and constructive criticism in each and every phase of this master thesis that were essential for its improvement and progress.

Furthermore, I owe special thanks to Hugo Furtado, MSc PhD, for helping me with all Matlab programming issues and for advising and supplying the CPD2-package.

I would like to thank Wolfgang Lechner, PhD, and Dr. DI Markus Stock for supervising my project and giving me handy tips, especially according the treatment planning system, that I could also apply throughout this master thesis.

I am grateful for the mental support and useful tips of all my friends and colleagues. Thank you for your friendship and having a sympathetic ear!

I owe special thanks to my parents, who made my course of study possible in the first place, with their encouragements and financial support.

Last but not least I want to express my deepest thanks to my husband David. Thank you for your love and for making me laugh anytime I was frustrated or exhausted due to all the little detail-issues of this master thesis. I wouldn't have come this far without your calming and loving arms!

Abstract

Purpose & Objectives:

It is well known that motion, tumor regression and filling variations of organs occur during radiotherapy and can thus affect treatment outcome. Therefore adaptive radiotherapy (ART) aims for adaptation of the treatment to the respective anatomic situation.

This thesis tackles ART for cervix cancer, where it is postulated that this kind of advanced radiotherapy would be beneficial for the patients in terms of better coverage of the tumor and improved sparing of organs at risk. This can be achieved by adapting the treatment plan to the current organ constellation of the patient immediately before the fraction is delivered. Currently no commercial turnkey solutions are available to perform such a treatment-plan-adaption. Furthermore only few clinical data have been gathered so far regarding the effects of ART for cervix cancer patients.

The clinical workflow of adaptive treatment of cervical cancer at the Vienna General Hospital / Medical University of Vienna will be based on a pre-treatment established motion model. The main aim of this thesis is to establish and improve this workflow by means of the development of a stand-alone Matlab contour-interpolation tool. Finally, the achievable treatment plan quality of ART for cervix cancer was assessed by dosimetric evaluation of resulting treatment plans.

Materials & Methods:

Patient Cohort: The delineated imaging data sets of 3 cervix cancer patients were acquired. Each data set included the planning-CT, weekly CTs and 3-5 CBCTs per week. All patients were treated with 3D-CRT with a total dose prescription of 45Gy that was delivered in 25 fractions of 1.8Gy each and a concomitant chemotherapy of 40mg/m² cisplatin weekly. The patients were classified to be either mover or non-mover by measuring the top-of-uterus-motion (ToUM). With a classification threshold of 2cm two patients were non-movers and one was a mover. In total 69 image data sets and their according structure contours of the organ constellation were analyzed in this planning study.

OAR- and CTV-Definition: The CTV was split into a primary CTV (CTVP) and a nodal CTV (CTVN). The CTVP includes the primary tumor, uterus, parametria and proximal third of the vagina and is enclosed by a safety-margin of 1cm. The CTVN is composed of obturatorial, iliac lymph nodes, groins and para-aortic lymph nodes and contained within a setup-margin

of 0.5cm. Bladder, rectum, sigmoid and bowel were considered as OARs.

Motion Model/ "Plan of the Day"-Approach: Our method depended on an interpolated intermediate structure from the data of full and empty bladder scan, which had to be generated by use of OrCA¹. By overlaying full with intermediate or intermediate with empty bladder volume CTV we obtained full and empty stage CTV. Adding a safety margin of 1cm resulted in the needed corresponding PTVs. This 2-stages- or "plan of the day"-approach (PotD) gives in the clinic the possibility to decide which plan to deliver for each fraction individually.

Motion Robust Plan: For the patients categorized as non-movers a motion robust treatment plan was generated following a similar attempt. The two CTVs of the full and empty bladder scans were fused and a safety margin of 1cm was added to obtain the motion robust PTV.

Both planning strategies were based on two full 360° VMAT-arcs in the transversal plane where the isocenter equals the center of the tumor. *Evaluation through TPS:* The overall evaluation of the planning strategies was possible by image registration of the bony anatomy of all available scans to the planning-CT and import of all according contour data sets to this one scan. Placing all available contour data in the planning-CT scan gives the possibility to evaluate all DVH-values of all structure contours by calculating just one treatment plan.

Results:

The analyzed OAR DVH-data showed only minor differences between non-ART and motion robust plans, except for the increase of the D_{mean} of the bladder by about 6Gy for one patient. The other patient seemed to benefit from the motion robust plan in terms of an increased cervix-uterus target coverage. The analysis of dose distributions and DVHs showed especially for the PotD-approach good results by means of a substantial increase of cervix-uterus target coverage from $74 \pm 18\%$ to $98 \pm 3\%$. The OAR DVH-values showed an increase of D_{mean} of the bladder from $30 \pm 4\text{Gy}$ to $41 \pm 2\text{Gy}$.

An additional analysis focused on the question of the CTV-PTV-margins. For the nodal CTV we found that the setup margin of 0.5cm should not be decreased, since reducing it to 0.2cm led to approximately 5% less nodal target coverage for all 3 patients. Reducing the primary CTV margin from 1cm to 0.5cm seemed to lead to approximately 2 – 3Gy lower D_{mean} of the bladder for all patients. On the other hand for the mover-patient and her PotD-approach we found that the cervix-uterus target coverage went down about 3% through this margin reduction. All other OAR DVH-values did not seem to be significantly influenced by this margin-modification.

Conclusion:

In conclusion we can state that all the necessary building blocks for a functioning radiotherapeutic treatment workflow for cervix carcinomas are now ready for clinical use. Conceived

¹OrCA is a Matlab program that was developed in the scope of this thesis and generates intermediate contours of the CTV as well as bladder.

in general terms, according to the findings of our planning study the mean dose of the bladder will increase with the adaptive approach, but patients will benefit due to improved target coverage. Anyhow the pre-determined motion models have to be verified and monitored on a regular basis during the treatment course and more patients need to be included in future studies.

Kurzfassung

Zweck & Ziele:

Bekanntermaßen treten während einer radiotherapeutischen Behandlung Organbewegung, Tumorregression und Veränderung des Füllungsstandes von Organen auf, deren zeitlicher Verlauf im Weiteren den Behandlungserfolg beeinträchtigen können. Aus diesem Grund zielt die adaptive Radiotherapie („adaptive radiotherapy“ - ART) auf die Adaptierung der Behandlung auf die aktuelle, jeweilige anatomische Situation ab.

Diese Masterarbeit behandelt ART für Zervixkarzinome. Für diesen Teilbereich der Onkologie wird im Speziellen postuliert, dass adaptive Bestrahlungsplanung sich positiv auf die Tumorabdeckung auswirkt und eine geringere Risikoorganbelastung zur Folge hat. Dies kann durch eine Anpassung des Bestrahlungsplans an die momentane Organkonstellation der Patientin unmittelbar vor der Bestrahlungsfraction erreicht werden. Zur Zeit ist keine kommerzielle Komplettlösung zur Durchführung einer solchen Bestrahlungsadaptierung erhältlich. Außerdem sind bisher nur wenig klinische Daten zur ART von Zervixkarzinomen gesammelt worden.

Der klinische Workflow der adaptiven Behandlung von Zervixkarzinomen am AKH Wien / Medizinischen Universität Wien basiert auf einem vorab entwickelten Bewegungsmodell. Das Hauptziel dieser Arbeit besteht darin, diesen Workflow mitzubegründen und im Weiteren durch die Entwicklung eines autarken Matlab Kontur-Interpolations-Programmes zu verbessern. Abschließend werden die erreichbaren Qualitäten der Bestrahlungspläne von ART für Zervixkarzinome anhand einer dosimetrischen Auswertung von Bestrahlungsplänen ermittelt.

Material & Methoden:

Patientengruppe: Die konturierten Bilddatensätze von drei Zervixkarzinom-Patientinnen wurden in der Planungsstudie untersucht. Jeder Bilddatensatz inkludiert das Planungs-CT, wöchentliche CTs und 3-5 Kegelstrahl-CTs („cone beam CT“ - CBCT) pro Woche. Alle Patientinnen wurden mittels dreidimensionaler konformaler Strahlentherapie („three dimensional conformal radio therapy“ - 3D-CRT) mit einer totalen Dosisverschreibung von 45Gy behandelt, die in 25 Fractionen von je 1.8Gy verabreicht wurde und einer begleitenden Chemotherapie von wöchentlich 40mg/m² Cisplatin. Die Patientinnen wurden entweder als „Mover“ oder als „Non-Mover“ anhand der Messung der Bewegung des Uterus-Fundus klas-

sifiziert. Mit einer Klassifikationsgrenze von 2cm waren zwei Patientinnen „Non-Mover“, während eine „Mover“ war. Insgesamt sind 69 Bilddatensätze und ihre zugehörigen Strukturkonturen der Organkonstellation in dieser Planungsstudie analysiert worden.

OAR- and CTV-Definition: Das klinische Zielvolumen („clinical target volume“ - CTV) wurde in ein primäres (CTVP) und ein nodales (CTVN) geteilt. CTVP inkludiert den Primärtumor, Uterus, Parametrium und das obere Drittel der Vagina und wird mit einem Set-Up Sicherheitssaum von 1cm ausgestattet. Das CTVN setzt sich aus obturatorialen, ilioakalen Lymphknoten, Leisten- und den paraaortischen Lymphknoten zusammen und erhält einen Sicherheitsrand von 0.5cm. Blase, Rektum, Sigmoid und Darm wurden als Risikoorgane („organs at risk“ - OARs) berücksichtigt.

Bewegungsmodell / „Plan of the Day“-Ansatz: Unsere Methode hängt von interpolierten, intermediären Strukturen zwischen den CT-Aufnahmen der vollen und leeren Blase ab, welche mit Hilfe von OrCA² erstellt wurden. Basierend auf einem Bewegungsmodell erhielten wir durch eine Überlagerung dieses intermediären CTVPs mit dem jeweiligen Extrem-CTVP (Blase voll bzw. leer) „full“ und „empty stage CTVP“. Das Hinzufügen eines Sicherheitsrandes von 1cm führte zu den benötigten zugehörigen PTVs. Dieser „2-stages“- oder „plan of the day“-Ansatz (PotD) gibt in der Klinik die Möglichkeit vor jeder Strahlungsfraction individuell zu entscheiden welcher Bestrahlungsplan abgestrahlt werden soll.

Bewegungsrobuster Plan: Für die Patientinnen, die als „Non-Mover“ kategorisiert wurden, ist ein bewegungsrobuster Plan erstellt worden, der einem ähnlichen Ansatz folgt. Die beiden CTVPs von vollem und leerem Blasenvolumen-CT-Scan wurden fusioniert und mit einem Sicherheitsrand von 1cm versehen, um das bewegungsrobuste PTV zu erhalten.

Beide Planungsstrategien basierten auf zwei vollen 360° VMAT-Bögen in der transversalen Ebene, wobei das Isozentrum dem Zentrum des Tumors entsprach. *Auswertung durch das Planungssystem:* Die gesamte Auswertung der Planungsstrategien war möglich durch Bildregistrierung der Skelettanatomie aller verfügbaren Scans auf das Planungs-CT und Importierung von allen zugehörigen Konturdatensätzen in diesen einen Scan. Die Platzierung aller verfügbaren Konturdatensätze in den Planungs-CT-Scan macht es möglich alle DVH-Werte aller Strukturkonturen mit nur einer einzigen Behandlungsplanberechnung auszuwerten.

Resultate:

Die analysierten OAR DVH-Daten zeigten nur kleine Unterschiede zwischen non-ART und bewegungsrobustem Plan, abgesehen von dem Anstieg der mittleren Dosis der Blase von ungefähr 6Gy bei einer Patientin. Die andere Patientin schien von dem bewegungsrobusten Plan zu profitieren, da sich ihre Zervix-Uterus-Zielabdeckung verbesserte. Die Analyse der Dosisverteilung und DVHs zeigte vor allem für den PotD-Ansatz gute Resultate im Sinne

²„Organ Contour Adaptor“ ist ein Matlab Programm, welches im Rahmen dieser Arbeit entwickelt worden ist und intermediäre CTVP- und Blasenkonturen generiert.

von einer deutlichen Verbesserung der CTVP-Abdeckung von $74 \pm 18\%$ auf $98 \pm 3\%$. Die OAR DVH-Werte zeigten einen Anstieg der mittleren Blasendosis von $30 \pm 4\text{Gy}$ auf $41 \pm 2\text{Gy}$. Eine zusätzliche Analyse untersuchte die Fragestellung einer CTV-PTV-Rand-Verringerung. Für die nodalen CTVs wurde festgestellt, dass der Rand von 0.5cm nicht reduziert werden sollte, da eine Verringerung auf 0.2cm zu einem Abfall der nodalen Zielabdeckung von ungefähr 5% für alle drei Patientinnen führte. Eine Reduktion des primären CTV Randes von 1cm zu 0.5cm schien eine ungefähr $2 - 3\text{Gy}$ niedrigere mittlere Blasendosis für alle drei Patientinnen zur Folge zu haben. Andererseits zeigten die Daten für die Mover-Patientin und den PotD-Ansatz, dass dadurch die Zervix-Uterus-Zielabdeckung um 3% verschlechtert wird. Alle weiteren OAR DVH-Werte zeigten keine signifikanten Abweichungen durch diese Veränderung des Sicherheitsrandes.

Fazit:

Abschließend können wir festhalten, dass alle notwendigen Bausteine für einen funktionierenden radiotherapeutischen Behandlungs-Workflow für Zervixcarzinome für den klinischen Gebrauch bereit sind. Generell können wir aus den Ergebnissen unserer Planungsstudie schließen, dass die Blase mit dem adaptiven Ansatz einer höheren mittleren Dosis ausgesetzt werden wird, aber die Patientinnen durch die verbesserte Zielabdeckung profitieren werden. Auf jeden Fall muss das zuvor definierte Bewegungsmodell während des gesamten Behandlungsverlaufs regelmäßig verifiziert und kontrolliert werden und zukünftig müssen weitere Studien mit einer höheren Anzahl an Patientinnen durchgeführt werden.

1 Introduction to some Principles of Radiation Therapy

1.1 Introduction

The interdisciplinary field of radiation therapy is one of the three pillars for the treatment of cervical cancer. Besides surgery and chemotherapy, radiotherapy is an approach which is continuously improved and a focus of research. We distinguish between brachytherapy (BT), which applies dose by bringing radionuclides in close proximity of the tumor site and external beam radiotherapy (EBRT, also referred to as teletherapy), which is split into particle and photon radiation applications.

The main aim of radiotherapy is to apply a prescribed dose to the tumor volume to induce controlled cell death (apoptosis). For clarity the definition of different physical dose concepts are presented in section 1.2. Photon irradiation is delivered by treatment linear accelerators (linacs) that can be seen as the "workhorses" of radiooncology. Their main components and principle of functionality are therefore presented in section 1.3. Through availability of highly dynamic multileaf collimators (MLC), sophisticated treatment planning systems (TPS) and advanced dose calculation algorithms, the development of many elaborated delivery methods became possible, starting from 3D-conformal radiotherapy (3D-CRT) through static and dynamic intensity modulated therapy (IMRT) to rotational IMRT. The different aspects of these delivery modes are highlighted in section 1.4 and the advantages of flattening filter free beams (FFF beams) in contrast to filtered beams will be outlined.

Section 1.5 explains common volume concepts in oncology that are needed for an accurate and standardized prescription in order to be consistent during all radiotherapeutic treatment planning processes, while section 1.6 gives background information about the state of the art clinical planning process.

The above mentioned sections are mainly based on the *Handbook of Radiotherapy Physics - Theory and Practice* [1] and *The Physics of Radiation Therapy* [2] and loosely recite some of their contents.

In today's practice of radiotherapy the delivered dose distribution is based on snapshot imaging information; i.e. dose calculation, treatment planning and dose response assessment are linked to a rigid anatomy. Since the availability of built-in cone-beam CTs (CBCT), that

allowed to check the patients anatomy in treatment position, it is well known that motion, tumor regression and filling variations of organs occur during treatment and can thus affect treatment outcome. Current technology research and developments aim for adaptation of the treatment to the respective anatomic situation ("adaptive radiotherapy" - ART). The section 1.7 describes the idea and benefits of adaptive radiotherapy at first in general and gives more detail for the most recent findings for ART for cervical cancer cases.

1.2 Dose

First of all it is important to point out that there are diverse dose concepts that should not be confused with each other. They are presented in the following.

According to the ICRU [3, 4] **absorbed dose** is defined as the quotient of $d\bar{\epsilon}$ by dm , where $d\bar{\epsilon}$ is the mean energy deposited by ionizing radiation to matter of mass dm . This relation is given in equation 1.1

$$D = \frac{d\bar{\epsilon}}{dm} \quad (1.1)$$

The unit of absorbed dose is the Gray (Gy) which is 1 Joule per kilogram (J/kg). The **energy imparted**, ϵ , by ionizing radiation to the matter in a volume is given in equation 1.2 and was also defined in the ICRU reports of 1980 and 1998.

$$\epsilon = R_{in} - R_{out} + \sum Q, \quad (1.2)$$

where

R_{in} is the radiant energy, which is the sum of the energies of all ionizing particles that enter the volume

R_{out} is the sum of the energies of all ionizing particles that leave the volume and

$\sum Q$ is the sum of all changes of the rest mass energy of nuclei and elementary particles in any nuclear transformations that occur in the volume. If the rest mass energy increases the contribution receives a negative sign and vice versa.

The **kerma** (**k**inetic **e**nergy **r**elaxed per unit **m**ass), K , is measured in Gray like the absorbed dose and is defined as the quotient dE_{tr} by dm . dE_{tr} (transferred energy) is the sum of the initial kinetic energies of all the charged ionizing particles released by uncharged ionizing particles, like photons, in a material of mass dm . Equation 1.3 displays this relation.

$$K = \frac{dE_{tr}}{dm} \quad (1.3)$$

The **ion dose** J is a physical quantity for measuring ionizing radiation and is defined as the electrical charge dQ of all ions with the same sign that are released by ionizing radiation in a material of mass dm . Thus, its dimension is charge per mass with the unit Joule, $J=C/kg$. The mathematical definition of ion dose is given in equation 1.4.

$$J = \frac{dQ}{dm} \quad (1.4)$$

Various types of ionizing radiation do not have the same effect on biological tissue. To account for these discrepancies the concept of **relative biological effectiveness** (RBE) has been developed. It's definition is given in equation 1.5.

$$RBE = \frac{D_{ref}}{D_R}, \quad (1.5)$$

where

D_{ref} is a reference absorbed dose of radiation of a standard type and

D_R is the absorbed dose of radiation of type R that causes the same amount of biological damage.

An extension of this idea is the **equivalent dose** H_T that was established by the ICRP in 1991 [5], which is used in radiation protection. It can be determined by multiplying the mean absorbed dose $D_{T,R}$ deposited in body tissue T by radiation type R with the radiation weighting factor W_R . This weighting factor is dependent on the type and energy of the radiation R and represents the relative biological effectiveness of the radiation. It is a function of the linear energy transfer (LET)¹. Equation 1.6 shows the mathematical definition of the equivalent dose.

$$H_{T,R} = \sum W_R \cdot D_{T,R} \quad (1.6)$$

Although the physical unit of the equivalent dose is J/kg, like for the absorbed dose and kerma, it is expressed in Sievert (Sv).

Not only the type and energy of radiation influences the effects on biological tissue, but also the kind of tissue that is irradiated. To account for the different sensibilities of organs, we can use the **effective dose** (E). In its definition the equivalent dose is used as starting point and multiplied by a tissue weighting factor (W_T), which are determined by the ICRP and have been revised twice in the last 15 years. For better clarity, the relation is shown in eq. 1.7.

$$E = \sum W_T \cdot H_{T,R} \quad (1.7)$$

¹The LET describes how much energy an ionizing particle transfers to the material transversed per unit distance. It depends on the nature of the radiation as well as on the material traversed.

Both equivalent and effective dose are not intended as a measure of deterministic health effect, but stochastic health risk.

1.3 Medical Linear Accelerators

An external view allows only to see the stand, the gantry and the couch of the linac treatment system. Gantry and couch both have one rotational axis, i.e. two degrees of freedom that allow the delivery of various incident angles in little time. The actual linac is inside the gantry head and in some design versions in the stand. The basic principle of a medical linear accelerator is to accelerate electrons that are emerging from the electron gun using high frequency electromagnetic waves onto a high-density target (commonly made from tungsten). Its main components are a RF power generator, an electron gun, an accelerating waveguide and a target. Their arrangement can be seen in figure 1.1 in three different linac-designs.

The RF power generator consists of a magnetron as power source and a modulator. The modulator transfers high voltage pulses to both the magnetron and the electron gun. The magnetron is a high power oscillator that generates microwave pulses which are transported to the acceleration tube via a waveguide system. The electron gun consists from a cathode that thermo-ionically emits electrons, which are then focused into a pencil beam by a curved focusing electrode and accelerated towards the perforated anode. Through this anode they are injected in the acceleration tube (also referred to as accelerating waveguide in figure 1.1). The electrons gain kinetic energy through interaction with the sinusoidal electromagnetic field of the standing wave in the acceleration tube.

After the acceleration, they are guided by means of bending magnets into the treatment head, where they collide with the water cooled target. From the interaction of the accelerated electrons with the matter of the target results bremsstrahlung. The emerging bremsstrahlung-photon beam is characterized by an X-ray spectrum corresponding to the maximum energy of the incident electrons. The linac head contains several components that influence the shaping, localizing and monitoring of the clinical photon beams. In figure 1.2 the main components of the treatment head are depicted.

The treatment head consists of a primary collimator, flattening filter, monitor chamber, multi-leaf collimator and x and y jaws, which prepare the photon beam for the radiotherapy. The treatment head is shielded against leakage radiation in accordance with radiation protection guidelines.

The primary collimator is circular, close to the target and constrains the radiation directions to ensure that only the required part of the patient is irradiated. Due to the various energies of electrons hitting the target, the angular distribution of x-rays the intensity is peaked forward. To achieve a uniform beam intensity across the field a flattening filter is arranged between

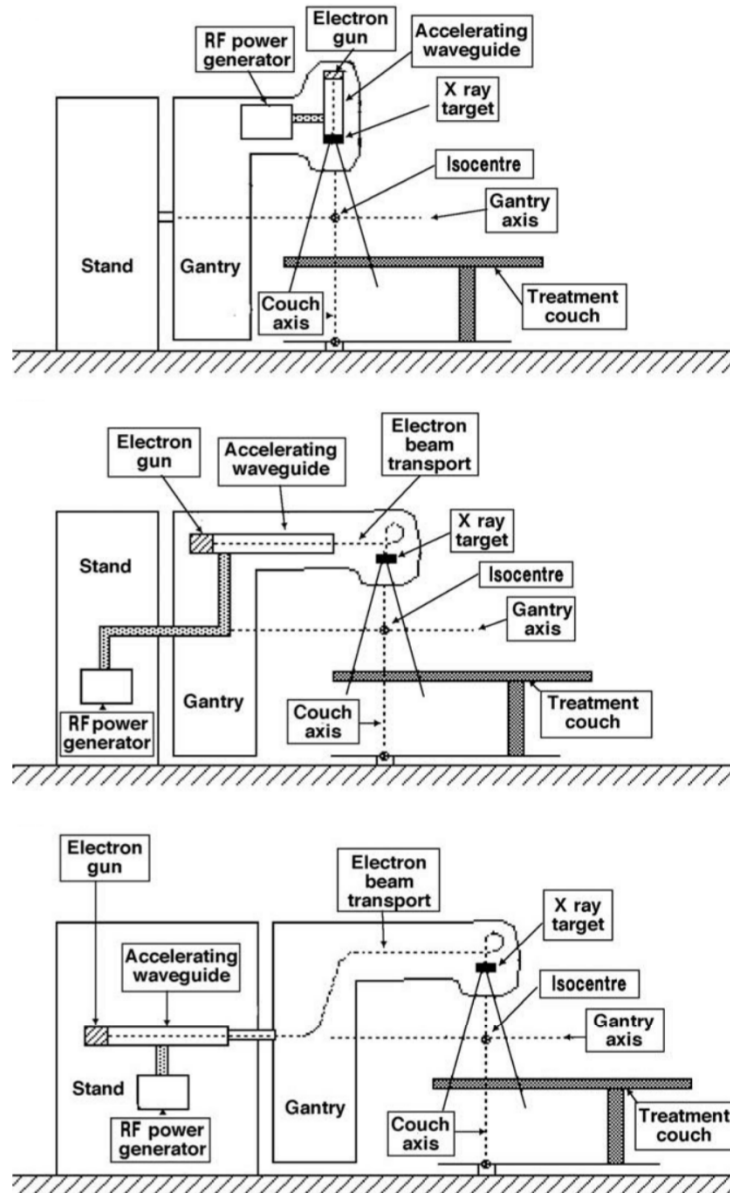


Figure 1.1: Schematic structure of three different linac-designs. The straight-through beam design (top) allows the machine only to produce X rays with energies of 4-6 MV, the other two designs allow to produce megavoltage X rays as well as electrons.[6]

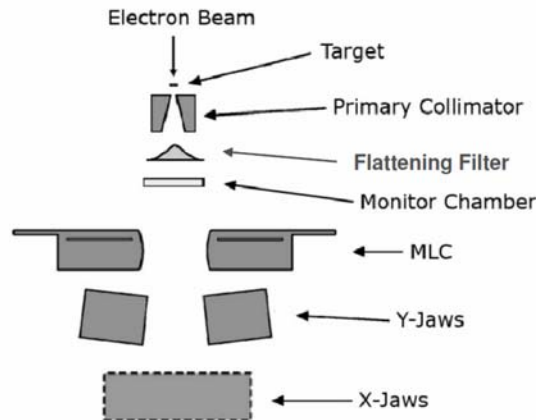


Figure 1.2: Schematic constellation of the components of a linac treatment head.[7]

the primary collimator and the wedge. A dose monitoring chamber is an ion chamber for monitoring dose rate, integrated dose and field symmetry. A wedge filter causes a progressive decrease in intensity across the beam, resulting in a tilt of the isodose curves from their normal positions. The lower jaws, the multileaf collimators (MLCs) and the backup jaws define the correct field size and are usually made of flat-faced blocks of lead. A MLC for photon beams consists of a large number of leaves that can be driven independently and automatically to generate irregular field shapes.

1.4 Delivery Methods

1.4.1 Three-Dimensional Conformal Radiotherapy (3D-CRT)

In recent years, radiotherapy has become increasingly complex. The current trend is toward the implementation of conformal radiotherapy and intensity modulated radiotherapy (see subsection 1.4.2). These aim to reduce normal tissue toxicity by limiting irradiation of normal tissues while still irradiating the tumor in its entirety. In conformal radiotherapy the treatment volume of the patients body is being positioned in the overlap-region of the different beam directions. The multiple fields are configured by individually produced lead diaphragms to fit the target shape and by wedges to account for varying tissue thickness. Conventional coplanar techniques include single beam, two-beam, four-beam or multiple beam arrangements, where the beam-weight can be modified.

In 3D-CRT numerous coplanar as well as non-coplanar fields from different directions can be used and the beam profile is optimized with a computer-controlled multileaf collimator (MLC) for each delivery angle to cover the projection of the PTV.

Increasing the number of fields decreases the dose deposition per beam, but distributes the dose over a larger volume. The planning process for CRT is called "forward planning". This

means the planner applies a number of fields in the planning system by making use of prior experience of similar cases. Then the treatment planning system (TPS) calculates the dose distribution according to the MLC settings. The planner decides afterwards whether or not to make adaptations to the field directions, weights and/or beam number. It is important to point out that the intensities of the applied fields are uniform and not modulated, in contrast to the later introduced methods like IMRT and VMAT. This means that it is generally not possible to produce concave dose distributions with this technique.

1.4.2 Static and Dynamic Intensity Modulated Radiotherapy (IMRT)

Static IMRT can be seen as an advanced CRT method. Numerous fields and various incidence angles are used to apply the prescribed dose to the target volume. The beam profile is adjusted with a computer-controlled MLC for each delivery angle. Moreover and in contrast to 3D-CRT, the field for each delivery angle is divided into a number of subfields that can overlap with each other and are irradiated uniformly. The superposition of this static subfields results in an intensity modulation. If the Linac is turned off while the collimator leaves are moving to arrange the next subfield the method is called "step and shoot" IMRT. Another IMRT delivery method is the fully dynamic delivery or "sliding window" method where the leaves do not stop or take steps but sweep smoothly during the irradiation phase from one side to the other with variable velocities. Assuming the simplest case, in particular that the beam output is constant and the transmission through the leaves is zero and neglecting penumbra and scattering, we obtain that the profile intensity at the position x depends on the time interval at which the beam is not blocked due to any collimator leaf corresponding to x . This relation is represented in equation 1.8 [2].

$$I(x) \propto t_1(x) - t_2(x) \quad (1.8)$$

$$\frac{dI(x)}{dx} \propto \frac{dt_1(x)}{dx} - \frac{dt_2(x)}{dx} \quad (1.9)$$

$$\frac{dI(x)}{dx} \propto \frac{I}{v_1(x)} - \frac{I}{v_2(x)} \quad (1.10)$$

with t_1 and t_2 as time instances at which the edges of the first and the second collimator leaf are reaching the position x . v_1 and v_2 are the velocities of the first and second collimator leaf as a function of the position x . These relationships are illustrated in Figure 1.3.

In contrast to the planning method of 3D-CRT, the one used for IMRT is called "inverse planning". Cost functions are essential for the inverse treatment planning process. In order to define a mathematical goal, cost functions are associated with the various outlined structures and the composite cost function (CCF) is minimized by the TPS during optimization process. The value of the CCF is a measure of the violation of the target prescription. The objective function is an anatomy-specific function that establishes dose and/or biological re-

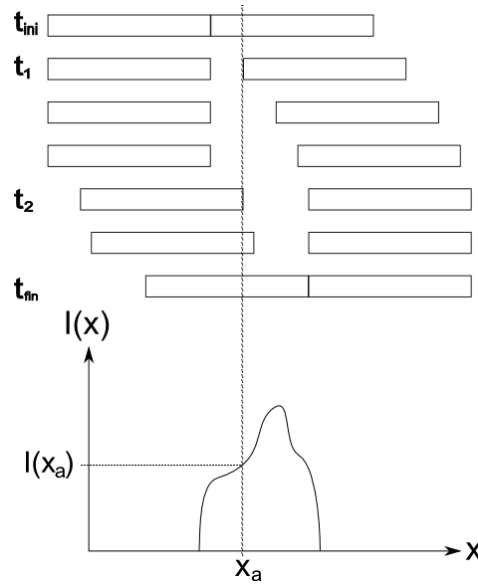


Figure 1.3: Schematic illustration of IMRT: A pair of collimator leaves corresponding to x_a at different times and the produced intensity profile. t_1 and t_2 are depicted for the marked position x_a

sponse goals and target prescription is its only input. These goals do not necessarily have to be met, in contrast to constraint functions. When both are used simultaneously, the objective will always be limited so that constraints are met. The system explores a range of options for beam weights, calculates the applied dose and accepts options that decrease and rejects options that increase the value of the CCF. This is repeated until the cost converges to a minimum. Optimization is always an iterative process.

We distinguish between biological and physical or dose-volume cost functions. Although physical cost functions are easy to handle, they do not account for the location of dose discrepancies. The importance factor, a simple dimensionless number, allows the user to weight certain regions higher than others in terms of optimization, by giving each of the various contributions to the CCF an own weighting.

But still, just the weighting of the physical cost functions was not enough and better specifications were required for OARs. Consequently biological cost functions have been developed. These functions can take advantage of the biological volume effect of structures. Each structure is associated with its particular volume-effect, in contrast to the physical cost functions, where the system treats all structures as if they had the same dose response mechanism. Those volume-effects are split into the two main groups serial and parallel. As the name indicates, they are designed for serial and parallel OARs as mentioned in section 2.3.

1.4.3 Rotational Intensity Modulated Radiotherapy

Rotational Intensity Modulated Radiotherapy or "Volumetric Modulated Arc Therapy" (VMAT) is also based on a modulation of intensity of the beam. It is quite similar to IMRT but the gantry is moving during the whole irradiation phase following an arc. Clearly the MLC

works in dynamic mode to shape each subfield as the gantry rotates, enabling highly conformal dose distributions to be delivered also to irregularly shaped tumors. Gantry speed and dose rate can be varied freely within the given range of the Linac. Several overlapping arcs can be used that are programmed to deliver one subfield at each gantry angle. The chosen intensity steps per arc and number of arcs strongly correlate with the complexity of the case. As in static IMRT the superposition of those subarcs creates the desired intensity modulation. Irradiating while the gantry is moving gives possibility to use more and continuously changing irradiation directions. An increase in low dose exposure of the patient compared to the other mentioned techniques occurs when using VMAT which might enhance the possibility of therapy-induced secondary malignancies. However, the time efficiency in contrast to other methods is evident. The great time saving is given by the fact that the irradiation angle is continuously altered during irradiation. Less starting positions have to be approached and the fraction of overall treatment time in which the Linac has to be turned off is decreased compared to other techniques.

1.4.4 Flattening Filter Free Beams (FFF Beams)

The use of flattening filters has historical roots. In early days of computer assisted dose calculation the computation of photon fluences was not as accurate and fast as nowadays, because the performance of computers is continuously increasing. Calculations had to be done by hand and were often based on only one calculated point, therefore a flat profile was most practical. Also the uniform treatment of target volumes can be seen as a paradigm of radiation therapy, because it was assumed that tumor tissue was homogeneous and had constant cell density. For this reason the beams were flattened to obtain a nearly uniform dose at a given depth. Today more sophisticated calculation algorithms, like Finite Size Pencil Beam (FSPB) or Monte Carlo (MC) (see subsections 2.4.2 and 2.4.1), allow the estimation of dose distributions induced by non-flattened photon beams. Additionally the optimizers and sequencers of the TPSs have improved.

Georg et al have reviewed the properties and advantages of flattening filter free beams [8]. The unfiltered beam profile shows a prominent peak, especially for high energies. Two main differences can be observed in the photon spectrum when removing the flattening filter. It is typically softer and the photon energy fluence increases and consequently the dose rate increases to more than $1000\text{MU}/\text{min}$. This leads to lower net delivery times. The off-axis softening is less pronounced which may lead to a higher dose calculation accuracy. Additionally, one of the major sources of electron contamination and photon scattering drops out when removing the flattening filter. As a result the head leakage is reduced by 50% to 60% [8].

1.5 Oncological Volume Definitions

The three dimensional representation of patient anatomy available today call for standardized volume definitions. According to the *Handbook of Radiotherapy Physics - Theory and Practice* [1] [P.638, Part G]

"The adoption of these terms serves several purposes:

- Improves clarity of thought and encourages a logical approach to planning*
- Promotes consistency in physics planning and clinical practice*
- Allows standardisation of clinical trial protocols, particularly for complex, multiphase treatments*
- Facilitates communication between different centres and within clinical trials"*

For these reasons various radiotherapeutic volume concepts have been developed by the International Commission of Radiation Units and Measurement (ICRU) to account for uncertainties. The volume concepts from ICRU Reports 50 [9] and 62 [10] and are presented in the following.

Gross Tumor Volume (GTV)

The GTV denotes the visible or palpable tumor volume. It represents the macroscopic tumor extent. This is the volume that can be seen as a more or less clearly delineated structure on the CT or MR images. In some cases it may be difficult to distinguish between malign growth and inflammatory tissue reaction.

Clinical Target Volume (CTV)

The CTV encloses the GTV and tries to account for invisible microscopic spread of the disease with an additional empirical margin and often includes the affected lymph nodes. The use of PET can help to define the CTV with higher precision.

Internal Target Volume (ITV)

The ITV is the volume that encompasses the CTV and the Internal Margin, which accounts for internal physiological variations in size, shape, and position of the CTV relative to anatomic reference points, e.g. filling of the bladder, respiratory movement.

Planning Target Volume (PTV)

The PTV is the volume according to which the treatment plans are designed. It encompasses the GTV, CTV and ITV completely with a safety margin, that compensates uncertainties in patient position and inherent radiation delivery uncertainties. When defining the PTV one

has to make sure that every part of the CTV will receive the prescribed dose.

Treated Volume (TV)

As the name implies, the treated volume is the volume that receives more than a threshold dose that has a treatment effect on the tissue. For example this could be the volume that is enclosed by the 95% isodose surface depending on the specification through the clinician. In an optimized treatment plan the TV should not be significantly larger than the PTV.

Irradiated Volume (IV)

The irradiated volume consists of all the voxels that receive a significantly higher dose than the considered tolerance of the normal tissue due to treatment. This concept is for example used when comparing competing treatment plans. If two plans only differ in IV size, smallest IV is clearly preferable.

Organs at Risk (OAR)

With the term "Organs at Risk" the structures that fulfill an important purpose in the human body and/or are very sensitive to radiation are summarized. These structures are distinguished into serial and parallel organs. This refers to their behavior in case of tissue destruction. The organs consist of functional units.

For example the lung consists of non-depending alveoli. If only a small portion is damaged, the others can fulfill their function independently. It behaves similarly to a rope. If only few strings break, the rope still can carry load. Only if a critical amount of strings break the rope is broken. The human body only needs a certain amount of healthy alveoli to survive and to ensure sufficient oxygen supply. Therefore the lung is considered as a parallel organ.

If we take a look at nerves that are damaged in a very small part of their volume, it is not possible to pass on stimuli any more. The functional units are aligned like a chain. The function of the whole is lost if one functional unit is damaged. Hence, nerves are considered to be serial organs.

Serial-parallel OAR show attributes of both types (e.g. the heart).

A schematic drawing of the various volumes is given in figure 1.4.

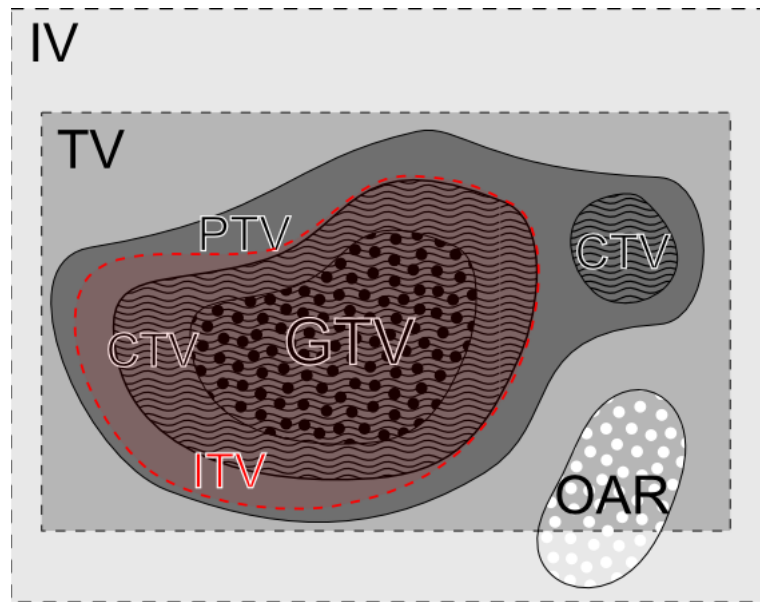


Figure 1.4: Oncological volume concepts: The small CTV on the right could depict an involved lymph node. The PTV is not necessarily one combined volume as illustrated in this example but can also be decomposed in two or more PTVs. The ITV accounts for physiological movements of the CTV.

1.6 Treatment Planning Process

According to the *Handbook of Radiotherapy Physics - Theory and Practice* [1] [P.635] "Treatment planning is the process of determining the most appropriate way to irradiate the patient. It is a combination of the following five essential steps:

1. *Choosing an appropriate patient positioning and immobilisation method so that treatments will be reproducible;*
2. *Identifying the shape and the location of the tumour (i.e. the target) and of the neighbouring organs at risk;*
3. *Selecting a suitable beam arrangement;*
4. *Evaluating the resulting dose distribution;*
5. *Calculating the treatment machine settings to deliver the required absolute dose."*

Any state of the art radiotherapeutic treatment planning procedure begins with obtaining an initial planning-CT of the region of interest of the patients anatomy. Of course the patient positioning with help of various tools, like thermoplastic masks, supporting vacuum bags etc. has to be consistent for planning-CT and irradiation fractions and therefore determined beforehand. Based on the obtained CT images, the organ contours for organs at risk and the oncological volumes like CTV and PTV are delineated by a clinician using the tools of the TPS. The TPS has to base its planning process on these contours, the selected beam model

of the chosen treating Linac and MLC and the electron density distribution of the tissue. In order to guarantee a precise treatment, it is important to determine the relationship between CT Hounsfield units and electron densities, which is the basic input for radiotherapy planning systems that consider tissue heterogeneities. In other words, the electron density distribution can be obtained via the calibration curve of the Hounsfield units of the CT images to correct for tissue inhomogeneities in dose calculation during radiotherapy treatment planning. Radiotherapy can be based on single, two or multiple beam arrangements with coplanar or non-coplanar techniques. Also more sophisticated methods are suitable like in our case VMAT (see subsection 1.4.3 and section 2.9). In clinic often appropriate templates of beam arrangements are available for the various indications. One of these is usually selected and if necessary adjusted in the TPS. All IMRT planning processes are based on so called inverse planning. The planner decides initially which aims he wants to achieve in terms of dose distribution. This happens by the use of cost functions that are applied to the structures of interest. The TPS tries to minimize the sum of the cost functions by modulating the various dose profiles and beam weights of the different beam directions. If the goal is feasible it will show the computed dose distribution after some time of calculation. The planner then decides whether to adapt the different parameters of the cost functions or to accept the calculated treatment plan. The evaluation of the treatment plans requires usually DVH curves of all structures of interest and a visualization of the resulting 3D dose distribution, which both are provided by the TPS. It is essential to ensure that no cold spots in the PTV are allowed to prevent a significant decrease of TCP. For a closer look at the TPS used in this thesis see section 2.4, details about cost functions are shown in subsection 2.4.3, examples and definitions of structures of interest are explained in subsections 1.5 and 2.3 and for more information about dose calculation algorithms see subsections 2.4.1 and 2.4.2.

1.7 Adaptive Radiotherapy

1.7.1 General Concept

A human being is not a rigid body. Movement and deformation of anatomical structures with respect to the skeleton are more challenging to estimate than errors in patient positioning. It is very difficult to control and measure them. A frequently used tool is the implantation of gold markers to increase the visibility of the position changes and make them easier to measure. We distinguish between *interfractional* and *intrafractional* movements.

The most pronounced source of intrafractional movement is breathing motion of the patient during the treatment. This causes severe interferences during the irradiation of thoracic and upper abdominal regions (e.g. mammary, pulmonary or hepatic cancer). Studies have shown that the motion and deformations of diaphragm, lung, liver and kidneys can range of up to

a few centimeters [11, 12, 13]. Solution concepts often rely on gating, tracking or free or enforced breath holding via active breath control (ABC) [14, 15, 16, 17, 18, 19, 20].

Interfractional organ movements are typically encountered in the abdominal and pelvic region. Research through comparison of CTs from different days of treatment fractions have shown that the position of colon, rectum, small bowel, bladder and prostate can vary by centimeters [21, 22]. The position of the bowel is assumed to change over minutes due to peristaltic contractions and the volume of bowel and bladder fluctuates according to the uptake of fluids and food. The snapshot position of organs at each fraction don't seem to correlate in any way and therefore are random and can be seen as a stochastic process. One example of restricting such organ-motions is by stabilizing the prostate with the aid of an endorectal balloon. At other indications tools that apply external pressure on the belly to push the bowel out of the irradiation field have been used to spare it from high doses. Beside the mentioned kinds of organ movements, also tumor regression may occur during the course of treatment or the tumor biology might change by means of hypoxicity [23].

The goal of Adaptive Radiotherapy (ART) is to minimize the influence of these individual geometrical variations to the treatment outcome. The Concept of ART had first been proposed in 1997 by Yan et al. [24, 25]. The general idea was to adapt the safety margin of the radiotherapeutic treatment based on obtained data from the individual patient in contrast to data from population. Consequently this is leading to a change of the target volume. During the first couple of treatment fractions data are gathered containing information about the position and movement of organs. Based on this data the PTV is adapted. This can be called feedback loop.

Nowadays the term ART has grown bigger and contains sub-categories. Lu et al. have not adapted the safety margin but the fractionation and made it dependent on the PTV-OAR distance [26]. They found that OAR would benefit from this adaption strategy in terms of up to 20% less cumulative dose by maintaining the same cumulative dose for the tumor. Such strategies are based on realtime replanning and often use in room CBCTs (see subsection 2.2.1) and are called online-adaptive methods.

ART is therefore just the first step of implementing image guided adaptive radiotherapy (IGART) into clinical practice.

1.7.2 ART for Cervical Cancer Cases

State-of-the-art radiotherapeutic treatment of cervical cancer cases nowadays consists of two components based on different delivery methods: external beam radiation therapy and brachytherapy. To optimize OAR sparing IMRT and VMAT are suitable irradiation techniques in combination with image guidance and reduced margins. The whole cervix-uterus

shape as well as the lumbar and adjacent lymph nodes are defined and delineated as CTV in the planning process.

Both the cervix-uterus shape and position depends on bladder and rectum filling [27, 28, 29, 30, 31]. Moreover large individual differences in the obtained cervix-uterus motion pattern can be found. For some patients the influence of the bladder filling is close to zero, meaning that the uterus stays erected. These patients are categorized as "non-movers". For other patients the uterus position shows a significant dependency on the bladder filling by means of bending over the bladder. These cases are called "movers". For a non-adaptive planning strategy on average 20 to 25% of the CTV can be outside the PTV for such patients showing much bladder filling variation [32].

The effect of non-adapted treatment can be seen in figure 1.5.

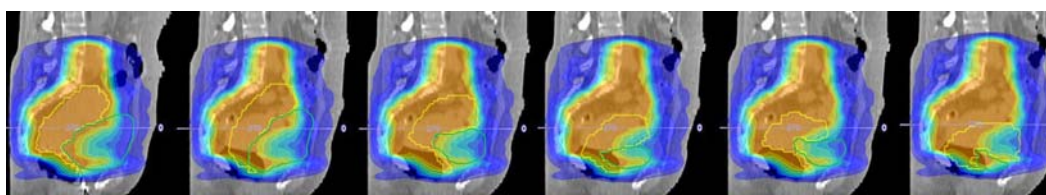


Figure 1.5: Planned dose distribution based on the planning-CT and changing uterus positions for different bladder filling stages during the treatment fractions. The yellow contour depicts the uterus while the green one shows the bladder. [courtesy by webpage of Christian Doppler Laboratory for Medical Radiation Research and Radiation Oncology ¹]

To overcome these discrepancies, adaptive radiotherapy (ART) might be a solution. Adaptive radiotherapy for cervical cancer patients can have different levels of feedback and re-planning frequency. It can vary between a single re-planning phase after one week of treatment, weekly re-planning and plan of the day (PotD) approaches. Recent studies showed that approaches based on a predefined treatment plan library reduce radiation induced complications to normal tissue, while still maintaining target coverage [33, 34, 35, 36]. To create plan libraries it is necessary to obtain a range of CT scans with different bladder volumes and pre-plan according to defined bending or position sub-ranges. Previous to each treatment fraction a cone-beam CT (CBCT) is gathered and the appropriate plan from the library can be selected and delivered according to the daily anatomy. Heijkoop et al. have investigated a method to adjust the treatment plans after a certain time to account for tumor regression and changes in patient weight or anatomy [37].

The extra imaging and the necessary image processing time have an important impact on the associated clinical workload. Thus prior to clinical implementation of ART an evaluation of the costs of ART against its benefits has to be made. This is especially important since little clinical proof of the benefits of ART have been furnished yet.

¹<http://www.meduniwien.ac.at/hp/radonc/workpackages/workpackage-2-image-guided-adaptive-radiation-therapy-igart/>

1.8 Motivation

The Concept of ART had first been proposed in 1997 by Yan et al. [24, 25]. During the first couple of treatment fractions data are gathered containing information about the change of position and shape of organs. The PTV is adapted through a "feedback loop". Nowadays the term ART has grown bigger and contains sub-categories some of which are shortly introduced in the next paragraphs.

Lu et al. have not adapted the safety margin but the fractionation in simulated treatment courses and made it dependent on the PTV-OAR distance [26]. Wu et al. [38] found a method for on-line re-optimization of prostate IMRT plans for ART using deformable image registration (DIR). Some studies investigated methods to adjust the treatment plans after a certain time to account for tumor regression of cervical cancer patients and/or changes in patient weight or anatomy [23, 37].

Some groups have focused on adaptive radiotherapy concerning the bladder as tumor site, since the deformation of this organ is one of the largest occurring in the human body (e.g. [39, 40]). This applies also for cervix carcinomas, since uterus and cervix are in close proximity to the bladder. Tanderup et al. [41] gave an overview of the use of image-guided adaptive radiotherapy (IGART) in the multimodal management for this tumor site.

Many recent studies showed that approaches based on a predefined treatment plan library reduce radiation induced complications to normal tissue, while still maintaining target coverage [33, 34, 36]. Bondar et al [35, 42, 43] have based their plan library on a pretreatment established motion model for the highly deformable target volume in cervical cancer patients.

The workflow of adaptive treatment of cervical cancer borrows strategies from the last mentioned group and still has to be established and improved at the Vienna General Hospital / Medical University of Vienna to obtain better time efficiency and higher accuracy of PTV delineation for every bladder filling state. Furthermore IGART for cervix carcinomas is still focus of research and very little is known about the benefits and practicability of the different approaches that have been developed so far.

1.9 Objectives

This master thesis aims to tackle the issue of ART for cervix cancer, where it is postulated that adaptive treatment planning would be beneficial for the patients in terms of better tumor-coverage and improved sparing of organs at risk, like the rectum, bladder and the bowel. Consequently a lower toxicity is predicted for these organs. In more details, a motion model for the highly deformable tumor volume in cervical cancer patients is implemented and verified, which builds the basis for a clinical workflow concept for ART at the Vienna General

Hospital / Medical University Vienna. The needed intermediate interpolated contours of the planned target volumes (PTVs) have to be generated by use of an application that fulfills also the tasks of data transfer and data processing. Such an application is not commercially available.

Therefore the development of a stand-alone Matlab program that closes this gap is one main task of the thesis. It shall automatize the step of organ contour interpolation of the workflow using two CT-scans at two extreme bladder filling conditions. Thus, it will allow to generate intermediate structures of the PTV as well as bladder according to the current bladder volume. Practicability and functionality of this program will be tested in the preliminary clinical workflow. Another main task of the thesis is to estimate potential dosimetric benefits of ART on the basis of a pilot study. The achieved treatment plan quality of ART for cervix cancer will be assessed by dosimetric evaluation of the resulting treatment plan properties and parameters of 3 cervical cancer cases. Furthermore an exact analysis and comparison of the 3 cases will be performed and the influence of the set up margin will be researched.

2 Materials and Methods

This chapter is dedicated to the materials and methods which were used for the purpose of this thesis. The first sections focus on the details of patient data and setup and the preparations that were necessary for treatment planning, including general information about cone-beam CT (CBCT). These chapters are mainly based on a study by Seppenwoolde et al [32]. Section 2.4 gives a closer look at the used treatment planning system (TPS), especially its dose calculation algorithms and the cost functions and is followed by an introduction to the concept of dose volume histograms in section 2.5. The section 2.6 explains the applied treatment strategies and section 2.7 the aims we tried to achieve within the treatment plans. The methods of evaluation and analysis of this study are introduced in section 2.8, including the requirements to the computer program tool that was developed and tested as main part of this thesis. The final TPS-settings are presented in section 2.9.

2.1 Patient Cohort

The delineated weekly CT scans and daily CBCT scans (see subsection 2.2.1) of 3 cervix cancer patients were acquired. They were selected from an available study data set of more than 20 patients. The other patients did not suit our purposes of this thesis either because the bladder filling variations were too small or because of missing delineations. Thus they were excluded since the main goal of this thesis was to investigate on the influence of large bladder filling variations on the treatment outcome. The selected patients from the study data set have the numbers 12, 20 and 21.

All patients were treated with 3D-CRT with a total dose prescription of 45Gy that was delivered in 25 fractions of 1.8Gy each. Additionally they received a concomitant chemotherapy of 40mg/m² cisplatin weekly and a following brachytherapy boost of the tumor at the end of the external beam radiotherapy. This was performed as high dose rate (HDR) image guided adaptive brachytherapy (IGABT) via MRI and using a tandem-ring applicator that functioned as dose carrier for the iridium-192 source [44]. Brachytherapy boosted the total dose up to 84Gy (normalized to 2Gy fractionation, $\alpha/\beta = 10\text{Gy}$) via 4 fractions of 7Gy [45]. Each data set included the planning-CT, weekly CTs and 3-5 CBCTs per week. For patients 12 and 21 also the planning-MRT scan was available, for patient 12 even two additional MRT scans from treatment-weeks 3 and 4. In total 69 image data sets and their according

structure contours of the organ constellation were analyzed in this planning study. For each patient the scan with the largest bladder filling volume was defined as "full bladder scan" while the opposite definition holds for the "empty bladder scan".

2.2 Patient Setup and Preparations for Planning

Patient Setup and Technical Data:

All imaging data was gathered in supine position with help of the ProSTEP system (Elekta, Germany) to stabilize the patient positioning and improve reproducibility. The planning-CT scan (Siemens MultiSlice CT Somatom Plus 4 Volume Zoom, Germany) was performed with oral contrast (Scannotrast) and intravenous contrast, with technical characteristics of a slice thickness of $4mm$, in-plane resolution of 512×512 pixels and a voxel size of $0.98 \times 0.98 \times 4mm^3$. The same imaging protocol was used for the weekly repeated fan-beam CT-scans (FBCT), but without giving the patients any contrast. CBCTs were performed by using the Elekta XVI^{TM} system¹ (Elekta, UK) with an optimized protocol to get a longitudinal scan length of $26cm$ encompassing the pelvic region. To minimize the amount of scatter radiation, a transversal field of view (FOV) measuring $41 \times 41cm^2$, a bow-tie filter and an energy of 120kV with 1040mAs were chosen. All Patients were instructed to have a full bladder for the scans and treatment fractions, but this was neither reported nor verified.

Delineation and OAR- and CTV-Definition:

An experienced radiation oncologist manually delineated all available image data sets according to contouring guidelines [46]. The CTV was split into a primary CTV (CTVP) and a nodal CTV (CTVN). The CTVP includes the primary tumor, uterus, parametria and proximal third of the vagina. In case of vaginal involvement, the CTVP was contoured 2cm below the distal tumor extension. The CTVN is composed of obturatorial, iliac lymph nodes, groins and para-aortic lymph nodes. By adding a safety margin of 1cm and 0.5cm to the CTVP and CTVN we obtain PTVP and PTVN, respectively. Bladder, rectum, sigmoid and bowel were considered as OARs. The delineation of the rectum started inferiorly from the anorectal junction and ended superiorly at the beginning of the rectosigmoid junction. The whole potential peritoneal space of bowel up to 2cm above the cranial end of the PTV was contoured as bowel bag excluding the rectum [47].

Patient Classification:

All patients were classified to be either mover or non-mover by measuring the top-of-uterus-motion (ToUM). This was performed with help of OrCA (see section 3.1) via checking the change of top-of-uterus-position from full to empty bladder scan. With a classification

¹XVI=X-ray volume imaging

threshold of 2cm the patients 12 and 20 are non-movers and patient 21 is a mover, since the movement found for her was about 7 cm, which is extraordinarily large. This classification allowed us to develop two different treatment planning strategies (see section 2.6).

2.2.1 Cone-Beam Computed Tomography

The possibilities of commercially available integrated CBCTs (also referred to as flat-panel-CT) allow to verify and compare the patients anatomy in treatment position immediately before delivering the treatment fraction. Therefore it can be seen as technical basis for ART. As the name implies X-rays are diverging from the source in a cone-like manner and are detected by a flat panel. The principle of both FBCT and CBCT are presented in figure 2.1.

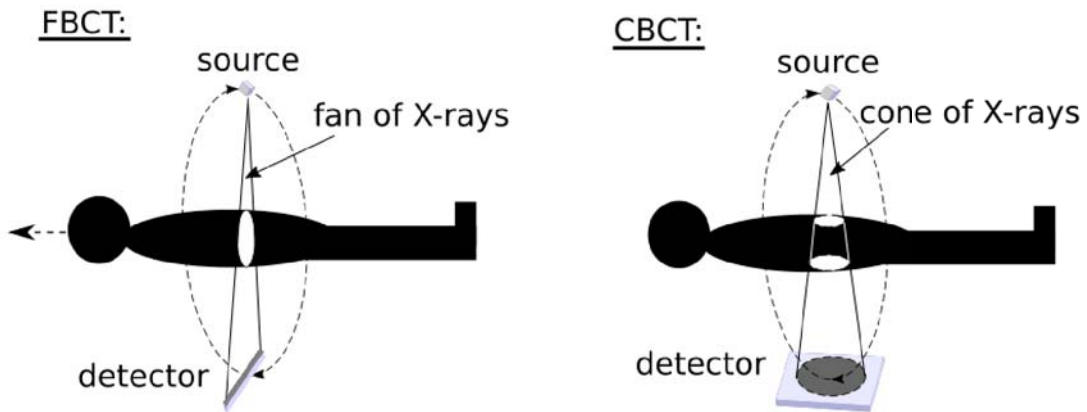


Figure 2.1: Principle of FBCT and CBCT in direct comparison.

The obtained projections from the various angles contain information about the scattered and absorbed X-ray-intensity and consequently one detector-pixel gives the attenuation along one ray-path, which is proportional to electron density. The basic principle of back-projecting the ray-paths is comparable for both CT types, although the mathematical algorithms have to be adapted to the different geometry. The sum of all back-projections give the final 3D-information of the scanned volume.

The main difference of CBCT and usual CT (=FBCT) is that slice-wise detection, where 1D data is acquired is replaced by a 2D detection. This increases scatter and consequently decreases image quality [48], but scanning time is dramatically reduced since only one full rotation is needed at maximum. The scanning time is therefore typically under one minute with a default gantry speed of $0.5rpm^2$. To achieve a suitable image quality at least 200° rotation is necessary which causes a dose of about 50mGy per scan in the isocenter [49]. Also Wen et al. [50] found comparable CBCT imaging dose values for OARs of prostate cancer patients. The detector position (or offset) defines the FOV as depicted in figure 2.2.

²rpm=revolutions per minute

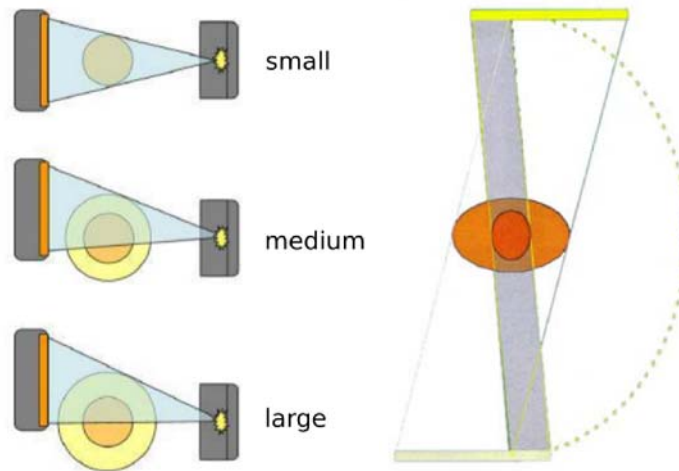


Figure 2.2: Small, medium and large FOV and detector offset (left) and 360° rotation with medium FOV (right)[51].

X-rays are maximal collimated to improve image quality as the FOV in cranial caudal direction is given by collimation and direct proportional to scatter irradiation. A bow-tie shaped filter further improves image quality and decreases skin dosage. The collimation filter has to correlate with the software settings and the detector position [51].

A built-in CBCT, such as was available for this study, consists of a X-ray source, that is shifted by 90° with respect to the Linac-head and an opposed flat detector panel. Consequently the isocenter of CBCT and Linac are identical which allows to visualize internal structures within the reference frame of the treatment system and reduce geometric uncertainties. According to the Elekta web-page³ further key visualization advantages offered by using x-ray volume imaging (XVI) at the time of treatment include:

- view of critical organs and tumors
- bony anatomy-alignment in 3D right away
- eliminate the need for surrogate markers
- ability to minimize the imaging dose
- overlay of structures defined in treatment planning system
- large field-of-view
- simultaneous acquisition and reconstruction

³http://www.elekta.com/healthcare-professionals/products/elekta-oncology/treatment-techniques/image-guided-radiotherapy-igrt/xvi.html?utm_source=xviutm_medium=redirectutm_campaign=redirects

2.3 Structures of Interest and Organs at Risk

In the following the OARs and structures of interest including the various target volumes for cervix cancer are introduced. Figure 2.3 gives the sagittal view of the female pelvic anatomy without bowel.

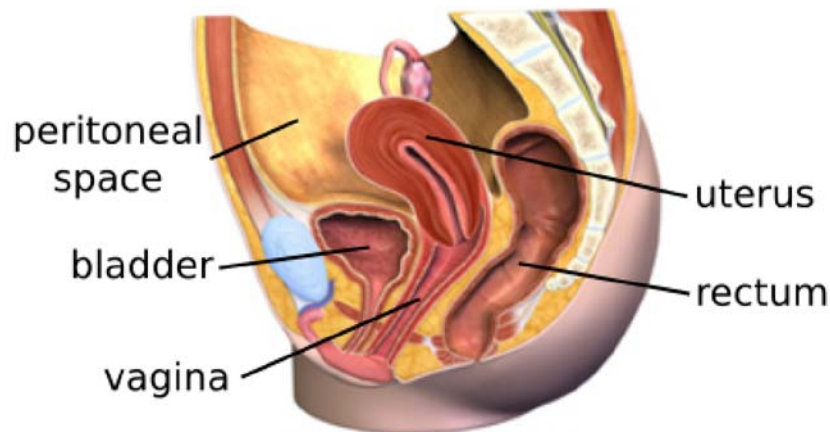


Figure 2.3: Sagittal view of pelvic region of female anatomy. The pelvic space contains the bowel which is not depicted here.

Bladder:

The urinary bladder is part of the urinary tract and a hollow, elastic, muscular sack. It is positioned on the pelvic floor ventral to vagina (female) or rectum (male). Its purpose is to collect and keep urine and to allow controlled urine excretion on purpose. The inside is lined by a layer of transitional epithelium. The bladder is connected via the ureters to the kidneys and on the bottom to the urethra. Maximum bladder filling volume of humans can vary approximately from 500 to 1000ml.

About 7 – 21% of patients receiving radiotherapy in the pelvic region develop lower urinary tract symptoms (LUTS) [52, 53]. Approximately 9% of these patients suffer from haematuria due to radiogenic cystitis. First symptoms of radiation damages by means of an acute tissue reaction usually occur 4 to 6 weeks after irradiation because of the slow regeneration of the transitional epithelium. Severity correlates with the applied dose and fractionation. Classifications (grading) of severity of adverse effects can be taken from table 2.1.

Bowel, Sigmoid, Rectum:

The bowel is an elastic, hollow, muscular tube and consists of small bowel and large bowel. The small bowel is about 6 to 7 meters long and provides an internal surface lined by mucosa of $30m^2$ for absorption of nutrients. Muscle layers allow peristaltic contractions to transport the bolus.

The large bowel is with 1.5 meters way shorter. Its main purpose is to absorb water through

Graduation	gastrointestinal tract	genitourinary tract
Grade 1	increased bowel movements without the need for medication, minor blood or mucus discharge	microhematuria, LUTS without need of medication
Grade 2	diarrhea with need for oral medication, abdominal cramping, mucus and temporary blood excretion without need of pads	moderate urinary frequency (<1/h), occasional hematuria, numerous telangiectases
Grade 3	diarrhea with need for pads or par-enteral substitution, stenoses requiring surgery, severe bleeding requiring transfusions	urinary frequency (>1/h), severe dysuria, hematuria frequent, bladder capacity of less than 150 ml
Grade 4	perforations, fistulae, life-threatening bleeding, necroses	perforations, fistulae, severe hemorrhagic cystitis, bladder capacity of less than 100 ml
Grade 5	each fatal complication	each fatal complication

Table 2.1: Late adverse effects of radiotherapy: Classification after Radiation Therapy Oncology Group (RTOG)

its about $2m^2$ large mucosa into the bloodstream. Especially the last sections of the large bowel are of special interest during planning, because they are closest to the target volume: the sigmoid flexure (or sigmoid colon) and the rectum. The name "sigmoid" is given by its shape and means S-shaped. "Rectum" means straight and as this name indicates it is the straight, final section of the bowel and about 12cm long. It acts as a temporary storage site for feces.

Almost all patients undergoing radiation to the abdomen, pelvis, or rectum will show signs of acute enteritis, but only 5 to 15% of them will develop chronic problems [54]. Patients suffering from acute enteritis may complain of nausea, abdominal cramping, tenesmus and diarrhea. Acute enteritis symptoms usually resolve 2 to 3 weeks after the completion of treatment, and the mucosa may appear nearly normal. Diarrhea (any grade) occurs in 20 to 49% of patients receiving pelvic radiotherapy.

Grading of severity of adverse effects caused by irradiation of the mentioned regions are shown in table 2.1.

Uterus (=CTVP):

The uterus is a muscular, fist-sized organ that is part of the female reproductive system. Within the uterus the fetus develops during gestation. Its position is inside the pelvis immediately dorsal to the urinary bladder and ventral to the rectum. It can be anatomically subdivided into fundus (top), corpus (middle) and cervix (bottom), which opens into the vagina. On both sides of the fundus an ovary is connected to it via the fallopian tube or oviduct.

Histologically its layers can be segmented into endometrium, myometrium (smooth muscle layer) and perimetrium (connective tissue) from inside to outside.

There are many different kinds of uterine cancers and even more subtypes. The most abundant cancer types are the endometrial carcinoma arising from the uterine lining (endometrium), cervical cancer originating from the transformation zone of the cervix and uterine sarcomas, which are most commonly leiomyosarcomas ("leio"=smooth, "myo"=muscle). Worldwide, cervical cancer is both the fourth most common cause of cancer and the fourth most common cause of death from cancer in women [55]. Figure 2.4 gives an overview of the various cervical cancer stages according to the cancer research UK (CRUK).

Patients included in this study suffered from stage IA, IB or IIA cervical cancer. It is very hard to give an estimation of the microscopic tumor spread, so in external beam radiotherapy usually the whole organ and neighboring structures including lymph nodes are defined as clinical target volume (see CTVP and CTVN definition of subsection 2.2).

2.4 *Monaco*[®] Planning System

Monaco[®] (Elekta/CMS, St.Louis, USA) is a commercially available complete IMRT treatment planning software. Comprehensive contouring and plan review tools are used to support the IMRT planning and evaluation process. It allows the application of biological cost functions and physical dose-volume constraints for treatment plan optimization, like the ones introduced in subsection 2.4.3. *Monaco*[®] uses a twofold optimization process composed of a fluence optimization in the first and a MLC segment weight and shape optimization in the second step. The dose distribution is preliminary determined via a so called finite size pencil beam algorithm (FSPB) and later on recalculated with either again FSPB or Monte Carlo (MC) simulation. It is essential that the correct electron density is calculated from the CT data.

The FSPB algorithm is a fast and accurate algorithm designed for IMRT optimization but has design limitations. Leaf transmission, MLC leaf details and dose distributions at prominent tissue inhomogeneities can't be modeled precisely. Therefore in this thesis MC was the chosen calculation algorithm for the second optimization step.

2.4.1 Principles of Pencil Beam Calculation

The pencil beam approach is a model-based algorithm that uses a convolution method. It is suited to model intensity-modulated radiation therapy, where the incident fluence is modulated over the field and as described in [1, 2]. This approach is based on a pencil made of the total energy deposited at a distance. To characterize this energy a pencil beam convolution kernel K_{PB} is introduced. It represents the energy distribution released from the pencil beam and normalized to unit fluence at the penetration point on the patient surface. The transport

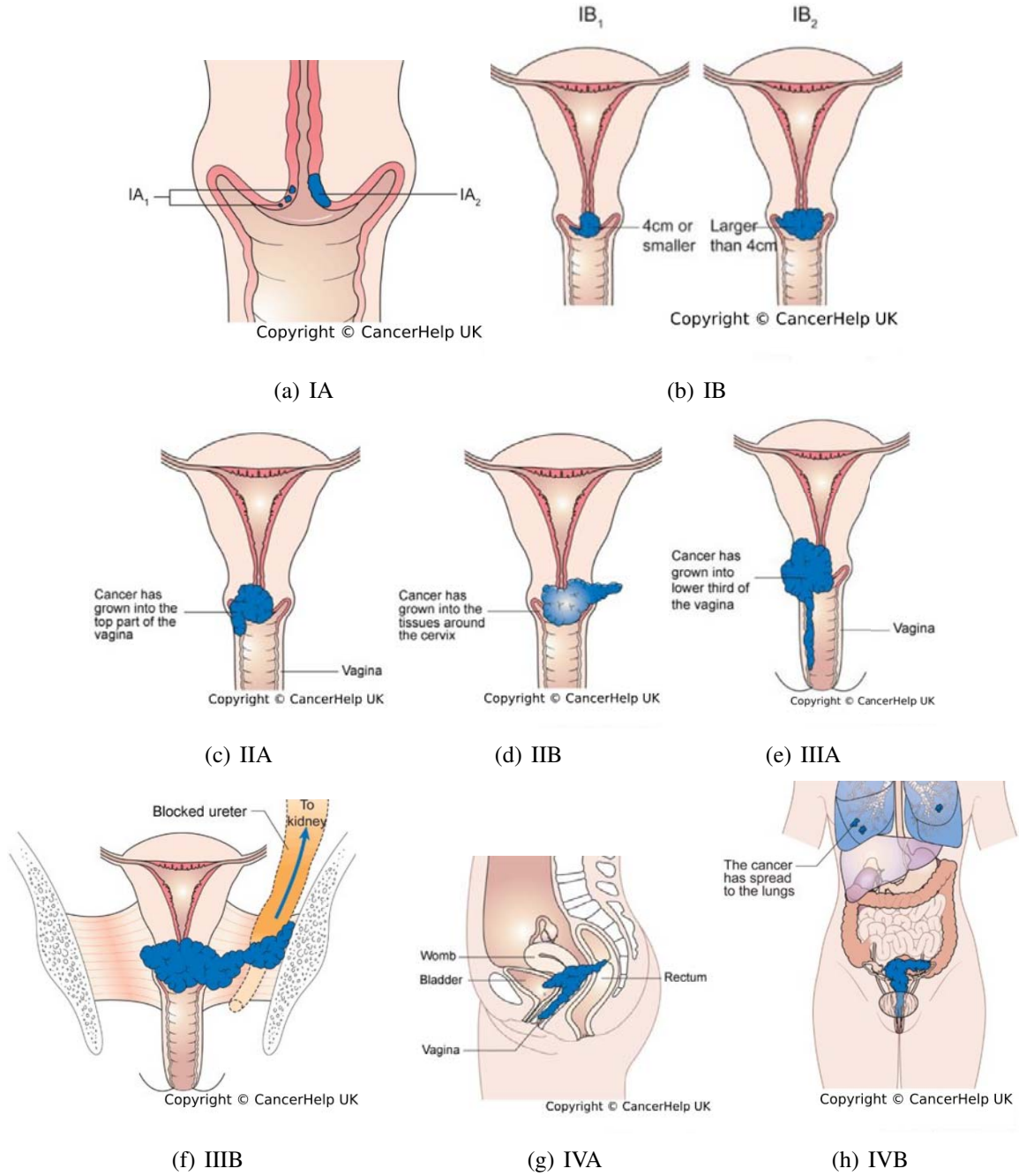


Figure 2.4: Visualization of the staging criteria for cervical cancer [56]. A common complication of stage IIIB is an occlusion of a ureter.

of primary photons, scattered photons and secondary electrons emerging from the primary photon interaction are separately considered in the convolution equation. The dose at a given point (x,y,z) is given in equations 2.1 and 2.2, cf. [1].

$$D(x,y,z) = \iint \frac{\mu}{\rho} \Psi_P(x',y') K_{PB}(x-x',y-y',z) dx' dy' \quad (2.1)$$

$$D(x,y,z) = \iint T_P(x',y') K_{PB}(x-x',y-y',z) dx' dy' \quad (2.2)$$

where the 2D integration is restricted to the field area and with

$$\begin{aligned}\Psi_p(x', y') &= \text{primary photon energy fluence at point } (x', y') \\ T_p(x', y') &= \text{total energy released per unit mass (terma)} \\ \frac{\mu}{\rho} &= \text{mass attenuation coefficient for medium} \\ K_{PB}(x - x', y - y', z) &= \text{value of the convolution kernel at } (x, y, z)\end{aligned}$$

The convolution kernel can be represented by a matrix of dose distribution deposited by scattered photons and secondary electrons originating at the primary photon interaction site. It can be obtained by calculation or direct measurement.

2.4.2 Monte Carlo Dose Calculation Algorithm

The main mathematical problem to be solved in dosimetry is the Boltzmann transport equation (BTE) that directly employs the fundamental microscopic physical laws of particle interactions and describes the trajectories of particles adequately [57]. The BTE is given in equation 2.3.

$$\left[\frac{\partial}{\partial s} + \frac{p}{|p|} \frac{\partial}{\partial x} + \underbrace{\mu(x, p)}_{\text{total macroscopic cross section}} \right] \psi(x, p, s) = \int dp' \underbrace{\mu(x, p, p')}_{\text{macr. differential scattering cross section}} \psi(x', p', s) \quad (2.3)$$

, where s is the path length, p the momentum and x the position of the particle.

$\frac{p}{|p|} \frac{\partial}{\partial x}$ is a directional derivative.

$\psi(x, p, s)$ is the probability of the presence of a particle at position x with momentum p and path length s .

The macroscopic differential scattering cross section (probability per unit length) describes scattering from momentum p to p' at location x .

The Monte Carlo method provides a numerical solution to this equation [58, 59] as it statistically reproduces the individual particle tracks by using the scattering and absorption cross-sections of the various particles and atoms of the irradiated matter. Macroscopic characteristics of the radiation field are computed as average over all individual microscopic simulations. To understand the principles of Monte Carlo simulations it is important to explain the Central Limit Theorem.

As part of the probability theory the *Central Limit Theorem (CLT)* states that the Monte Carlo estimator $\langle x \rangle$ for the arithmetic mean \bar{x} of a sufficiently large number N of particle histories simulated as independent random variables, each with a well-defined expected value $E(x)$ and well-defined and finite variance σ_x^2 can get arbitrarily close to \bar{x} (for energies from 1 keV up to 50 MeV [60]). According to the CLT, the distribution of $\langle x \rangle$ is Gaussian and

characterized by a variance $\sigma_{\langle x \rangle}^2$. Therefore the CLT predicts that if $N \rightarrow \infty \Rightarrow \sigma_{\langle x \rangle}^2 \rightarrow 0$. This limiting result is also proven by the Strong Law of Large Numbers [60]. In other words, the more particles are going to be simulated, the more reliable and accurate MC simulation will get.

Regarding this, we can make the following considerations:

Any human being undergoing radiotherapy has a mean Z of 7 to 8 with 65% of mass being oxygen (Z=8), 18% carbon (Z=6), 10% hydrogen (Z=1) and 3% nitrogen (Z=7) as the most abundant elements in the human body. This means it can be seen as low-Z-material where the photon's interaction distances in the energy range 10 keV to 40 MeV are of the order of 20cm [1][chapter 5.3]. With an interaction rate this low, it is with modest computational resources feasible to simulate hundreds of millions of particle histories considering only photon-transport. Consequently the accuracy of the MC simulation in human tissue is high and fits clinical requirements.

According to the *Handbook of Radiotherapy - Theory and Practice* [1] the photon and electron interaction processes that should be modelled by a Monte Carlo code for applications in radiotherapy and dosimetry are:

- Pair production in the nuclear and atomic fields
- Compton scattering from atomic electrons (=incoherent scattering)
- Photoelectric absorption and photoelectron production
- Rayleigh scattering from atomic and molecular fields (=coherent scattering)
- Møller scattering of electrons from atomic electrons
- Bhabha scattering of positrons from atomic electrons
- Bremsstrahlung photon creation in the nuclear and atomic fields
- Positron annihilation with atomic electrons
- Elastic scattering of electrons and positrons from nuclei
- Excitation of atoms and molecules by electrons and positrons

Figure 2.5 shows a flow chart for a photon MC simulation.

The particle paths are simulated until the whole energy is absorbed or the particles have left the region of interest (ROI). Figure 2.6 gives exemplarily a possible history of an incident photon in a MC simulation.

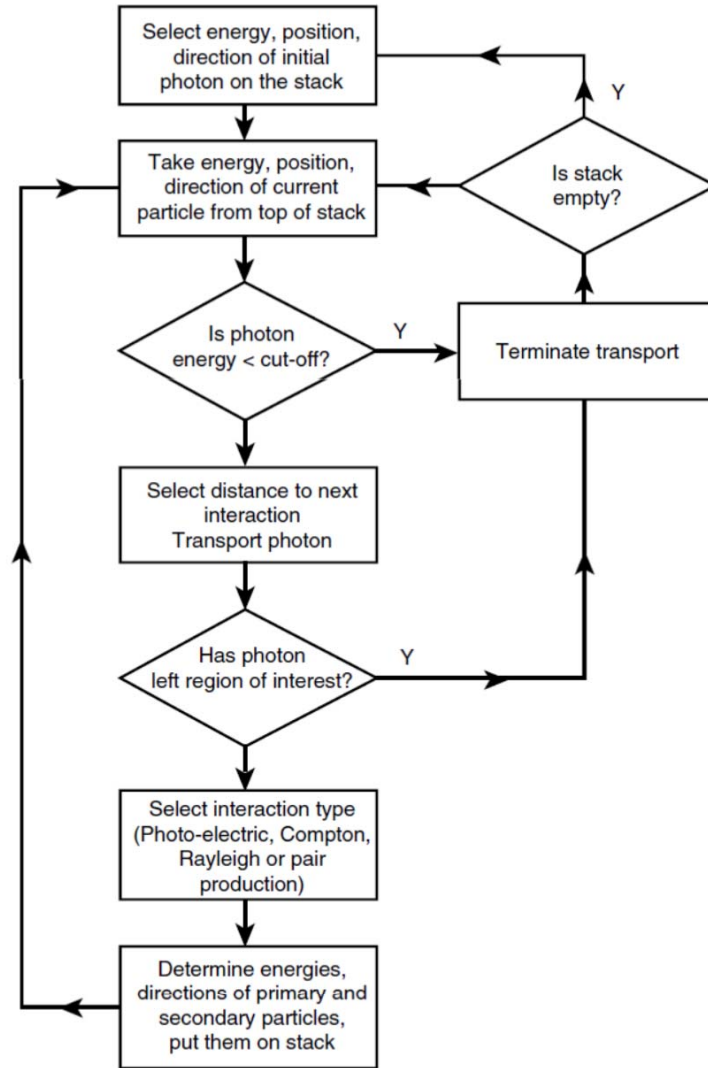


Figure 2.5: Flow diagram showing the essential steps in the Monte-Carlo transport of photons (excluding electron-transport) [1][Part A, Chapter 5.3]

The incident photon undergoes a Compton scattering, repelling an electron. After that a Rayleigh scattering event occurs, changing the photon direction. Another particle interaction lowers the energy of the photon to a value below the cut-off energy. Focusing back onto the Compton-electron we can see that it produces bremsstrahlung before leaving the region of interest. The new photon undergoes shortly afterwards a pair production where the electron again escapes the ROI. The positron is being annihilated producing two photons, one escaping, the other losing energy in another interaction process and falling below the cut-off energy.

Monte Carlo algorithms are most useful when it is difficult or impossible to use other mathematical methods. Moreover their provided numerical solutions have higher accuracy due to the stochastic approach compared with other mathematical approximation models. If one

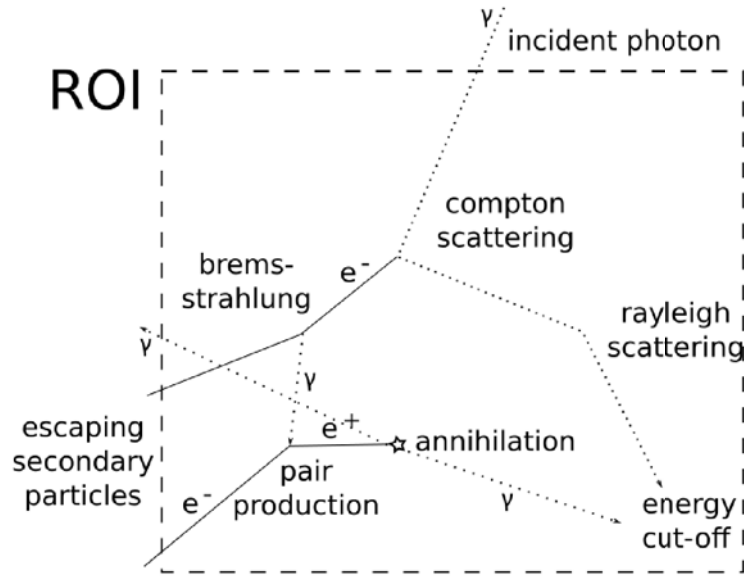


Figure 2.6: Possible photon history and particle transport in MC simulation. Dashed lines represent photon paths, while solid lines give the electron and positron paths.

knows the governing physical laws and particle transport mechanisms and has access to sufficient computing resources, the answer to the dose deposition question may be computed. This confluence of theory and computational ability are responsible for the rapid increase in the use of the MC-method in radiotherapy and dosimetric applications and reason that it is a vital element of the standard toolbox of the medical physicists, especially in research.

2.4.3 Cost Functions

The next subsections show details of selected cost functions and their parameters provided in *Monaco*[®].

Target EUD:

The concept of equivalent uniform dose (EUD) assumes that any two dose-distributions are assumed to be equivalent if they cause the same radiobiological effect on tissue independent of their homogeneity. The Target EUD is a biological cost function available in *Monaco*[®] and handled as an objective. It is the primary cost function for targets. Moreover, the field size is automatically formed to fit the target volume for each beam or sequence.

For all patients the first adaptable parameter for the Target EUD, the isoconstraint, was set to 45Gy, which represents the prescription (see also section 2.9). The second parameter that can be adapted is the cell sensitivity and has an impact on the dose distribution with respect to cold spots. In this thesis its value was set to 0.9 in all cases. The dependence of cell sensitivity and the penalty on cold spots is depicted in figure 2.7.

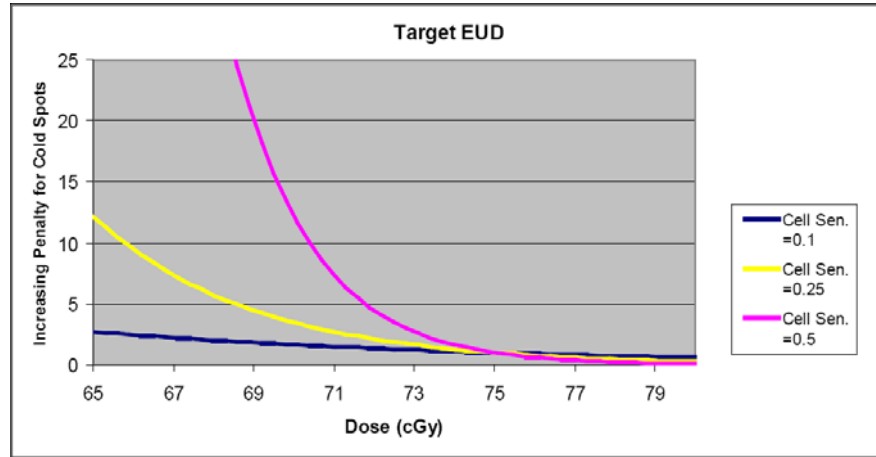


Figure 2.7: **Penalty curves:** cell sensitivities are shown for the values 0.1, 0.25 and 0.5 [61]

Target Penalty:

This physical cost function is the "objective" version of the Quadratic Underdose constraint for targets, which works analogous to the Quadratic Overdose cost function (see following paragraph) but implements a quadratic penalty for under-dosage instead of over-dosage. The isoeffect is a DVH based physical parameter. The Target Penalty is a quadratic penalty which starts at the threshold dose. We can configure the dose and reference volume. This is a non-EUD based objective and consequently does not add hot spots to the target to compensate for cold spots. As a result, it produces steeper dose gradients after target threshold doses are met. Either Target EUD or Target Penalty or both must be used as target objective in the prescription.

Quadratic Overdose:

This physical cost function represents a constraint that can be used with both targets and OAR to limit high doses. It was the most frequent applied one in the Monaco prescription (see section 2.9). The quadratic overdose cost function requires as first parameter the maximum dose, beyond which a penalty occurs. The second parameter, the isoconstraint, is the root mean square (RMS) dose excess. This represents the amount of deviation of the prescription that is accepted. The root mean square of a set of values is determined using equation 2.4.

$$RMS = \sqrt{\frac{\sum D^2}{n}} \quad (2.4)$$

with D being the voxel dose in excess of the maximum dose and n the total number of voxels. Only dose values above the maximum dose are considered.

The most frequent application of the Quadratic Overdose is in combination with the Target EUD to prevent hot spots. Without this dose-limiting cost function, the Target EUD objec-

tive would push the dose far above the prescribed value. To prevent this, the maximum dose should be set to the prescribed dose, and the RMS dose excess to a moderate value.

Serial:

This biological cost function is a constraint designed for serial OARs. It takes into account that the functional units of the organ act as a chain. It applies large penalties for hot spots even if they are small in volume. The first required parameter is the power law exponent (k) volume-effect parameter. In general, when a large k value is used, there is less tolerance for excessive damage to small volumes of the assigned structure. In this case, low dose volumes receive a very small weight relative to high dose volumes. Figure 2.8 illustrates the changes in the penalty or weight of a dose value in the overall EUD calculation for various k values.

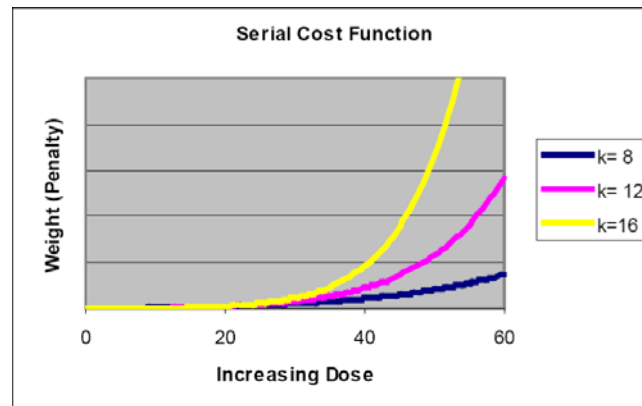


Figure 2.8: Serial penalty curves: k values are set to 8, 12 and 16 [61]

The k value defines the complication model that is applied to the tissue of the selected structure. The second parameter, the isoconstraint, is the EUD. Here the value is similar to an acceptable maximum dose when the k value is large and is equivalent to the mean dose when the k value is equal to 1.

Parallel:

This biological cost function is the first choice as constraint for parallel OARs. Some organs tolerate very high dose values in small sub-volumes, as long as the rest of the organ is spared. That means it loses its function if too many sub-volumes are damaged.

This cost function requires three parameters. The first parameter is the EUD which represents the dose that is only just acceptable for most of the structure and at which a clear dose effect can be observed. E.g. for the lung, this dose is about 20 Gy. Irradiating an organ homogeneously with the reference dose leads to a destruction of 50% of its volume. The second parameter is the isoconstraint, which is the mean organ damage to the structure in percent. The third parameter is the power law exponent (k). Analogous to the k -value of the serial cost function this value changes the shape of the dose response curve and determines

how strong the structure responds to the entered reference dose and mean organ damage values. A higher k -value translates to a steep dose response that often leads to into a pronounced kink in the DVH.

Figure 2.9 illustrates the shape of the cost function curve for different values.

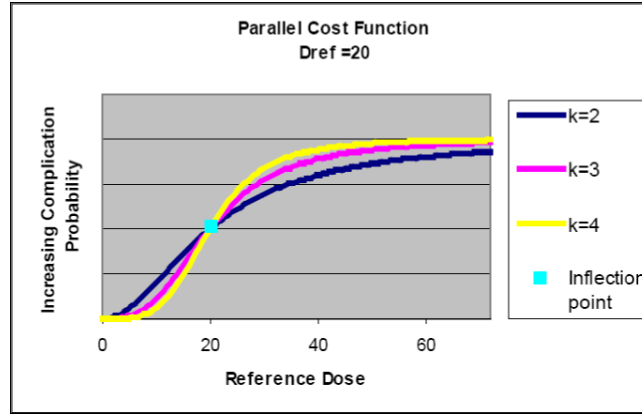


Figure 2.9: Parallel complication curves: k values are shown for 2, 3 and 4. The inflection point is marked. [61]

In figure 2.10 the effects on DVHs of applying serial and parallel cost functions to a structure are schematically depicted side by side.

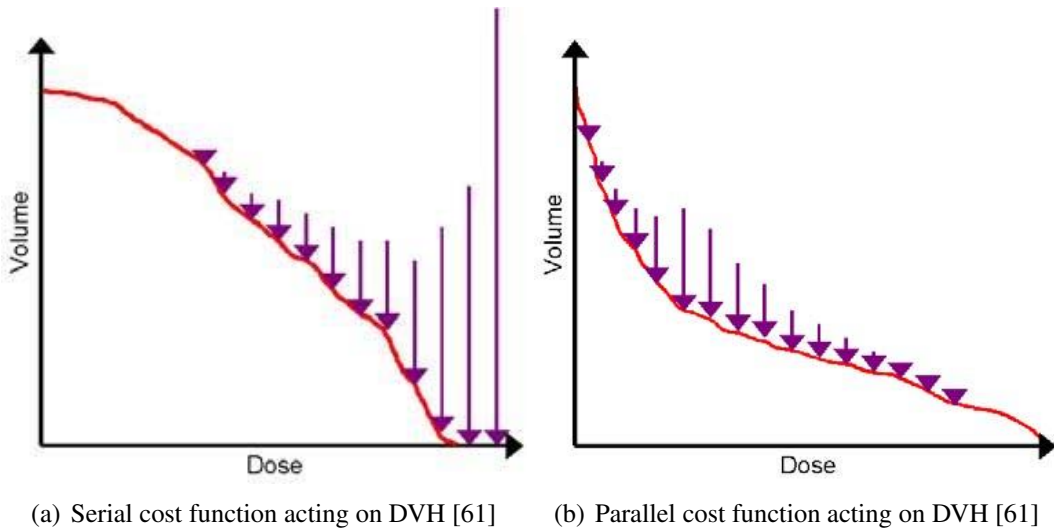


Figure 2.10: Effects of serial and parallel cost functions on a DVH: The length of the arrows represent the relative impact of the cost function on the various points of the DVH.

Of course it is possible to apply more than just one cost function to a structure (see subsection 2.9).

For the case of overlapping organ structures, they should be listed (layered) in the prescription in order of their importance so that voxels are prioritized and defined appropriately. The

layering order determines how the optimizer treats the voxels in the overlapping volume. The structure that is listed higher in the layering order "owns" the voxels in this region even if there is no cost function assigned to it in the prescription. Figure 2.11 illustrates examples of layering order applied to two overlapping structures. These voxel priorities represent the default behavior but can be overridden by individual cost functions with an additional parameter.

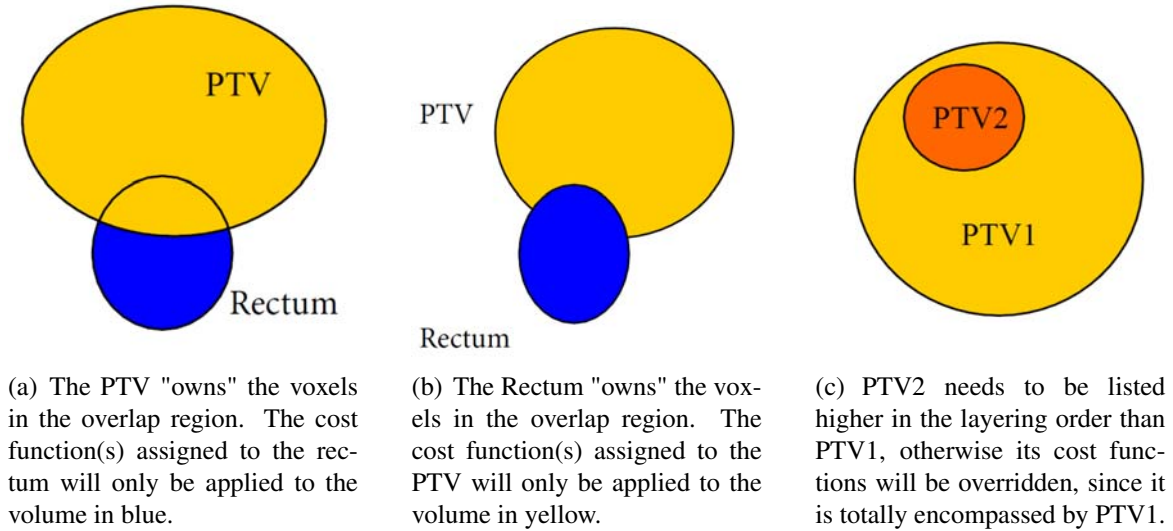


Figure 2.11: Structure layering of rectum and PTV or two different PTVs. [61]

Care should be taken that the order of overlap does not cause insolvable contradictions in the constraint list. The voxels can also be assigned completely to one structure with aid of the structure properties. The structure definition tools give the opportunity to define voxel priorities and physical properties for each structure in the prescription. In other words, one can determine which voxels a cost function will be applied to within a selected structure.

2.5 Dose Volume Histograms

For interpretation of treatment plans it is helpful to put the 3D dose distribution information to a dose volume histogram (DVH), which shows the dose within a specifically defined volume. This makes it easier to summarize and analyze the 3D data. The most commonly used DVHs are cumulative dose volume frequency distributions. They plot the percentage of volume of a structure receiving a dose equal to or greater than a given dose against dose. For better comparability of many treatment plans for different patients it may help to choose some dosimetric or volumetric values and compare the corresponding values on the DVHs.

- D_{max} corresponds to the maximum dose any voxel of the structure receives.

- D_{mean} analogous depicts the mean dose, that is to say the sum of the doses assigned to each voxel divided by the total number of voxels.
- $D_{x\%}$ stands for the dose that x% of the organ receives.
- V_{xGy} represents the volume of the organ in % or ccm that is receiving a minimum of x Gy.

Figure 2.12 will clarify these relations and gives a sketch of a standard DVH.

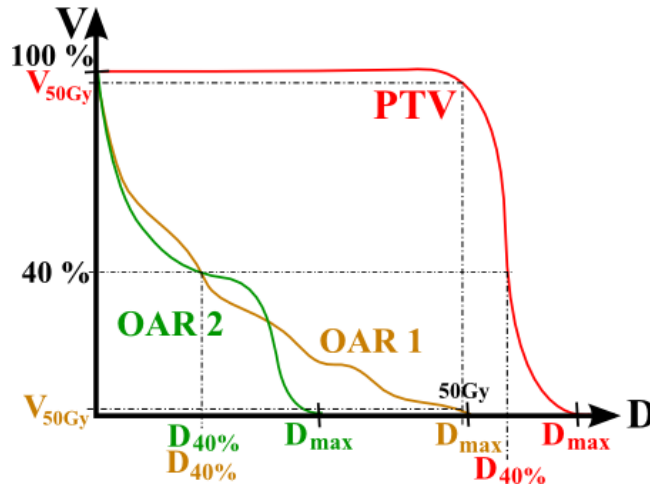


Figure 2.12: DVH-concept: The listed dose and volume values, except for the D_{mean} , are exemplarily plotted.

The main drawback of DVHs is the loss of spatial information. Therefore evaluation of treatment plans should always use other methods too, like observation of isodose curves.

2.6 Planning Strategies

2.6.1 Motion Model / "Plan of the Day"-Approach

Traditionally, radiotherapy of cervical cancer has been based on "rigid" treatment plans, which do not account for organ movement due to e.g. varying bladder filling conditions. This means that treatment planning was based on one snapshot imaging data set of the patients anatomy - the planning-CT. Bondar et al [35, 42, 43] have developed a strategy for individualized nonadaptive and online-adaptive treatment planning based on a pretreatment established motion model for the highly deformable target volume in cervical cancer patients. This motion model is used in this thesis as approach for the mover patients and is therefore presented in the following. Figure 2.13 shows the various dislocation- and deformation-graduations of Uterus/CTV correlating with the bladder filling volume.

If the structures are overlayed from empty to medium filled and from medium filled to full bladder we obtain CTVs like they are presented in figure 2.14.

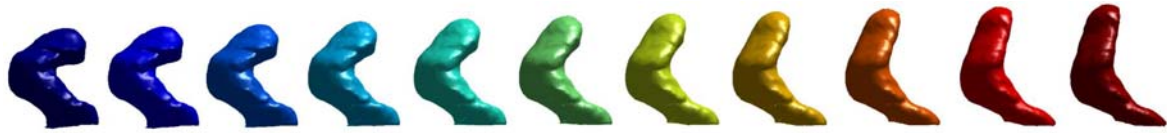


Figure 2.13: Deformation of CTV and dislocation of top of uterus in a mover-patient caused by bladder filling variations [42]. Lowest correlated bladder volume on the left, maximum on the right.

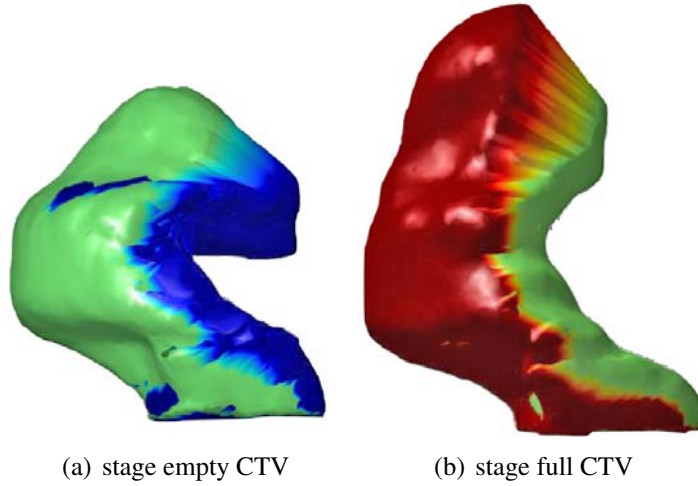


Figure 2.14: CTVs constructed via a motion model [43].

Our method depends on an interpolated intermediate structure from the data of full and empty bladder scan. By overlaying full with intermediate or intermediate with empty CTV we obtain full and empty stage CTV. The needed intermediate interpolated contours of the CTVs have to be generated by use of an application that fulfills also the tasks of data transfer and data processing. Such an application is not commercially available and was developed within the scope of this thesis (see section 3.1). Adding a safety margin of 1cm results in the needed corresponding PTVs. The full stage PTV should encompass any possible CTV-position that correlates with any bladder volume lying in the range from medium filled to full bladder. For the empty stage PTV the situation is analogous. Two different plans for these two PTVs are generated for each patient that is categorized as mover. This 2-stages-approach gives in the clinic the possibility to decide which plan to deliver for each fraction individually just by visual check of the current patient anatomy via the CBCT scan and by selecting the appropriate treatment plan. This is why this method is also called "plan of the day"-approach (PotD). In order to execute this visual check correctly, it is necessary to perform an image registration of obtained CBCT with bony anatomy of the planning CT first.

In future clinical implementation also a back-up plan will be created, by fusing full and empty stage PTV with each other to account for uncertainties in CTV position due to lacking image quality of the CBCT.

2.6.2 Motion Robust Plan

For the patients categorized as non-movers a motion robust plan is going to be generated following a similar attempt. Also for this plan structures are overlayed to obtain the motion robust PTV, but in this case no interpolated intermediate contour is needed. Just fusing the two CTVs of the full and empty bladder scans and adding a safety margin of 1cm results in the motion robust PTV.

The steps of these two planning strategies for movers and non-movers are essential building blocks of the future clinical workflow and presented in figure 2.15.

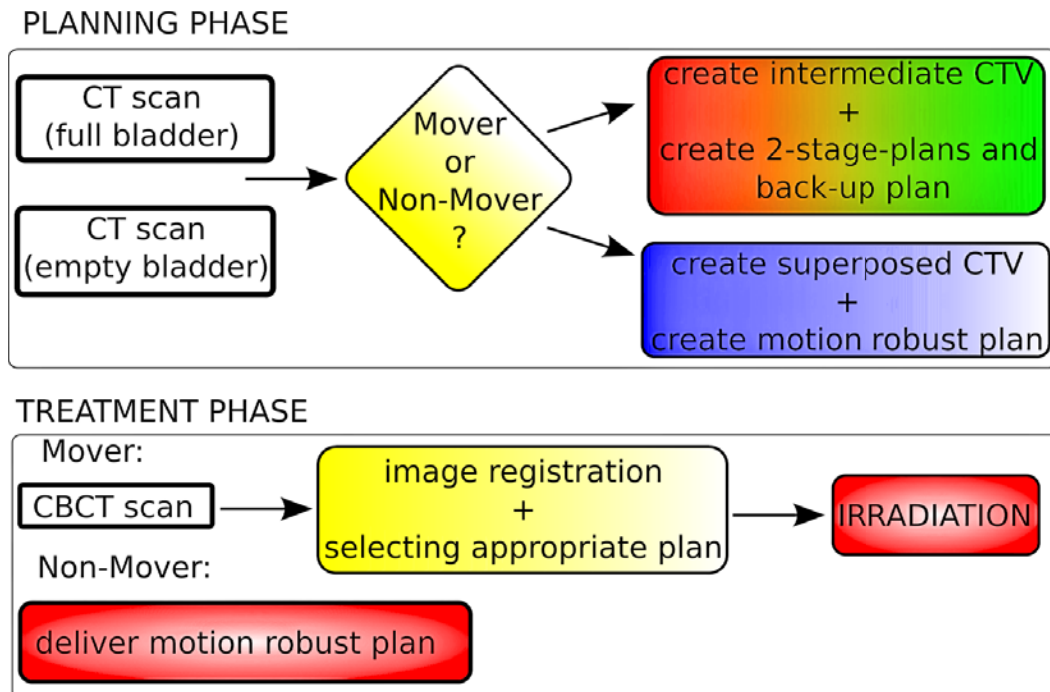


Figure 2.15: Schematic diagram of the future clinical workflow for PotD based ART of cervix cancer.

The main difference to what has been done in this thesis is the used patient data. In the future not only one pretreatment planning-CT but two will be gathered. The first with the patient having a full bladder and the second after the patient has emptied her bladder. These two scans will then be used to classify the patient and decide which planning strategy to pursue. In contrast, for this thesis the empty bladder scan was selected from one of the available CT-scans that were gathered during the course of the treatment. Not all available patients had enough variation in bladder volume and uterus position to be included in this study.

2.6.3 Non-ART Plan

For comparison, the original planning method (denoted as "non-ART" in the following) was also simulated and recalculated with VMAT delivery technique. Please remind that

this method is only based on the planning-CT and its correlated organ constellation, the margin that was used only accounted for set-up uncertainties and does not account for any internal organ movements. A clinical cervix cancer prescription plan optimization template was available, could be borrowed for this purpose and was slightly adapted (e.g. two PTVs instead of one).

PotD and motion robust plans of all 3 patients were designed analogous to the explanation above for a smaller margin of 0.5cm for PTVP and 0.2cm for PTVN too.

2.7 Planning Aims / Prescription

During the treatment planning process, some rules, constraints and the prescription had to be considered. As in subsection 2.1 mentioned, the clinical prescription for the PTV in cervical cancer cases is 45Gy, if combined with a follow-up brachytherapy. We set our aim to cover at least 95% of this volume with not less than 95% of the prescribed dose, thus 42.75Gy. $V_{95\%}$ of CTVP and CTVN is therefore going to be presented in the results. The upper limit was set to 110% of the prescribed dose to avoid overkill, thus 49.5Gy being the intended maximum dose. This is already a loosened constraint, since the ICRU recommends 107% being the maximum limit in radiation therapy [9], but in clinical practice larger variations are widely used. On the other hand one can not emphasize enough how important it is to avoid cold spots in the target volume (see e.g. [62]). For fixed size of a cold spot the calculated values of TCP decrease rapidly with increasing degrees of cold dose even if its size is just 1% of the fractional volume. We decided to keep an eye on the D_{2ccm} instead of D_{max} of CTVP and CTVN because hotspots in a very small volume are likely to smear out during the treatment because of inter-fraction patient motion. Therefore they should not be considered as clinically relevant. However, the optimization is often steered by limits on D_{max} . Very local non relevant hotspots may then 'disturb' the optimization process.

In general the OARs explained in subsection 2.3 were taken into account during planning. This is why the following DVH-values are important and presented in the results: D_{2ccm} of sigmoid, rectum and bladder and D_{mean} of the latter and V_{40Gy} , V_{45Gy} , D_{200ccm} and D_{400ccm} of the bowel. For all OARs the principle of ALARA applies. ALARA is an acronym for "*as low as reasonable achievable*" and states that the dose to OARs should be lowered as far as possible while maintaining a reasonable PTV coverage and thus achieve reasonable TCP. Moreover we focused on the elimination of hotspots in the dose distribution. Large attention was paid to the bowel via setting constraints: 200ccm should receive less than 45Gy and 400ccm less than 40Gy. These constraints should ensure enough bowel sparing to reduce adverse side effects to a minimum. This explains why the mentioned DVH-values of the bowel were chosen to be presented in chapter 3. The ALARA concept was preserved via the applied costfunctions (see section 2.4.3 and 2.9). After the second calculation step

of Monaco their constraints were tightened while still maintaining a PTV-coverage of at least 95% volume receiving 95% prescribed dose. Converging to the "optimum"⁴ plan was possible by paying attention to weighting-values and relative impact of the cost functions. They can give an idea of how hard the TPS is working on each cost function and how large its influence on the whole treatment plan is.

2.8 Evaluation and Analyzing Methods

The overall evaluation of the planning strategies was possible by image registration of the bony anatomy of all available scans to the planning-CT and import of all related contour data sets to this one scan. Huddling all contour data together into the planning-CT scan made it hard to keep the overview during planning because of the large number of structures but gives the possibility to make any of the organ structures visible in the TPS in any direction of view, simultaneously with the dose distribution as well as in their DVH-curve for the designed plan. One has to emphasize that in contrast to this study, in the future clinical workflow only 2 CT-scans plus the current CBCT will be fused via image registration at maximum.

On one hand this approach enormously saved time by obtaining all DVH-values of all image data sets with one treatment plan calculation and made it easy to compare all the various bladder filling volumes and uterus positions, on the other hand consequently all treatment plans were calculated on the electron density distribution of the planning-CT although the delineated structures do not all fit exactly. Please read more about this issue in the section 4.3.

To evaluate and analyze this pilot study of 3 cervical cancer patients, the following questions were defined:

- Does the motion robust plan show any advantages over non-ART for the non-mover patients?
- Do inter-patient differences occur for the two non-mover patients?
- Is the PotD approach improving the dosimetric outcome for the mover patient compared to non-ART?
- Is reducing the CTV-PTV-margin dosimetrically reasonable?

These questions were investigated and analyzed in detail by comparing the selected DVH-values, DVH-curves and dose distributions that resulted from this study. As already mentioned, the D_{2ccm} of sigmoid, rectum and bladder and D_{mean} of the latter and V_{40Gy} , V_{45Gy} ,

⁴Please remind that there is no clear definition of an optimal treatment plan, but it is always a trade-off between maintaining target-coverage and sparing OARs.

D_{200ccm} and D_{400ccm} of the bowel were the selected DVH-values to examine. These values were visualized in boxplots for all three patients and all obtained treatment plans; in sum 11 treatment plans were created, as listed below:

- one non-ART plan for each of the three patients (only organ constellation of the planning CT was used for the planning)
- one motion robust plan for each non-mover patient
- one motion robust plan with decreased margins for each non-mover patient
- a stage empty plan for the mover patient
- a stage empty plan with decreased margins for the mover patient
- a stage full plan for the mover patient
- a stage full plan with decreased margins for the mover patient

The stage empty and stage full plans were not evaluated for all available imaging data sets but only for the appropriate ones. In sum 10 of the image data sets were assigned to the full stage plan, while the other 12 image data sets were simulated for the empty stage plan. The explicit attribution of the scans can be taken from table 2.2.

full	empty
CT0	FBCT1
FBCT2	FBCT4
FBCT3	FBCT6
FBCT5	CBCT2b
MR0	CBCT2c
CBCT1a	CBCT3b
CBCT1b	CBCT3c
CBCT2a	CBCT4a
CBCT3a	CBCT4b
CBCT4c	CBCT5a
	CBCT5b
	CBCT5c

Table 2.2: Attribution of the several available imaging data sets of patient 21. Numbers stand for the treatment week. Therefore planning-CT and MR are symbolized by 0.

The findings of the study are presented in the chapter 3 and summarized and discussed in chapter 4.

2.8.1 Clinical and Technical Requirements to an ART Interpolation Tool

The future clinical workflow of cervix cancer radiotherapy is going to consist in general of the following steps:

- obtaining the two planning CTs
- importing the CT scans into the TPS
- delineating the organ contours
- generating intermediate organ contours of the CTVs
- creating the necessary treatment plans
- exporting the treatment plans to the treatment machine

The step of creating new intermediate organ contours is not implemented in the TPS. Therefore the dicom-RT-file of the patients CT-scan has to be exported from the TPS, adapted in a suitable program tool and imported back again to the TPS in order to generate a new organ contour. Currently no commercial turnkey solutions are available to fulfill the tasks of data processing as well as data transfer. Such a tool should conserve the dicom standard of the file format to guarantee a successful import back to the TPS. Furthermore it should interpolate linearly and correctly between two given contour data point sets, according to the simplest mathematical model. It is important that the resulting organ contours are smooth and can be made visible in the TPS to allow a validation. In this thesis Matlab was chosen as basis for the development of such an interpolation tool called OrCA (Organ Contour Adaptor). Matlab community supplies some dicom-functions that are handy for reading, processing and saving dicom files and a package for continuous point drift simulations (CPD2). For more information about OrCA see section 3.1 or its program report in the appendix.

DICOM-Standard:

About 30 years ago, it was very difficult for anyone other than manufacturers of CT or MRT devices to decode the images that the machines generated. Additionally the interoperability of devices and systems from different manufacturers was not ensured. Based on these issues the development of a standard for handling, storing and transmitting information in medical imaging was initiated. Digital Imaging and Communications in Medicine (DICOM) was developed by the DICOM Standards Committee. It includes among others a file format definition for image and patient data. The defined data structure allows researchers from all over the world to develop and improve all kinds of useful program tools for image visualization and processing (e.g. diverse modifications and applications of 3Dslicer).

2.9 VMAT Settings, Monaco-Prescription

In contrast to the clinical plan that was delivered to the patients taking part in this study, VMAT-delivery method instead of 3D-CRT technique was chosen as delivery technique for dosimetric simulations. The plans simulate two full Linac-head rotations in the transverse plane of the patients, the isocenter being the center of the PTV. This situation is depicted in figure 2.16 which gives a 3D view of the anatomy of patient 21.

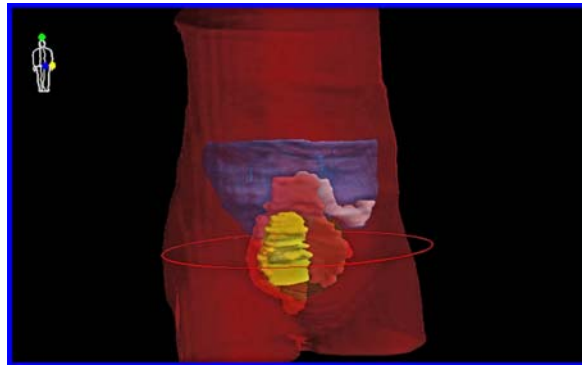


Figure 2.16: Anatomical 3D-view of patient 21 and her contoured organs. The red line symbolizes the rotation of the gantry during treatment.

The used cost functions are presented in figure 2.17.

PTVs are declared by both Target EUD and Target Penalty function in the TPS. All OARs have a serial cost function imposed to prevent high-dose regions in their volume. The many Quadratic Overdose cost functions make sure that the dose distribution is steep and smooth at the transition zone of target and OARs or normal body tissue. With the aid of the "RectumAir"-structure we ensured that no lower electron density than 0 occurs for the air in the rectum to prevent calculation errors and eliminate very low-density artifacts.







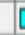
Structure	Cost Function	Enabled	Status	Manual	Weight	Reference Dose (Gy)	Multicriterial	Isoconstraint	Isoeffect	Relative Impact
	PTVCT0 ▶ Quadratic Overdose	<input checked="" type="checkbox"/>	On	<input checked="" type="checkbox"/>	2.21	46.500	<input checked="" type="checkbox"/>	0.400	0.400	+++
	Target EUD	<input checked="" type="checkbox"/>	On	<input checked="" type="checkbox"/>	1.00			45.000	45.254	
	Target Penalty	<input checked="" type="checkbox"/>	On	<input checked="" type="checkbox"/>	1.00			45.000	44.140	
	PTVNC0m0.5 ▶ Quadratic Overdose	<input checked="" type="checkbox"/>	On	<input checked="" type="checkbox"/>	8.05	46.500	<input checked="" type="checkbox"/>	0.400	0.403	+++
	Target EUD	<input checked="" type="checkbox"/>	On	<input checked="" type="checkbox"/>	1.00			45.000	43.712	
	Target Penalty	<input checked="" type="checkbox"/>	On	<input checked="" type="checkbox"/>	1.00			45.000	42.380	
	bowelbagCT0 ▶ Quadratic Overdose	<input checked="" type="checkbox"/>	On	<input checked="" type="checkbox"/>	0.01	45.000	<input checked="" type="checkbox"/>	0.250	0.147	
	Serial	<input checked="" type="checkbox"/>	On	<input checked="" type="checkbox"/>	0.04		<input checked="" type="checkbox"/>	30.000	29.701	+
	Quadratic Overdose	<input checked="" type="checkbox"/>	On	<input checked="" type="checkbox"/>	0.03	35.000	<input checked="" type="checkbox"/>	0.500	0.471	+
	sigmoidCT0 ▶ Quadratic Overdose	<input checked="" type="checkbox"/>	On	<input checked="" type="checkbox"/>	0.02	45.000	<input checked="" type="checkbox"/>	0.350	0.327	
	Serial	<input checked="" type="checkbox"/>	On	<input checked="" type="checkbox"/>	0.01		<input checked="" type="checkbox"/>	27.500	18.219	
	Serial	<input checked="" type="checkbox"/>	On	<input checked="" type="checkbox"/>	6.13		<input checked="" type="checkbox"/>	37.500	37.390	+++
	rectumCT0 ▶ Quadratic Overdose	<input checked="" type="checkbox"/>	On	<input checked="" type="checkbox"/>	0.88	45.000	<input checked="" type="checkbox"/>	0.250	0.249	+++
	Serial	<input checked="" type="checkbox"/>	On	<input checked="" type="checkbox"/>	0.01		<input checked="" type="checkbox"/>	40.000	37.336	
	Quadratic Overdose	<input checked="" type="checkbox"/>	On	<input checked="" type="checkbox"/>	0.01	46.000	<input checked="" type="checkbox"/>	0.500	0.362	
	Body ▶ Quadratic Overdose	<input checked="" type="checkbox"/>	On	<input checked="" type="checkbox"/>	1.56		<input checked="" type="checkbox"/>	25.000	24.800	+++
	Serial	<input checked="" type="checkbox"/>	On	<input checked="" type="checkbox"/>	0.22	40.000	<input checked="" type="checkbox"/>	0.250	0.222	++
	Quadratic Overdose	<input checked="" type="checkbox"/>	On	<input checked="" type="checkbox"/>	1.81	25.000	<input checked="" type="checkbox"/>	0.500	0.480	+++
	Quadratic Overdose	<input checked="" type="checkbox"/>	On	<input checked="" type="checkbox"/>	52.78	20.000	<input checked="" type="checkbox"/>	0.750	0.749	++++
	Conformality	<input checked="" type="checkbox"/>	On	<input checked="" type="checkbox"/>	0.05		<input checked="" type="checkbox"/>	0.85	0.71	+
	RectumAir ▶									

Figure 2.17: Monaco prescription of patient 21 (non-ART plan) showing the applied cost functions and their correlating parameters.

3 Results

The following sections present the developed ART interpolation tool OrCA as well as the findings of the pilot planning study that was performed as part of this MSc thesis project. The first section describes details about the dicom data structure OrCA uses, the interpolation process it is based on and the way the contour data is smoothed. Section 3.2 demonstrates the benefits of adapted treatment planning that were found in comparison with non-adapted treatment planning. The third section summarizes the findings of the the second part of the planning study, that focused on the question of the influence of decreasing the CTV-PTV margin. All presented values are rounded to integers, because the calculation accuracy is assumed to be in the range of $\pm 1\text{Gy}$ or $\pm 1\%$ in case of volumes.

3.1 Organ Contour Adaptor Tool - OrCA

OrCA is a MATLAB-based tool that was developed within the scope of this thesis and intended to support in the future clinical ART planning workflow of cervical cancer. It allows to generate intermediate contours of PTVP as well as bladder according to the current bladder volume. Its main purpose is to interpolate linearly between two extreme positions and/or filling states of patient's organ contours. These have to be loaded from two dicom-files beforehand. A intermediate contour is created by simply using 0.5 interpolation factor. It is up to the user whether a current contour according to the given min. and max. bladder volumes is created too. The registration of the two structures is based on the continuous point drift code package (CPD2)¹. The interpolated contour can be added to an existing dicom file chosen by the user. The newly generated file is a copy of the original file plus the new contour(s).

OrCA has been tested in a simulated clinical ART workflow for cervical cancer within the scope of a pilot planning study and proven to be both functional and useful. It fulfills the tasks of loading organ contours, downsampling, registering two organ contours as well as interpolating in between them, data processing, adapting the newly generated structure by means of a hull function, smoothing the resulting points of the slices automatically (or manually by the user) and saving the new dicom file, which contains the contour data and can

¹Coherent Point Drift (CPD) Matlab package (version 2.1).
Copyright (C) 2006-2009, Andriy Myronenko

be imported back to the TPS. OrCA gives the user the possibility to change the parameter of the hull function and therefore one can influence the adaption of the interpolated contour. Manual smoothing allows the user to adapt the number of breaks of the spline fit that is calculated for each slice, the center of coordinate transformation or to save the non-smoothed contour data points of particular slices. This is especially useful if the fit function does not work reasonable for a specific slice due to a too pronounced concaveness.

3.1.1 Datastructure

To add a new organ contour to the input dicom file, it is necessary to configure and to add new information to its metadata. Dicom files and especially dicom-RT-structure files contain many various and quite treelike branched metadata fields. The main modifications to the file occur in the 'ContourData' field containing the raw contour data in form of x, y and z coordinates of the point cloud that defines the new organ contour. Most TPS need the contour data in a slicewise manner with 4mm intervals (as it is in regular CT scans). ContourData consists of n fields called 'Items', where n equals the number of slices and each Item contains only points with consistent z coordinate. The points have to be ordered in a clockwise manner for correct illustration and composition of the contour in the TPS.

3.1.2 Interpolation

The above mentioned contour data has to be generated in the first place before the file can be saved. For this purpose the CPD2 code for point registration is used [63]. In a nutshell, CPD registers point cloud to point cloud and gives a vector of correspondences. Not every point has to be represented by another point in the second data set, making this method suitable for structures with an unequal number of points. Based on these correspondences, linear interpolation between the registered points can be performed. Downsampling is done for contour data that are larger than 200 points per slice in order to allow convenient calculation times. The newly generated point cloud that represents the interpolated organ contour needs to be processed in order to fit the data structure of dicom files. For this purpose a triangulated surface of the contour is created and "sliced" in 4mm z-intervals. The obtained point coordinates are then formatted and put in the needed Items.

Figure 3.1 shows the point clouds of full and empty bladder scan CTVp contours and the generated interpolated CTVp contour on the left and the triangulated surface of the latter on the right of patient 21.

3.1.3 Smoothing

For a smooth and clear contour depiction in the TPS the data from the newly generated Items have to be smoothed. The slice data is converted and transformed to polar coordinates where

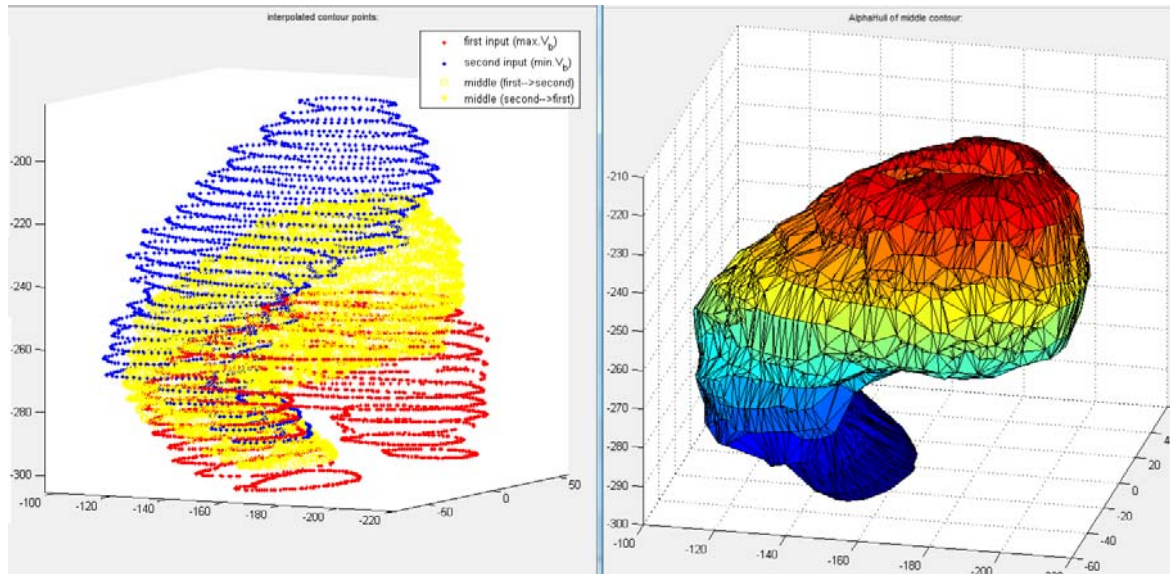


Figure 3.1: Point clouds of two input CTVP contours (red and blue) and interpolated middle CTVP contour (yellow). On the right its triangulated surface is shown.

the origin is set to the center of each contour slice. A number of points are read out from the applied fit-function and afterward transformed back to Cartesian coordinates and ordered in a clockwise manner. Figure 3.2 shows the user interface for adaption of the smoothing function.

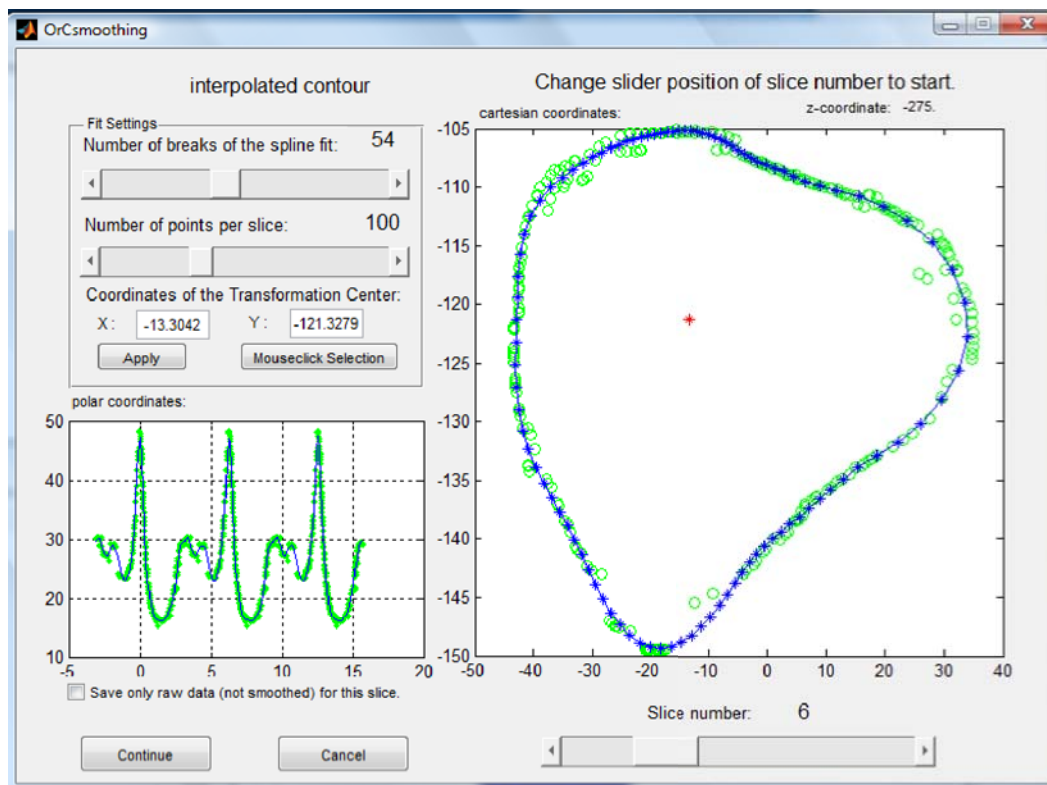


Figure 3.2: User interface of OrCSmoothing. blue x = smoothed points, blue curve = fit function, green o = raw data points

The large axis shows one slice of the new structure in cartesian coordinates, while the small axis shows the very same slice in polar coordinates. The red "*" indicates the actual center of transformation.

For a closer look at the mentioned steps and more details about the user interface of OrCA, please see its program report in the appendix.

3.2 Non-Adapted vs. Adapted Radiotherapeutic Treatment Planning

This section presents at first the results for the motion robust plans of the non-movers and secondly the data of the mover-patient with the PotD-approach.

3.2.1 Non-Movers

3.2.1.1 DVH-Values

The obtained PTV-coverages ($V_{95\%}$) for the planning-CT are presented in table 3.1. All plans fulfilled the objectives of $V_{95\%}$ of at least 95% of the prescribed dose of 45Gy. The D_{2ccm} were 49-50 Gy.

		non-ART	motion robust
P12	$V_{95\%}$ PTVP [%]	96	96
	$V_{95\%}$ PTVN [%]	95	95
P20	$V_{95\%}$ PTVP [%]	98	97
	$V_{95\%}$ PTVN [%]	96	96

Table 3.1: Planning PTV-coverages for patient 20 (P20) and patient 12 (P12).

The values of all imaging data (CBCTs, FBCTs, MR) from the different days of the treatment course were analyzed and compared to assess the influence of organ deformation. The results for the two treatment strategies (non-ART and motion robust) were obtained and the calculated mean values and standard deviations are presented. Performing a t-test showed which pairs of values differed statistically significantly. Significant but minor DVH-Value discrepancies of the results for patient 12 are the D_{2ccm} for CTVN and sigmoid. Only the D_{mean} of the bladder showed a much higher value for the motion robust plan. This can be explained by the larger target volume and a stronger bending of the PTV over the bladder. Moreover the bladder volume is on average smaller. The ART planning results for patient 20 showed just for two (of the in subsection 2.7 explained) observed DVH-values significant discrepancies to the non-adapted treatment plan: the $V_{95\%}$ of the CTVP and the D_{2ccm} of the rectum differed slightly. The explicit values can be taken from table 3.2.

(a) patient 12		
	non-ART	motion robust
D_{2ccm} CTVN [Gy]	50	49
D_{2ccm} sigmoid [Gy]	48 ± 1	47 ± 1
D_{mean} bladder [Gy]	32 ± 2	38 ± 3
(b) patient 20		
	non-ART	motion robust
$V_{95\%}$ CTVP [%]	99 ± 2	100
D_{2ccm} rectum [Gy]	45 ± 1	46 ± 1

Table 3.2: Statistically significant mean DVH value discrepancies of all fractions for both non-mover patients.

For patient 12 we observed an increase of mean bladder dose with the motion robust plan due to the smaller bladder volume and the larger PTV. Through the motion robust planning strategy an increase of the CTVP-coverage was obtained in patient 20.

All other discrepancies are in the size of the assumed computation accuracy and don't seem to be clinically significant, so they can be neglected.

All above mentioned values and also the insignificant data is depicted in the following box-plots for better visualization. The $V_{95\%}$ and D_{2ccm} of the CTVs are plotted in figure 3.3.

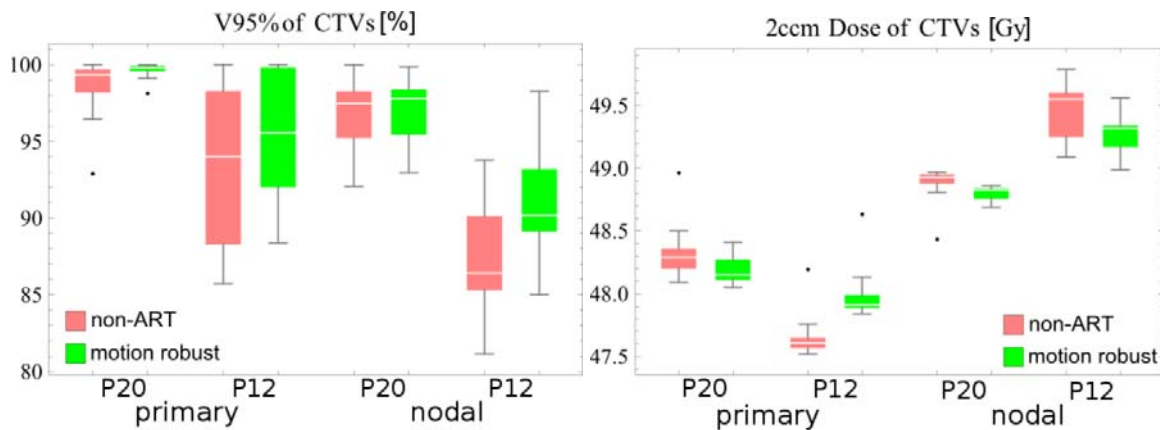


Figure 3.3: DVH value boxplots of the CTV data for patient 12 (P12) and 20 (P20).

In the left panel of figure 3.3 a grave discrepancy of the two non-mover patients can be observed in terms of CTV-coverage. The CTVP-coverage is quite bad in patient 12 with $V_{95\%}$ of $(94 \pm 5)\%$ (non-ART) or $V_{95\%}$ CTVP $(96 \pm 4)\%$ (motion robust). For comparison the respective mean values for patient 20 are approximately 4% higher and have a smaller standard deviation. The CTVN-coverage in patient 12 shows the same behavior and is even worse with a $V_{95\%}$ of $(89 \pm 6)\%$ (non-ART) or $(92 \pm 4)\%$ (motion robust). Again patient 20 shows superior mean DVH values that lie about 8% and 5% above these values, respectively. Moreover the standard deviation is by a factor 2 smaller. This is caused by the fact that P20 was really a non-mover and the uterus of P12 still moved quite a lot during the treatment.

It also moved in another direction during the treatment than was predicted by the motion model.

The D_{2ccm} of rectum, sigmoid and bladder can be seen in figure 3.4 in the top panel. The bottom panel shows the mean dose of the bladder and the D_{200ccm} and D_{400ccm} of the bowel, respectively.

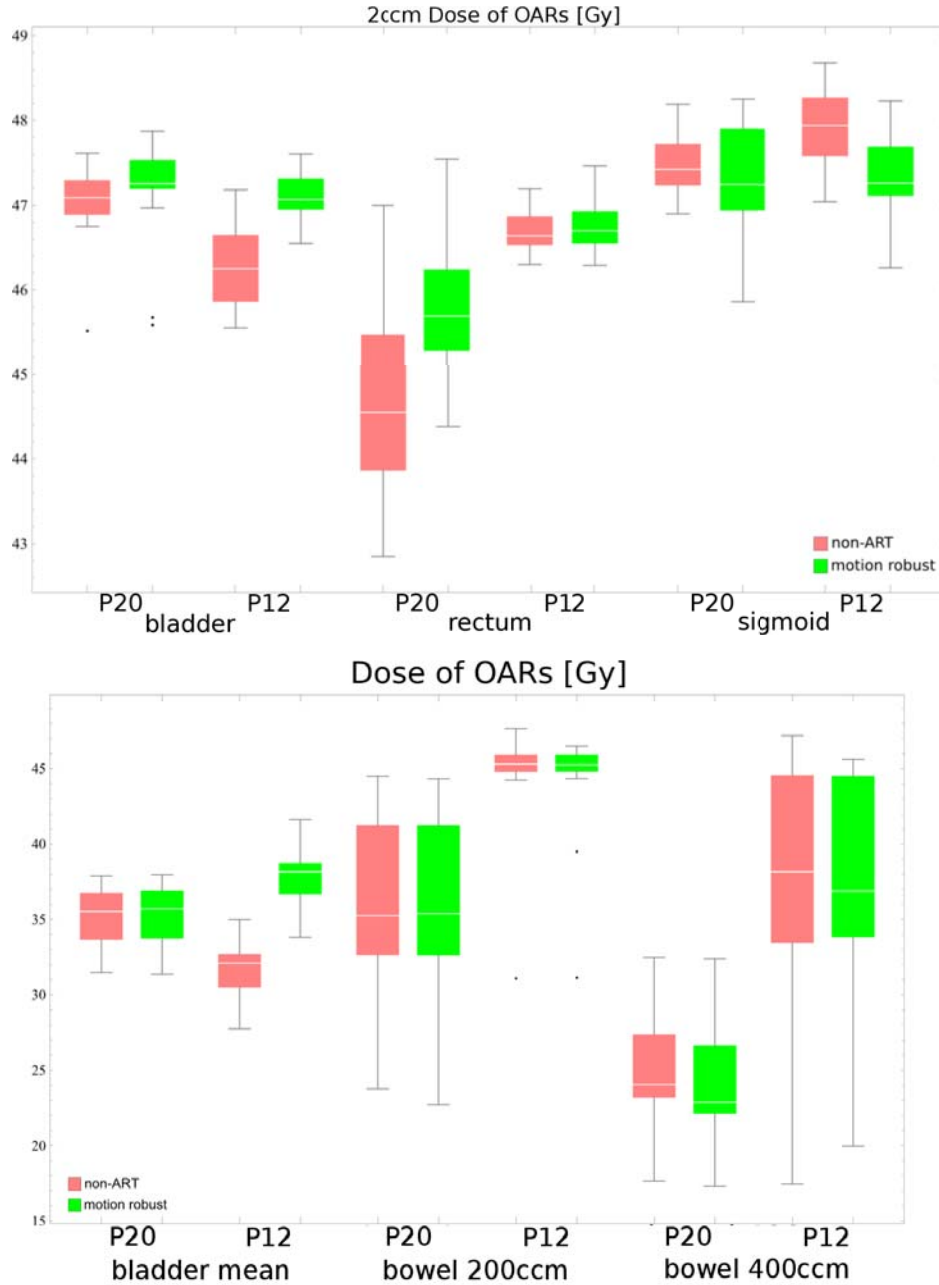


Figure 3.4: DVH value boxplots of the OAR data for patient 12 (P12) and 20 (P20).

The top panel of figure 3.4 shows no significant inter-patient-variations that were larger than the assumed accuracy of dose-calculation. In contrast, the bottom panel gives an idea of a higher bowel exposure of patient 12. The same holds for the corresponding V_{40Gy} and V_{45Gy} of the bowel that are shown in figure 3.5.

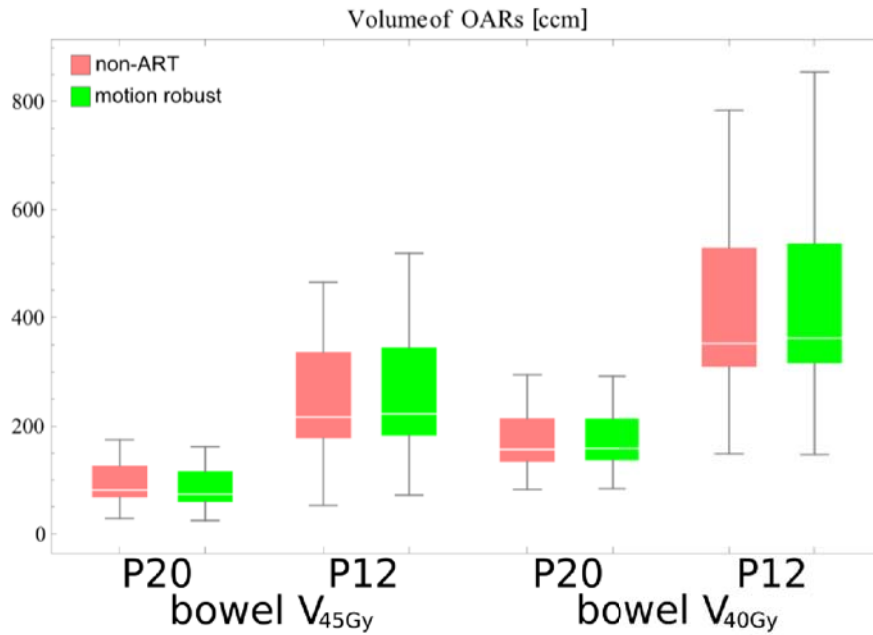


Figure 3.5: DVH value boxplots for V_{40Gy} and V_{45Gy} of bowel of patient 20 (P20) and 12 (P12).

3.2.1.2 DVH-Plots

To provide a better overview of the dose-volume correlations, figure 3.6 shows the DVHs of patient 20 and patient 12 for the two different plans with OAR-constellation and CTVs from the planning-CTs.

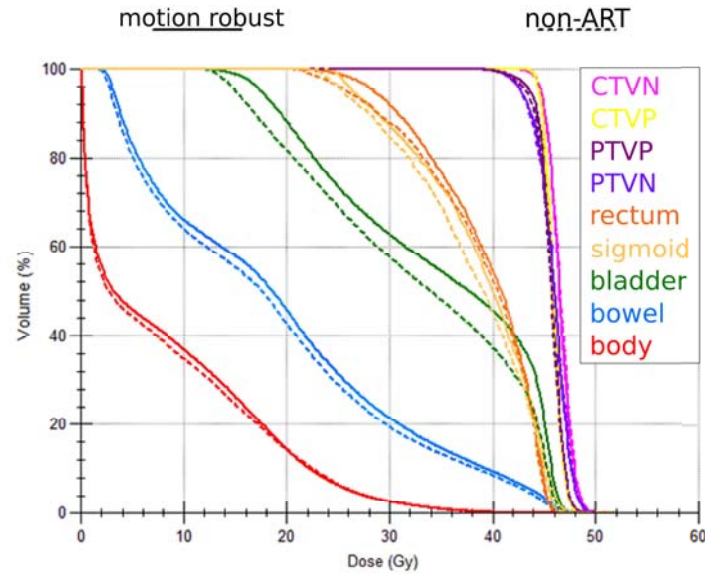
In the DVH of patient 20 the PTPV of the motion robust plan is shown too, which of course is not covered by the non-ART plan, because it is larger than the non-ART PTPV. The received dose of the bladder seems to change stronger for patient 12 with the new planning strategy, while in patient 20 no difference can be observed. In contrast, patient 20 shows a larger difference by means of rectal dose than patient 12. The DVHs in figure 3.7 are clarifying the CTV variations that are occurring during the course of the treatment for both non-movers.

The influence is more significant in patient 12 and even stronger for the CTVN than for the CTVP. Just some of the CTVs were selected to cover the range of variation nicely and giving the viewer the possibility to recognize the single curves. Therefore the lowest lines depict the "worst case" fractions for the patient with the worst coverage and the top lines the "best case" with the best achieved coverage. All other available CTVs lie in between these two lines like the few that are exemplarily plotted.

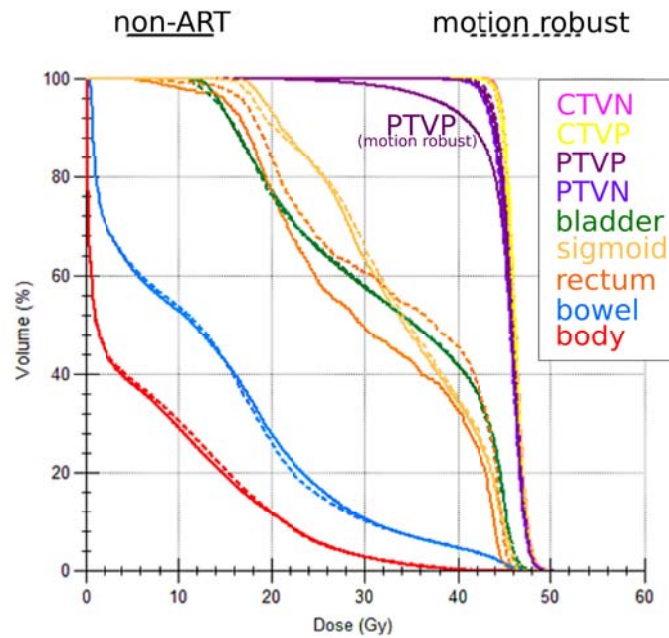
3.2.1.3 Dose Distributions

The DVHs can not give any information about the spatial dose distribution. Thus, in the following the sagittal, coronal and transversal view of the obtained dose distributions for the re-planned non-ART and motion-robust plans are presented in figures 3.8 and 3.9.

The dose distributions seem to be comparable as well as for inter-patient as for inter-plan



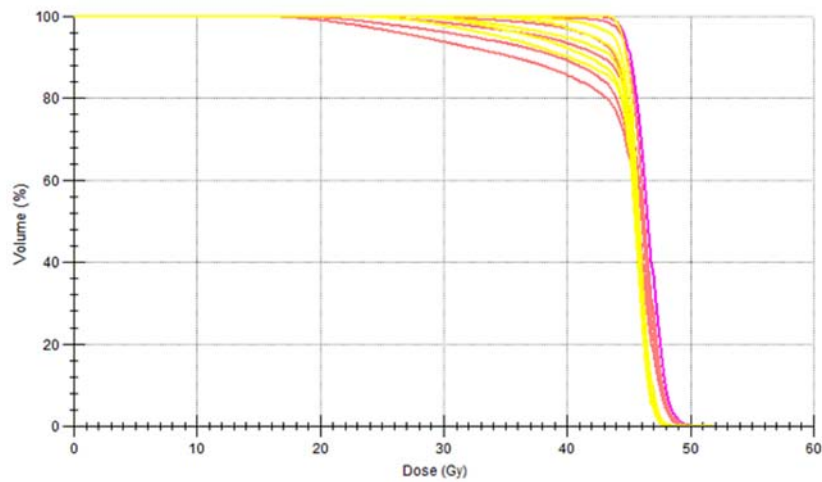
(a) Patient 12



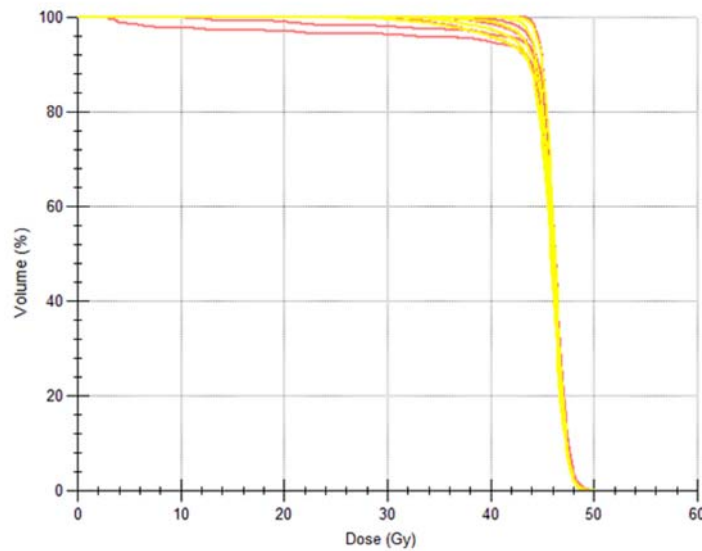
(b) Patient 20

Figure 3.6: DVHs for motion robust and non-ART plan of both non-mover patients.

comparison. The contours that are shown are the bowel (blue), bladder (green), sigmoid (light orange), rectum (orange), CTVP (yellow), CTVN (pink), PTVN (light blue/violet) and PTVP (violet). In the motion robust plans the CTVs of the two extreme bladder filling fractions are shown that were fused to obtain a motion robust CTVP.



(a) Patient 12



(b) Patient 20

Figure 3.7: DVHs of some selected CTVs of various imaging data sets (CBCT, FBCT) for non-ART plans of both non-mover patients. Yellow lines depict the CTVs, pink lines the CTVs.

3.2.2 Mover

In this subsection the findings of the planning study for the patient 21, who was categorized as mover, are presented. The adapted planning was based on the PotD-approach. The data is going to be presented in a similar manner as in subsection 3.2.1.

3.2.2.1 DVH-Values

During planning the PTV-coverages that are presented in table 3.3 were obtained for the various plans.

All D_{2ccm} values of the PTVs are on average 49Gy. Like for the non-movers, all PTV-

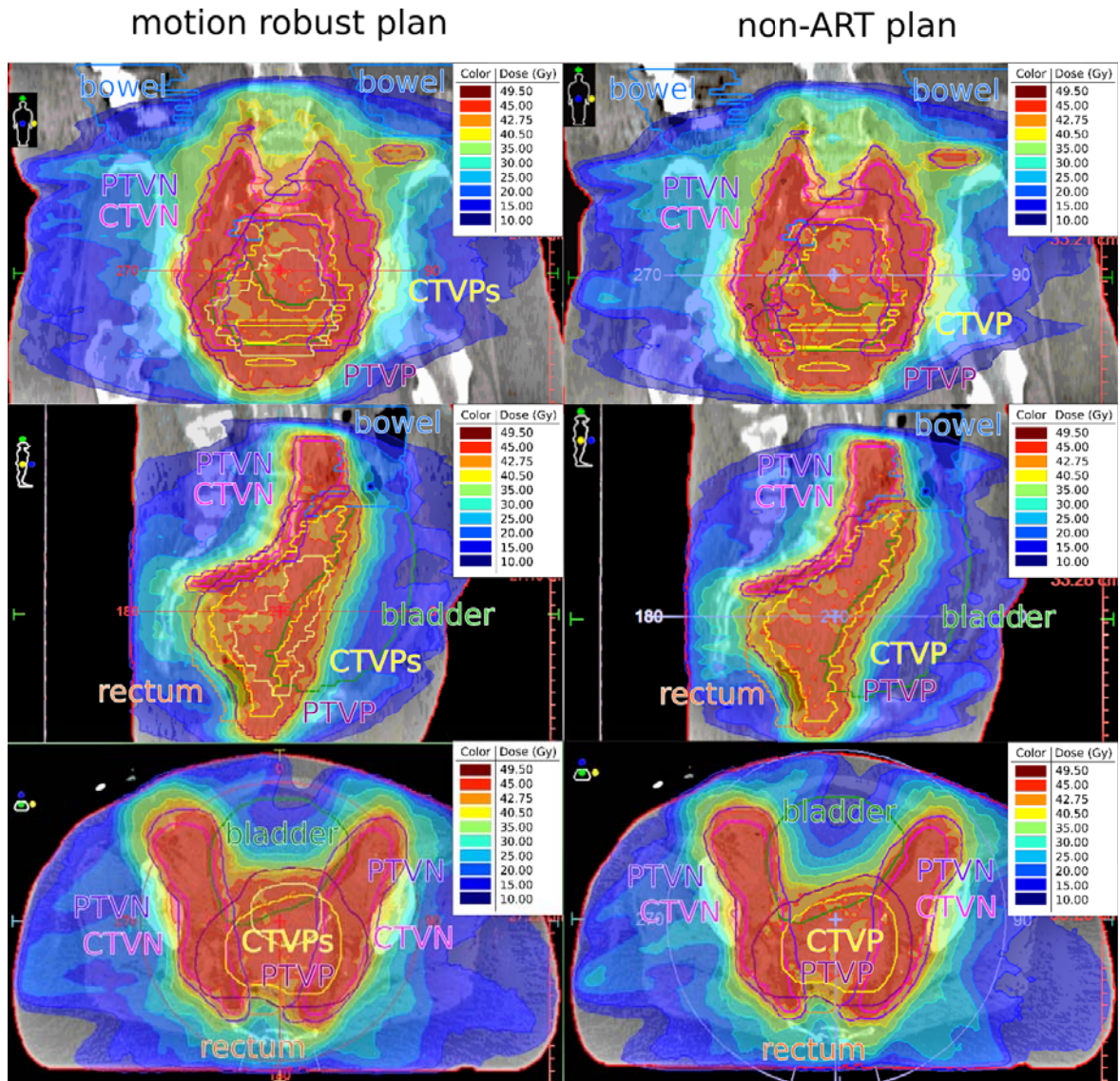


Figure 3.8: Comparison of the dose distributions of non-ART and motion robust plan of patient 12 in coronal, sagittal and transverse view.

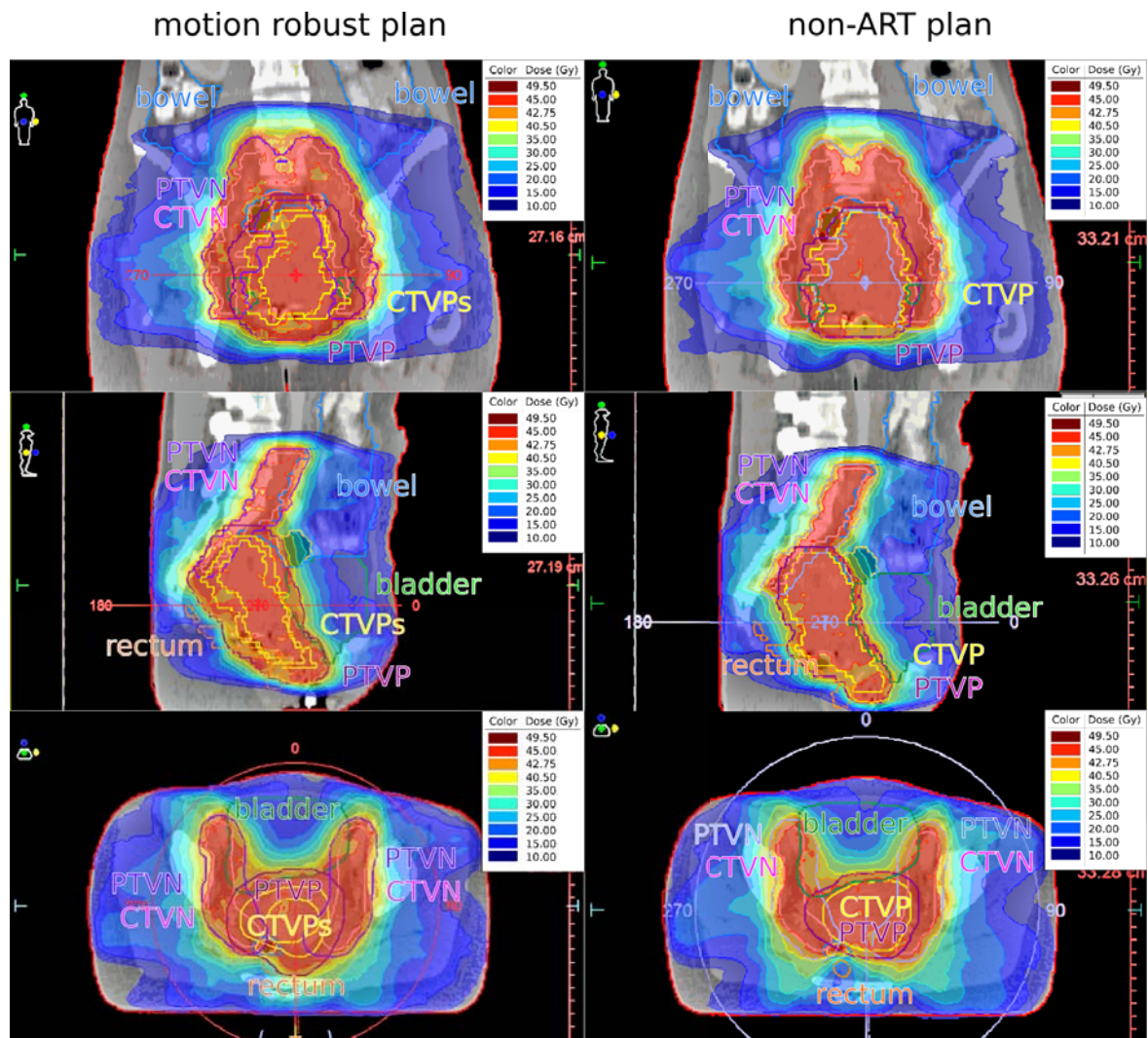


Figure 3.9: Comparison of the dose distributions of non-ART and motion robust plan of patient 20 in coronal, sagittal and transverse view.

	non-ART	stage full	stage empty
$V_{95\%}$ PTVp [%]	99	99	96
$V_{95\%}$ PTVn [%]	96	99	98

Table 3.3: Planning values of patient 21.

coverages lie above the intended 95% and all D_{2ccm} below 50Gy.

These mean values of the $V_{95\%}$ of the CTVs and D_{mean} of the bladder are presented in table 3.4. These are the statistically significant value discrepancies found for the two different planning strategies.

	non-ART	ART
$V_{95\%}$ CTVp [%]	74 ± 18	98 ± 3
D_{mean} bladder [Gy]	30 ± 4	41 ± 2

Table 3.4: Statistically significant mean DVH value discrepancies of all imaging data sets (CBCT, FBCT and MR0) for patient 21.

Note the grave effect of the target motion on the CTVp-coverage for the non-ART plan that can also be seen in figure 3.10 in the left panel.

Visualizations of the values from table 3.5 and all other obtained DVH values are given in the boxplots in figures 3.10 and 3.11.

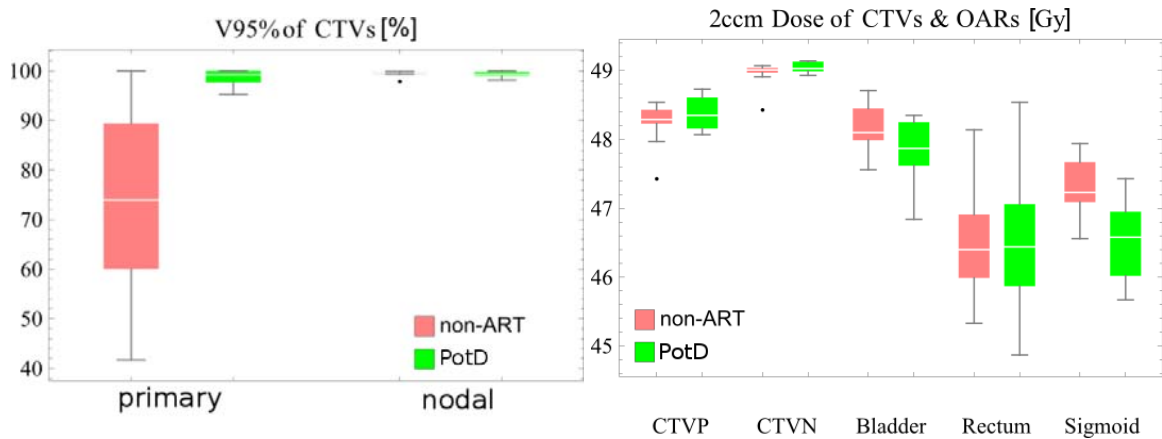


Figure 3.10: All obtained DVH values for CTVs and D_{2ccm} for OARs of patient 21.

Table 3.5 gives a comparison of the mean DVH-values that were obtained for both full and empty planning strategy for patient 21.

These values give an idea how the empty stage plan becomes important in reducing doses for bladder and bowel.

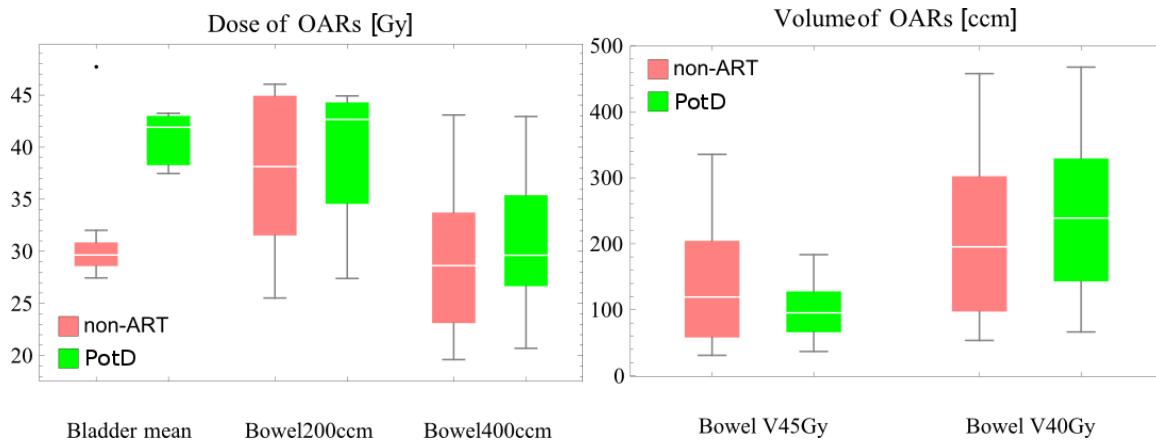


Figure 3.11: Remaining obtained DVH values for OARs of P21.

	stage full plan	stage empty plan
$V_{95\%}$ CTVP [%]	99 ± 2	97 ± 3
D_{2ccm} CTVP [Gy]	49	48
$V_{95\%}$ CTVN [%]	99	100
D_{mean} bladder [Gy]	43	38 ± 1
D_{2ccm} sigmoid [Gy]	46	47
D_{2ccm} rectum [Gy]	47 ± 1	46 ± 1
D_{200ccm} bowel [Gy]	43 ± 2	36 ± 7
D_{400ccm} bowel [Gy]	34 ± 4	26 ± 4
V_{45Gy} bowel [ccm]	104 ± 36	108 ± 54
V_{40Gy} bowel [ccm]	297 ± 80	163 ± 76

Table 3.5: Statistically significantly and insignificantly (grey) diverging mean DVH values of imaging data sets selected for empty and full stage planning strategy for P21, respectively.

3.2.2.2 DVH-Plots

Figure 3.12 depicts the DVH of the three obtained treatment plans for the planning-CT of patient 21 for direct comparison.

The bladder receives a higher dose in the adapted plans than with the non-ART plan. This behavior is similar to what had been found for patient 12, but with nearly twice the discrepancy (see also table 3.4). This can be explained by the decrease in bladder volume and especially the partly overlap of PTV and bladder.

Both the PTVP of the full stage and the empty stage plan are better covered by each other than by the non-ART plan. An explanation is the overlap of stage empty and stage full PTVP. This gives some decision-buffer for medium-filled bladder organ constellations and implies that for such cases the results of CTV coverage from any of the stage-plans will exceed the ones of non-ART. Figure 3.13 shows DVHs for all various CTVPs from all available imaging data sets. The non-ART plan is depicted in the top panel, the two stage-plans below.

The DVHs show clearly how the CTVP-coverage is being improved by ART.

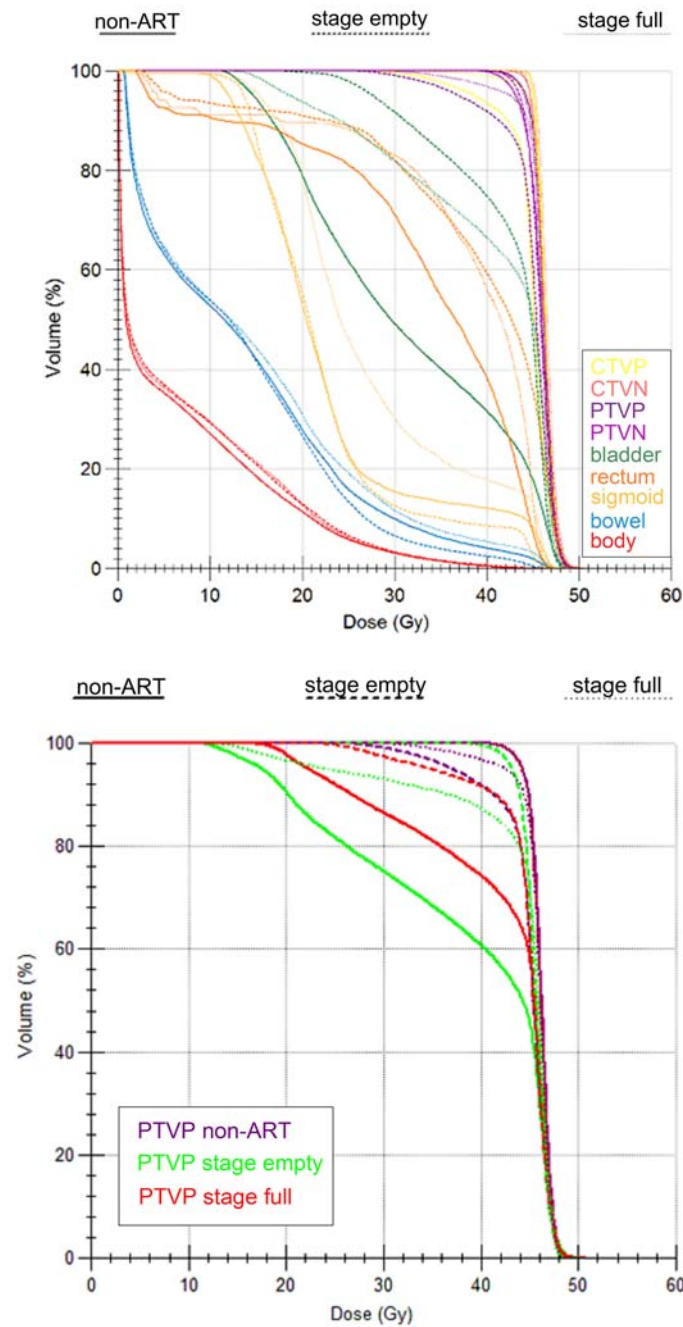


Figure 3.12: DVH of patient 21 for the non-ART plan and empty and full stage plan of the OAR-constellation (top) and the PTVs (bottom) of the planning-CT.

3.2.2.3 Dose Distributions

In the following the dose distributions of patient 21 are presented for all designed plans showing the PTVs and CTVs of the planning-CT (=full bladder scan) as reference structures and OAR-constellation which were taken into account according to the planning strategy. The non-ART and stage full plan show OARs from the full bladder scan, in the stage empty plan dose distribution the OARs from the empty bladder scan are depicted. The structures were outlined as follows: bowel (blue / purple), bladder (green), sigmoid (light orange),

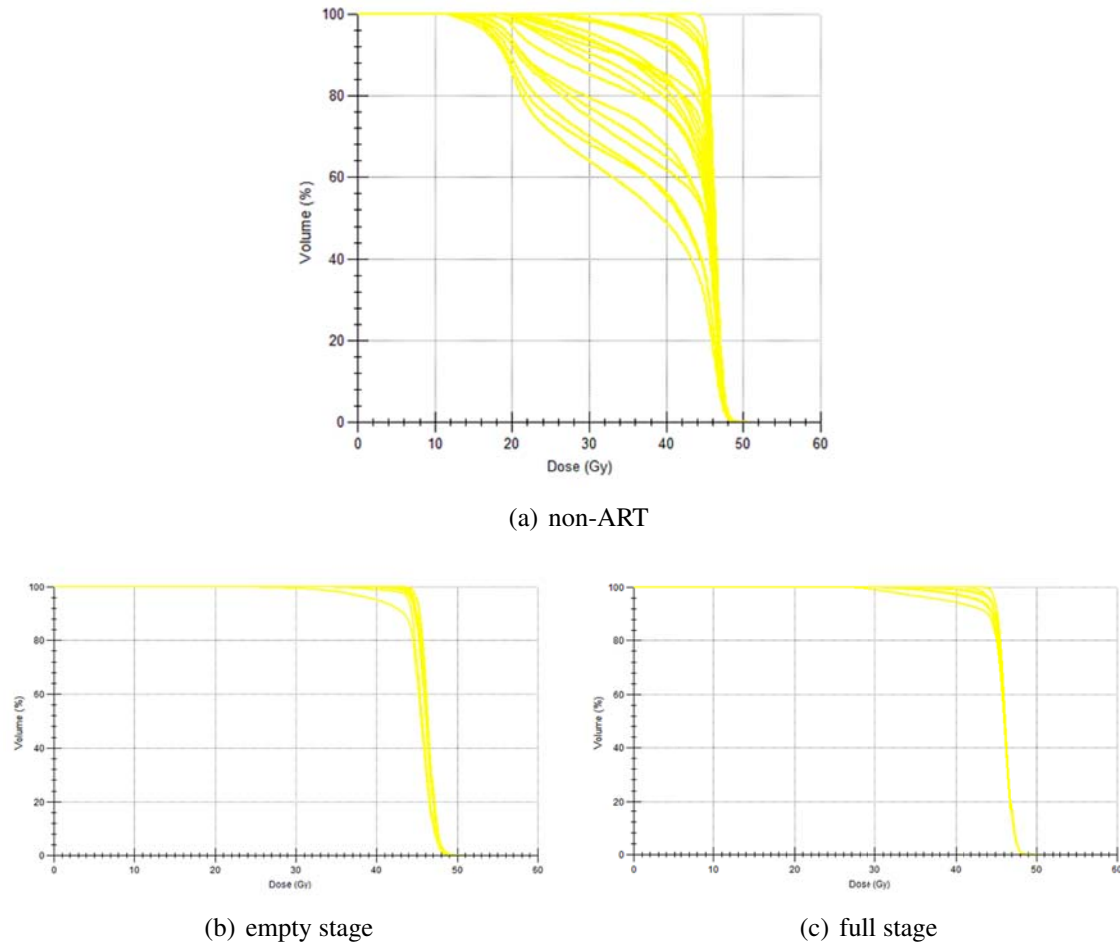


Figure 3.13: DVH of all CTVs of patient 21 for the non-ART plan and empty and full stage plans with the corresponding CTVs.

rectum (orange), CTV (yellow), CTN (pink), PTN (violet) and PTVP (violet / dark red).

In general the dose distributions can be considered as being quite similar, especially when looking at the PTN, but differences occur for the various PTVPs. The increased ITV can easily be seen in the sagittal views of the empty and full stage plan. In the non-ART plan the lack of the dose in the region of the bladder is obvious in coronal and sagittal view, when considering empty bladder contours and the according CTVs (see also figure 3.15). Figure 3.15 gives the contours of all CTVs with respect to their corresponding plan dose distribution in the sagittal view.

According to these dose distributions and the included CTV-constellations, the CTV-coverages seem to be satisfying.

3.3 Influence of Decreasing the CTV-PTV-Margin

3.3.1 DVHs

In figure 3.16 the DVHs for patient 12 and patient 20 with OAR-constellation, CTVs and PTVs of the planning-CT are exemplarily presented.

PTVN and PTVP with reduced margins are not plotted here, but the plans were re-optimized to fit the pre-defined goals. The small margin plan shows clearly less coverage for big-margin-PTVs because the plan is designed for smaller PTVs. For both patients a trend towards lower OAR doses can be seen like it would have been expected.

3.3.2 DVH-Values

During the planning for the reduced margin plans the values for PTV-coverage from table 3.6 were achieved.

	P20	P12	P21(full)	P21(empty)
$V_{95\%}$ PTVP [%]	97	96	99	98
$V_{95\%}$ PTVN [%]	96	95	99	98

Table 3.6: Planning DVH values for all small margin plans of all three patients.

The intended PTV-coverage of 95% was therefore exceeded and the enlarged border of 50Gy maximum D_{2ccm} was achieved for all plans. The following table 3.7 contains the statistically significantly diverging mean DVH-values from all three patients.

It is obvious that the mean CTVN-coverage for all patients went down approximately by 5%. This gives strong evidence to the fact that 0.2cm is a too small safety margin for the CTVN. The average CTVP-coverage in patient 20 decreased by 1% too, in patient 21 even by 3%. In all cases the standard deviation is increasing when using the small margin approach. The mean dose of the bladder decreased in all cases by 2 to 3Gy. In patients 12 and 20 also the rectum is spared moderately better. Reducing the margin is thus a trade-off between decreasing target coverage and increasing OAR sparing.

For better visualization, all obtained DVH values are presented in the following boxplots in figure 3.17 and 3.21. Figures 3.17 to 3.19 give the data of the non-mover patients, figures 3.20 and 3.21 the respective values of the mover.

(a) patient 12		
	big margin	small margin
D_{2ccm} CTVP [Gy]	48	49
$V_{95\%}$ CTVN [%]	92 ± 4	87 ± 6
D_{2ccm} CTVN [Gy]	49	50
D_{mean} bladder [Gy]	38 ± 2	35 ± 2
D_{2ccm} rectum [Gy]	47	48 ± 1
(b) patient 20		
	big margin	small margin
$V_{95\%}$ CTVP [%]	100	99 ± 1
$V_{95\%}$ CTVN [%]	97 ± 2	93 ± 3
D_{mean} bladder [Gy]	35 ± 2	33 ± 2
D_{2ccm} rectum [Gy]	46 ± 1	45 ± 1
(c) patient 21		
	big margin	small margin
$V_{95\%}$ CTVP [%]	98 ± 3	95 ± 5
$V_{95\%}$ CTVN [%]	99 ± 1	94 ± 3
D_{2ccm} CTVN [Gy]	49	50 ± 1
D_{mean} bladder [Gy]	41 ± 2	39 ± 3

Table 3.7: Significant mean DVH value discrepancies of all fractions of the patients.

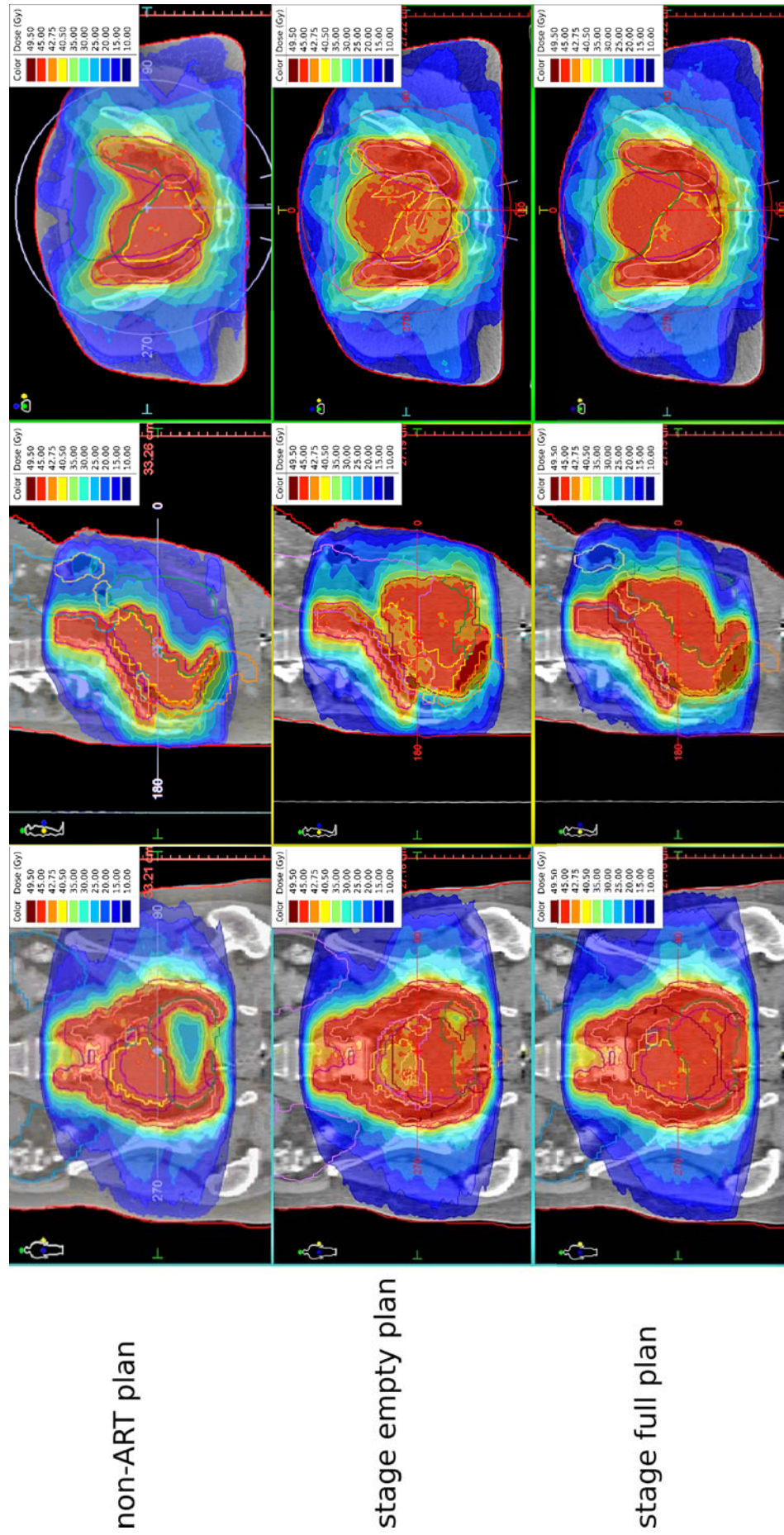


Figure 3.14: Comparison of the dose distributions of the non-ART (top) and the empty stage (middle) and full stage (bottom) plan of patient 21 in coronal, sagittal and transverse view.

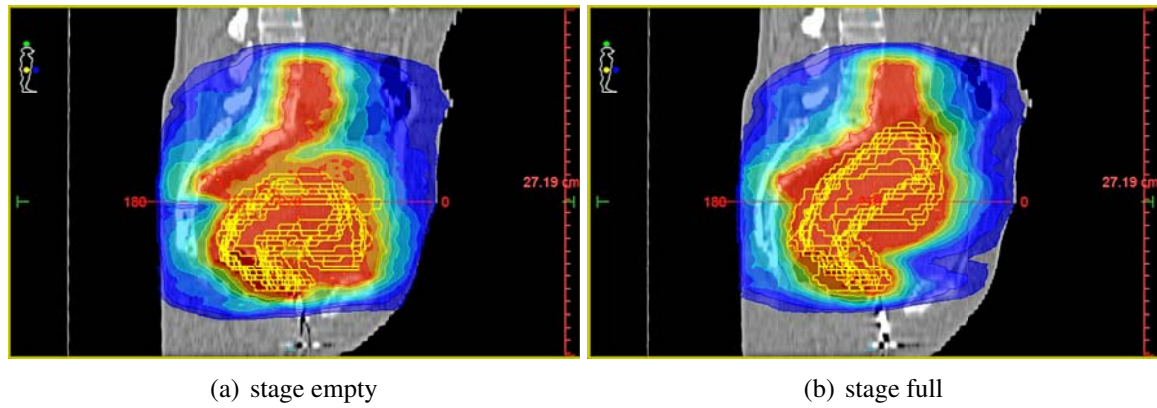


Figure 3.15: CTV variations and dose distribution of the two stage-plans. Yellow lines represent the CTV contours.

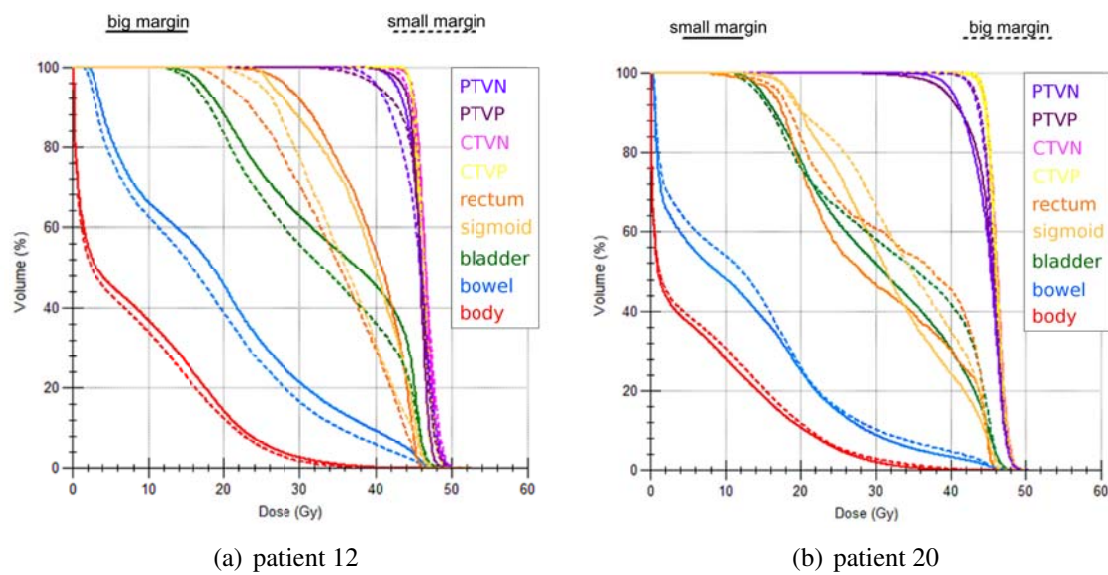


Figure 3.16: DVH of patient 12 and patient 20. Plotted PTVs all include big margin.

big margin = motion robust plan with normal (big) margins
(1cm CTV, 0.5cm CTVN)

small margin = motion robust plan with smaller margins
(0.5cm CTV, 0.2cm CTVN)

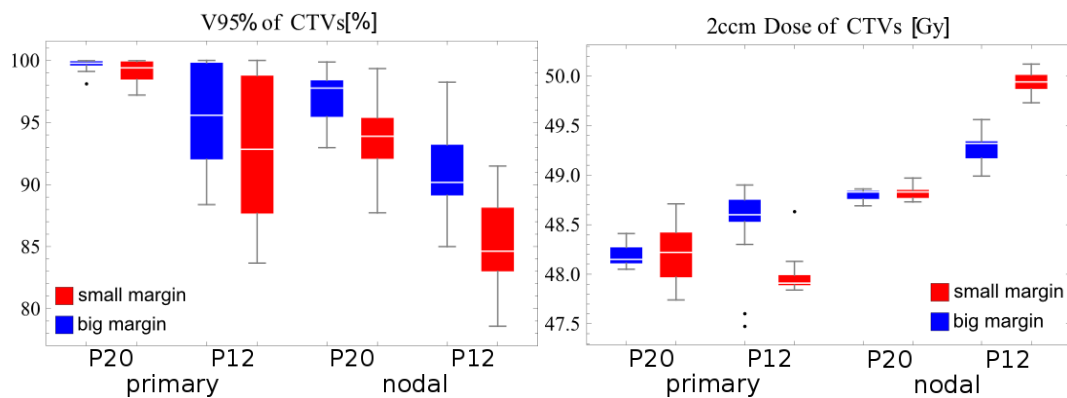


Figure 3.17: Influence of margin: DVH value boxplots of CTV data for patient 12 (P12) and 20 (P20).

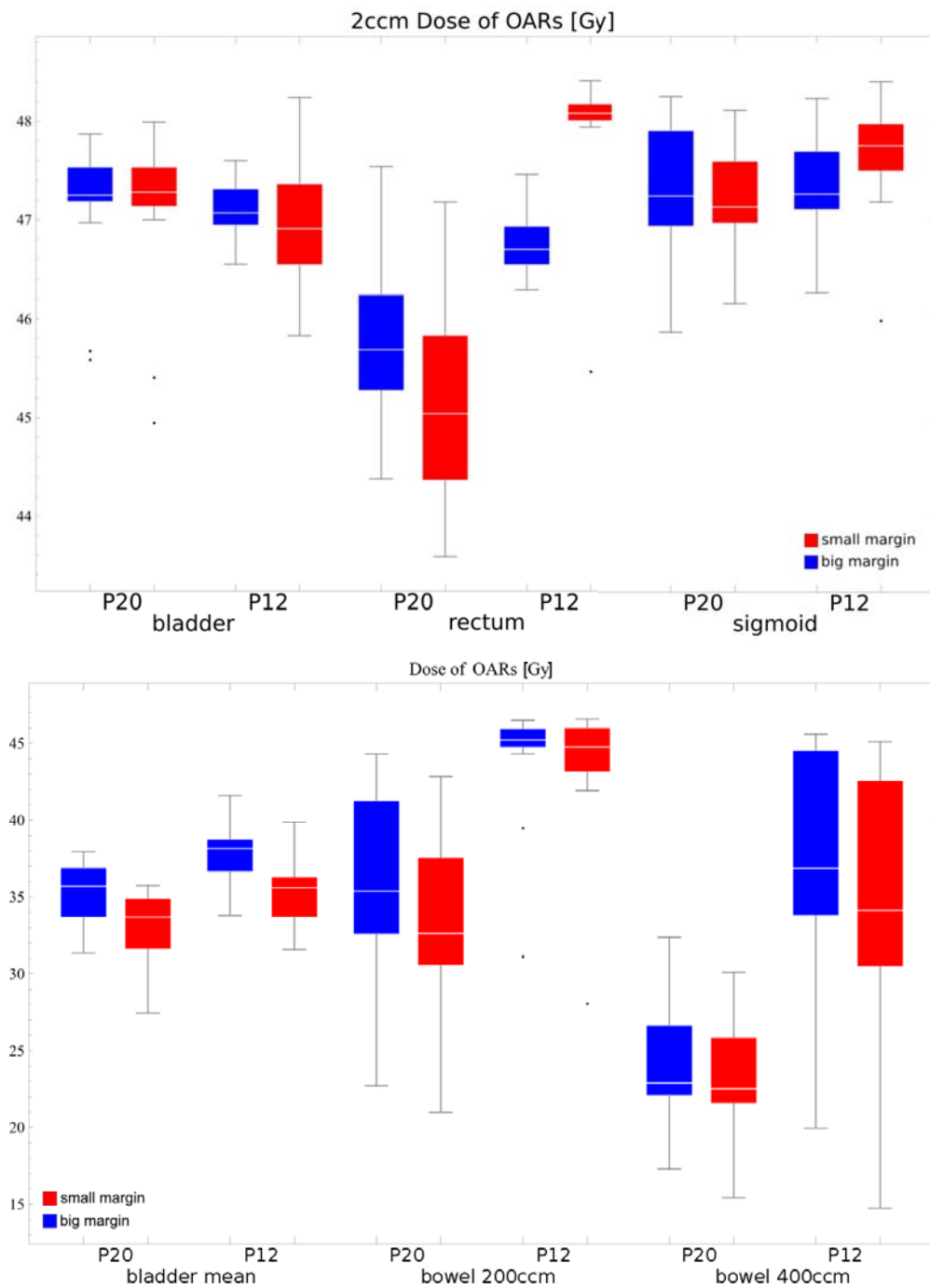


Figure 3.18: Influence of margin: DVH value boxplots of OAR data for patient 12 (P12) and 20 (P20).

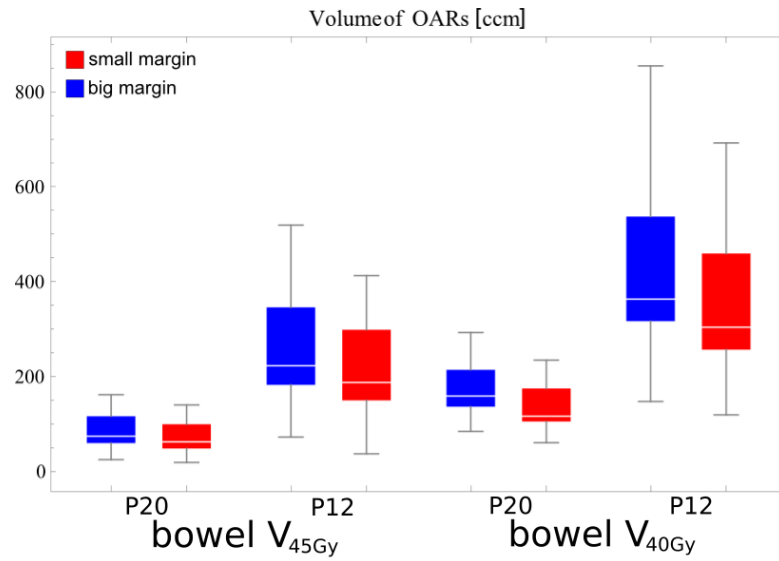


Figure 3.19: Influence of margin: DVH value boxplots of V_{40Gy} and V_{45Gy} of bowel of patient 12 (P12) and 20 (P20).

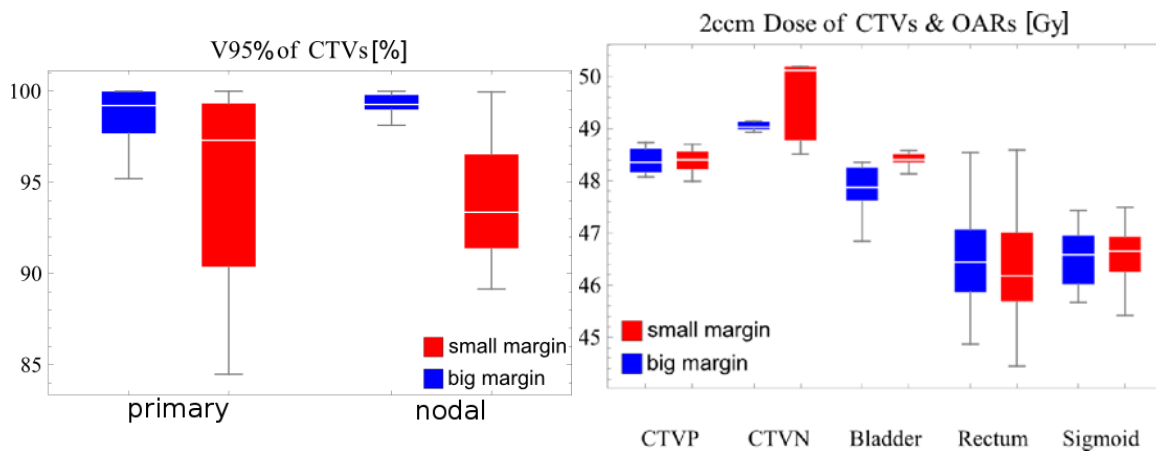


Figure 3.20: Influence of margin: DVH value boxplots for CTVs and D_{2ccm} of OARs for P21.

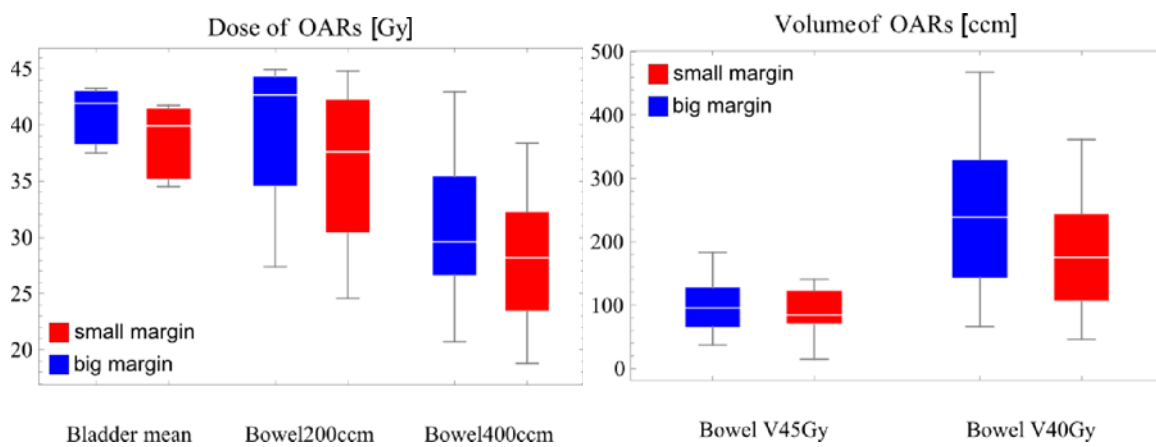


Figure 3.21: Influence of margin: DVH value boxplots of OARs for P21.

4 Summary and Discussion

The main goal of improving and establishing a proper and feasible clinical workflow of radiotherapeutic treatment of cervical cancer for future implementation has been achieved and the evaluation of dosimetric impacts of ART have been investigated. By acquiring two different planning-CTs of the patient with maximum and minimum bladder filling it is possible to classify the patient as mover or non-mover and either construct a motion robust plan if the changes in organ constellation are not big or by applying the PotD-approach based on two or more stage-plans. In fact this second approach has been made possible via the program tool OrCA which has been developed within the scope of this thesis. To check practicability and functionality of OrCA and to see how the adapted radiotherapy treatment planning approaches influence the treatment outcome, a simulated planning study with 3 patient data sets has been performed. Additionally the influence of a decreased setup margin has been addressed.

The analyzed OAR DVH-data showed only minor differences between non-ART and motion robust plans, except for the increase of the D_{mean} of the bladder by about 6Gy for patient 12. On the other hand patient 20 seemed to benefit from the motion robust plan because her cervix-uterus target coverage increased. The analysis of dose distributions and DVHs showed especially for the PotD-approach (patient 21) good results by means of a dramatic increase of cervix-uterus target coverage from $74 \pm 18\%$ to $98 \pm 3\%$. The OAR DVH-values showed an increase of D_{mean} of the bladder from $30 \pm 4\text{Gy}$ to $41 \pm 2\text{Gy}$.

An additional analysis focused on the question of the CTV-PTV-margins. For the nodal CTV we found that the setup margin of 0.5cm should not be decreased, since reducing it to 0.2cm led to approximately 5% less nodal target coverage for all 3 patients. Reducing the primary CTV margin from 1cm to 0.5cm seemed to lead to approximately 2 – 3Gy lower D_{mean} of the bladder for all patients. On the other hand for patient 21 and her PotD-approach we found that the cervix-uterus target coverage decreased by about 3% through this margin reduction. All other OAR DVH-values did not seem to be significantly influenced.

Of course there are some points that need further consideration which are discussed in the following.

4.1 Advantages and Disadvantages of ART

The main advantage of ART is that currently gathered CBCT image information can be used to improve the effectiveness of the dose delivery and with it the treatment outcome, in terms of superior target coverage and OAR-sparing. With ART the treatment plan can be adapted for each of the daily fractions individually to the current anatomical situation of the patient. The main drawback of ART is the increased dose burden due to the additional diagnostic imaging. Compared to the state of the art external beam radiotherapy for cervix cancer with just one planning CT scan, the diagnostic dose burden is doubled with ART, since two planning CTs scans are needed. Moreover the cumulative dose of all daily CBCTs scans during the course of the treatment is not negligible. Ongoing studies investigate this influence of the additional diagnostic dose burden. Only then it will become possible to weigh the benefits of the enhanced OAR-sparing against the increased diagnostic dose burden ART involves. Still, we can assume that the target coverage in cervical cancer cases will be improved and that therefore their TCP will benefit from ART.

4.2 Issues concerning Hollow Organs and Bladder Filling

Representations of organs, based on the planning-CT do not fit to the organ constellations for each treatment fraction. The error of planned vs. real organ contours is even enhanced by the fact that during the planning-CT the patients have a full bladder but for the treatment fractions a tendency to less bladder filling seems to occur. The advantages of a full bladder during treatment would include pushing up the bowel which consequently would move out of the irradiation field and the increasing distance of the distal bladder wall from the target-volume. As consequence a better OAR sparing can be achieved, especially because the bowel is more radio-sensitive than the bladder. Of course this bladder filling variations could be reduced by explaining the patients more clearly the importance of the organ position and by employing drinking protocols, but still the discrepancies between patients and between fractions can be large. There is no clear definition of a "full" bladder and the limit of bladder volume is patient-specific. The feeling of having a full bladder is highly subjective and changes during course of the treatment because of irritated bladder walls as a adverse effect of radiation. Methods that aim to determine the bladder volume just before treatment (for example with hand-held ultrasound) often fail because it is often not possible to reschedule the irradiation time slot for a patient on such a short notice in case her bladder is too empty or too full. ART is therefore the only alternative to effectively react on daily patient anatomy changes.

When it comes to dose estimation of hollow organs, as the most OARs in the pelvic region

and the bladder are, the dose to the contained volume does not really give good information about the exposure of the organ itself. According to the *Handbook of Radiotherapy* [1][Section 35.3.3]

"when considering the expected side effects, it is the dose to the wall of the organ that is likely to be relevant. A dose volume histogram of the whole organ may not be representative of the volume of the wall and the risk of side effects may be overestimated. Several approaches to this problem have been applied, with some centres outlining the outer and inner walls and others calculating dose surface histograms."

Other attempts of developing other useful concepts are for example dose-area frequency distributions that can be used for organ surfaces [64, 65]. For analysis of late adverse effects like assessing the risk of rectal bleeding in prostate irradiation, DVHs of the rectal wall or dose surface histograms may be beneficial [66, 67, 68, 69].

4.3 Dose Calculation of TPS with unchanged ED Distribution

As mentioned in section 2.7 the approach of putting all contours into the planning-CT image data set enormously saved time by obtaining all DVH-values of all image data sets with one treatment plan calculation. Unfortunately this means that all treatment plans were calculated on the electron density distribution of the planning-CT. The only alternative would have been to import the contour data for which the plan is designed (e.g. stage full PTV and the organ contours of the full bladder scan) to all other available scans (CBCT, FBCT, MR) and recalculating the plan for each scan separately. Consequently it would have been necessary to calculate each plan more than 20 times. This makes in sum approximately 220 calculations compared to 11 that were necessary with our approach. Calculation time varied from about two to three hours and therefore falls beyond the scope of my thesis. Assuming that the ED distribution has no sudden changes or sharp edges (which would only occur with large air enclosures in the bowel) we can estimate the calculation-error that comes with non-correlating delineation as small to neglectable. The differences are mainly due to changes in equivalent path length in the ventral side of the patient and because of air in the rectum. Since VMAT beams come from all directions, the beams of incidence angles that suffer from errors are among many others that do not experience changes. For cases with large weight-loss of the patient during the treatment course, calculation accuracy of this approach would have limitations.

4.4 Planning Study versus Future Clinical Workflow

During the planning study planned in the framework of this thesis more influences to organ variations than just the changes of bladder filling occurred due to selection of the empty bladder scan from the available data that was obtained during the treatment course. Firstly, tumor regression is taking place after some treatment fractions have been delivered. The reduced CTVP-volume is clearly visible for the non-mover patients 12 and 20 in figures 3.8 and 3.9. Thus, when planning with the non-regressed uterus as it is going to be practice in the future clinical workflow, the motion robust PTV will be larger than is necessary. Secondly, with selection of two scans from different days also day to day organ variations occur. The most prominent examples are the changes in rectum and bowel filling and peristaltic movements. Future ART planning of cervix cancer cases will therefore not account for the mentioned day to day variations, but only for the influences of changes in bladder filling volume.

4.5 Inferior Results of Patient 12

The results showed that patient 12 would have obtained by far worse treatment outcome than patient 20 with the motion robust approach. This can be explained by a complication that occurred for patient 12 from beginning of the treatment course - a lymphocele. This is a collection of lymphatic fluid in the retroperitoneal space. The phenomenon is usually a side effect after surgery and rarely develops spontaneous. In this case it was caused by surgical staging of lymph nodes. This led to enormous volume variations of the CTVN. In Figure 4.1 the behavior of the volume changes during the treatment course are plotted.

From the first to the second week, a lymph drainage reduced the volume of the lymphocele. The volume was most time nearly enlarged to the double of its normal size. Its 3D-view is even more impressive and shown in figure 4.2.

This enormous changes in volume led to poor CTVN-coverage and made plan optimization especially difficult. CTVP-coverage was also not sufficient for patient 12. We assume that the lymphocele pushed the CTVP out of the motion robust PTV. Another explanation could be, that we categorized this patient wrong, because of quite advanced tumor regression of the empty bladder scan. This finding also suggest that it can be rewarding to evaluate the CBCT scans regularly to ensure that organ configurations are still comparable to planning and take actions if something deviates (see also subsection 4.7).

4.6 Extreme Organ Movements of Patient 21

It is important to emphasize that patient 21 can not be seen as typical mover patient but represents an extraordinarily extreme case of organ movement. Typical top-of-uterus-motions

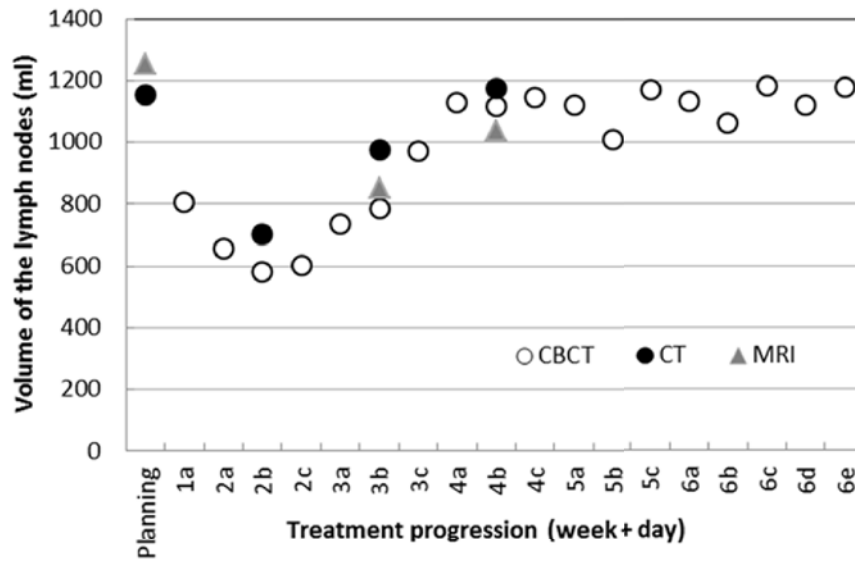


Figure 4.1: Volume changes of the lymph nodes (CTVN) [courtesy of Yvette Seppenwoolde].

(ToUM) of movers range from 2 to 5cm. Patient 21 showed more than 7cm ToUM resulting in quite big Potd PTV volumes. For this patient maybe a three stage PotD approach could have been considered. Anyhow, the benefits for even this single patient due to PotD-approach in terms of PTVP-coverage improvement are vital and give strong evidence that especially mover patients will benefit from ART.

4.7 Atypical Movement Patterns

For some cervix cancer patients atypical uterus movement patterns can be observed. Seppenwoolde et al [32] found for a patient an inverse motion model. The uterus bended backwards with decreasing bladder volume. Moreover it is possible that ventral motion occurs which leads to non-sufficient CTVP-coverage because the uterus is moving out of the field. It is possible that such a change of the motion pattern appears during the course of treatment. Therefore daily CBCTs should not only be used for on-line plan selection at the Linac, but should also be analyzed off-line to confirm the cervix-uterus shape prediction model or to verify that a patient labeled as non-mover did not change into a mover. Thus it is essential to monitor the prepared motion models carefully throughout the course of the treatment. In the future study, an update of the motion model is planned by rescanning the patient halfway the treatment.

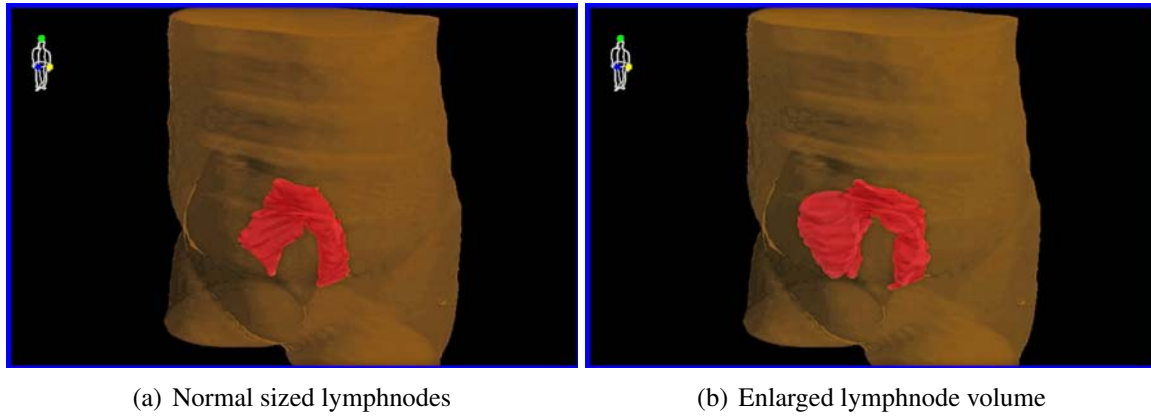


Figure 4.2: 3D-view of different CTVN / lymph node volumes of patient 12.

4.8 The Dose Summation Issue

Unfortunately it was not possible to superpose dose distributions to obtain the effective simulated delivered dose for patient 21 (the mover patient) because of lacking computation tools. Overlaying the several fractions of 1.8 Gy prescription dose full or empty stage plans, respectively, would have resulted in the real simulated dose distribution. In total 10 fractions / image data sets were decided to be covered by full stage plan, while the other 12 fractions / image data sets were simulated for the empty stage plan. The only possibility for evaluation was to select DVH-values accordingly to their attribution and calculate the overall mean DVH-values, which were presented in chapter 3.

4.9 Small Margin versus Big Margin

The idea of reducing the safety-margin is based on the assumption that this margin includes an ITV-margin. This would mean it accounts for a several amount of target position variation. Since in our approach the target movement is already included in our motion model, it was natural that this portion of the margin would no longer be needed. It was assumed that this would lead to a better OAR sparing. Therefore a reduction of the margin was analyzed and the results are presented in chapter 3.3. In fact, improvement of OAR sparing was less than would be expected, especially for the bladder. Moreover the CTVP-coverages especially for patient 21 decreased, meaning that for some fractions the motion was larger or different than was foreseen with the motion model. In general the differences between the small or big margin plans of the non-movers are quite small. Certainly more research is needed to determine the optimal margin recipe for ART of cervix cancer.

5 Conclusion and Outlook

Conclusion:

In conclusion we can state that all the necessary building blocks for a functioning radiotherapy treatment workflow for cervix carcinomas are now ready for clinical use. Conceived in general terms, from the findings of our planning study we can deduce that the bladder will receive a higher mean dose with the adaptive approach, but patients will benefit due to improved target coverage. Anyhow the pre-determined motion models have to be verified and monitored on a regular basis during the treatment course.

Outlook:

For further improvement of the clinical workflow, the implementation of OrCA into Slicer3D via MatlabBridge is planned. This will give the opportunity to export the newly generated organ structures directly into Monaco and therefore reduce the workload by one unnecessary step. Moreover the use of OrCA is not limited to the uterus only, but can also produce intermediate structures for other organs (i.e. bowelbag) as a function of bladder filling or generate a rectum-filling model. The linear model is furthermore not limited to the given bladder filling range by the two input structures but can also extrapolate to a certain extent in case a patient does not have a complete full / empty bladder during the first / second planning CT scan, respectively. In this case the resulting structure should be reviewed carefully to ensure that no exaggeration has been taken place.

To gather more general and reliable data for evaluation of the new adaptive treatment workflow for cervix cancer, further planning studies have to be performed. These studies need to obtain imaging data sets of the new approach including the two planning-CTs and need to be based on larger patient cohorts. Therefore more patients are needed to take part in these studies. Currently a follow up PhD thesis at the Vienna General Hospital / Medical University Vienna by Martin Buschmann will focus on this issues and expanding the scope also to head and neck cases, where tumor regression represents a major problem that has to be solved by ART.

Appendix

Program Report: **Organ Contour Adaptor Tool (OrCA)**

- What is OrCA and what can it be used for?

OrCA is a tool based on MATLAB that is intended to be useful in adaptive treatment planning of cervical cancer cases. Its main purpose is to load two extreme positions and/or filling states of a patient's organ contour (e.g. the PTV or the bladder) from two dicom files and to interpolate linearly between them. A middle contour is created by simply using 0.5 interpolation factor. It is up to the user if also a current contour according to the given min. and max. bladder volumes is created. The interpolation is based on the continuous point drift code package (CPD2¹). The interpolated contour can be added to an existing dicom file chosen by the user. The title of the newly generated file (a copy of the original file plus the new contour(s)) is entered by the user.

- How does it work?

DATASTRUCTURE AND SAVING PROCESS:

To achieve the intended goals it is necessary to change and add metadata of an input dicom file. Dicom files and especially dicom-RT-structure files contain many various and quite treelike branched metadata fields that can be accessed and adapted via 'dicominfo'² function and be deleted by using 'rmfield' function of Matlab.

OrCA adapts the following fields and saves the new file within 'dicomRTAddContour.m' by use of 'dicominfo' and 'dicomwrite'² functions:

```
StructureSetROISequence:
    ROINumber
    ROIName
ROIContourSequence:
    ROIDisplayColor
    ReferencedROINumber
    ContourSequence:
        ContourData
        ContourImageSequence:
            ReferencedSOPClassUID
        ContourGeometricType
        NumberOfContourPoints
refSOPInstanceUID
refSOPClassUID
```

The heart of the occurring changes lies within the ContourData field. It contains the raw contour data in form of x, y and z coordinates of the point cloud that defines the new contour. Most treatment planning systems (TPS) need the contour data in a slicewise manner with 4mm intervals (as it is in regular CT scans). Therefore ContourData consists of n fields called "Items", where n equals the number of slices and each Item contains only points with consistent z coordinate. The coordinates are alternatingly aligned in one column and the points are ordered in a clockwise manner which is important for a correct illustration and composition in the TPS.

THE INTERPOLATION:

The above mentioned contour data has to be generated in the first instance before the file can be saved. For this purpose the CPD2 code for point registration is used:

Abstract:

"Point set registration is a key component in many computer vision tasks. The goal of point set registration is to assign correspondences between two sets of points and to recover the transformation that maps one point set to the other. Multiple factors, including an unknown nonrigid spatial transformation, large dimensionality of point set, noise, and outliers, make the point set registration a challenging problem. We introduce a probabilistic method, called the Coherent Point Drift (CPD) algorithm, for both rigid and nonrigid point set registration. We consider the alignment of two point sets as a probability density estimation problem. We fit the Gaussian mixture model (GMM) centroids (representing the first point set) to the data (the second point set) by maximizing the likelihood. We force the GMM centroids to move coherently as a group to preserve the topological structure of the point sets. In the rigid case, we impose the coherence constraint by reparameterization of GMM centroid locations with rigid parameters and derive a closed form solution of the maximization step of the EM algorithm in arbitrary dimensions. In the nonrigid case, we impose the coherence constraint by regularizing the displacement field and using the variational calculus to derive the optimal transformation. We also introduce a fast algorithm that reduces the method computation complexity to linear. We test the CPD algorithm for both rigid and nonrigid transformations in the presence of noise, outliers, and missing points, where CPD shows accurate results and outperforms current state-of-the-art methods. "

(Point Set Registration: Coherent Point Drift, IEEE Transactions on Pattern Analysis and Machine Intelligence, December 2010 (vol. 32 no. 12), pp. 2262-2275)

Simply put, CPD registers point cloud to point cloud and gives a vector of correspondences. Based on these correspondences linear interpolation between the registered points can be performed.

Downsampling is done for contour data that are larger than 200 points per slice in order to allow convenient calculation times.

The newly generated point cloud that represents the interpolated organ contour needs to be processed in order to fit the data structure of dicom files. For this purpose 'AlphaHull'³ function is used to get a triangulated surface of the contour. This is then "sliced" in 4mm z-intervals and put in the needed Items. Those two steps happen in the 'alphahullslicing' function.

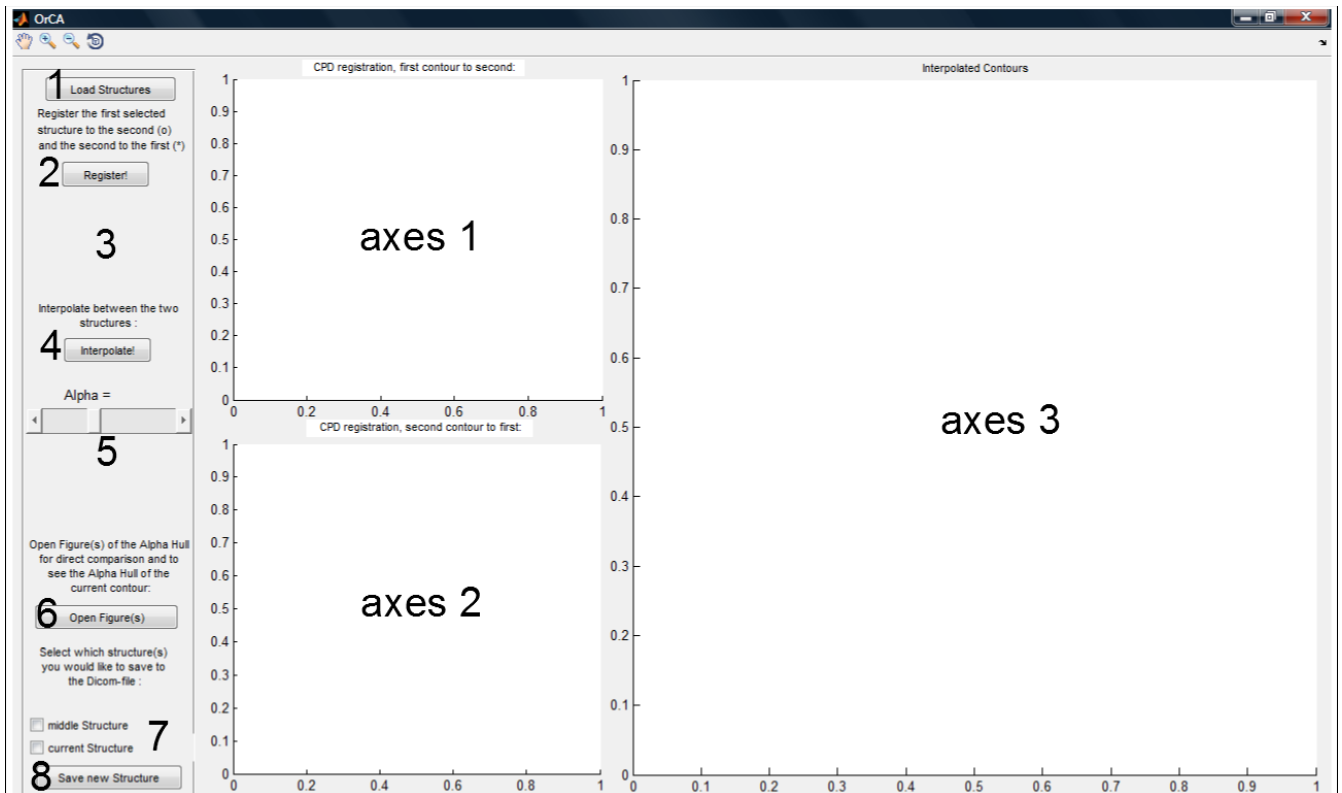
THE SMOOTHING:

For a smooth and clear contour depiction in the TPS the data from the generated Items have to be smoothed.

The slice data is converted and transformed to polar coordinates where the origin is set to the center of each contour slice by default. This can be adapted by the User (see point 3 of OrCsmoothing). OrCA uses the 'splinefit'⁴ function. A number of points are read out from the fit-function and afterward transformed back to Cartesian coordinates and ordered in a clockwise manner.

In case there are too less points to define the contour in a region, some are added by linear interpolation in order to prevent errors by the fit function. OrCA gives the possibility to let the user adapt the number of breaks for the fit, the number of points that are going to be saved per slice (Item) and the middle point of transformation in a separate user interface 'OrCsmoothing' or to run the smoothing with the default values of 50 spline breaks and 100 points per slice by using the 'contourdatasmoothing' function.

– How to use it - a short User Manual:



Step by step workflow and program description:

- 1.) 'Load Structures' Button: This button opens the browser to let the user select the dicom files and organ contours. The first contour should belong to the max., the second to the min. bladder filling status.
- 2.) 'Register !' Button: The button starts the CPD registration process in both directions. It will be visualized for the first direction in axes 1 and for the other in axes 2. At the end the patient categorization will pop up in a message box.
- 3.) Movement-Textfield: Here the average length of the top 10% of the registration vectors called “Movement” will show up after CPD registration is finished.
- 4.) 'Interpolate!' Button: Clicking opens a dialog that asks the user whether he wishes to create an interpolated structure according to the current bladder filling or just the middle structure. The point clouds will be visualized in axes 3. A message window will pop up that gives the number of registration vectors in each direction.
- 5.) Alpha Parameter Slider: Moving the slider will show the alpha hull of the middle contour in axes 3 for the chosen alpha parameter. Default value of the alpha parameter is 7.
CAUTION: Don't choose a too high alpha parameter just to obtain a closed surface, especially when working with concave structures!
- 6.) 'Open Figures' Button: Opens the figures of alpha hull of all available contour data sets for the current alpha parameter: middle and current structure (if generated) for both registration directions. This can be useful if you want to compare alpha hulls for different alpha parameters directly but is not necessary.
- 7.) Saving Checkboxes: Check the structure(s) you want to save, before you click 'Save new Structure'.

8.) 'Save new Structure' Button:

Pressing this button opens the browser window to let the user select a dicom file. The new structure(s) will be added to this file.

Afterward the user can choose which of the structure data he wants to save depending on which direction of registration he prefers or the merged data.

An input dialog will ask the user to enter the name of the new file and the new structure(s).

Then the color can be selected.

The user will be asked whether he would like to adapt the smoothing function or not.

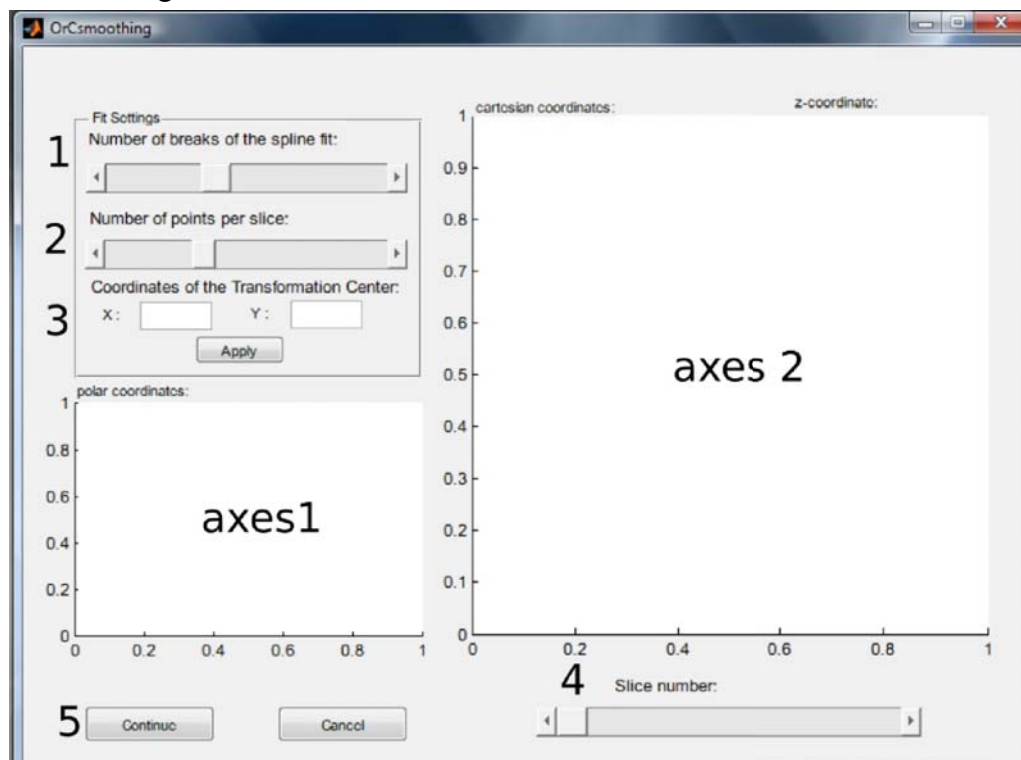
- If so see 9.) .

- If not OrCA saves the contours with the default values:

number of breaks: 50

number of points per slice: 100

9.) OrCsmoothing:



OrCsmoothing is an UI for visualization of the unprocessed (green) and processed/smoothed (blue) organ contour data in a slicewise manner and at the same time makes it possible to adapt the data smoothing process (fit function) by means of selecting the number of breaks for the spline fit. Points that were added by linear interpolation are shown in red.

axes 1 shows the polar, axes 2 the Cartesian coordinates of the contour slice as soon as any slider is moved.

- 1.) 'Number of breaks' Slider
- 2.) 'Number of points per slice' Slider
- 3.) x and y textfields and 'Apply'-Button

Adjust the number of breaks for spline-fit
Adjust the number of points per slice
Adjust the coordinates of the transformation
middle point

(this is also possible via click-selection)

- 4.) 'Slice number' Slider

With this slider the user can scroll through the
slices of the contour.

- 5.) 'Continue' Button

At button press the OrCsmoothing is closed and
the current values are used for smoothing before
saving the new contour.

- What is needed beforehand? / Further information:

You need to have the two dicom files that contain the organ structure for maximum and minimum filling state and should have determined the amount of bladder filling in ml if you want to create a structure according to a current bladder filling volume.

ATTENTION: Before you can import the generated dicom file to the TPS Monaco® you need to import and export in and from 3DSlicer.

- 1) Coherent Point Drift (CPD) Matlab package (version 2.1)
Copyright (C) 2006-2009, Andriy Myronenko
- 2) from the image processing toolbox of MATLAB
- 3) by Dylan Muir <dylan@ini.phys.ethz.ch>
- 4) by Jonas Lundgren

Bibliography

- [1] Philip Miles, Alan Nahum, and Jean-Cloude Rosenwald, editors. *Handbook of Radiotherapy Physics - Theory and Practice*. Taylor&Francis, 2007.
- [2] Faiz M Khan, editor. *The Physics of Radiation Therapy*. Wolters Kluwer | Lippincott Williams&Wilkins, 2009.
- [3] ICRU Report 33. Quantities and units for use in radiation protection. *Journal of the ICRU*, 1980.
- [4] ICRU Report 58. Dose and volume specification for reporting interstitial therapy. *Journal of the ICRU*, 1998.
- [5] ICRP Publication 60. Recommendations of the international commission on radiological protection. *Annals of the ICRP* 21, 1991.
- [6] IAEA. *Radiation Oncology Physics: A Handbook for Teachers and Students*. 2005.
- [7] Barbara Knäusel. Dosimetric characteristics of a flattening filter free photon beam. Master's thesis, University of Vienna, 2008.
- [8] Dietmar Georg, Tommy Knöös, and Brendan McClean. Current status and future perspective of flattening filter free photon beams. *Medical Physics*, 38(3):1280–1293, 2011.
- [9] ICRU Report 50. Prescribing, Recording, and Reporting Photon Beam Therapy. *Journal of the ICRU*, 1993.
- [10] ICRU Report 62. Prescribing, Recording and Reporting Photon Beam Therapy (Supplement to ICRU Report 50). *Journal of the ICRU*, 1999.
- [11] R M Henkelman and K Mah. How important is breathing in radiation therapy of the thorax? *International Journal of Radiation Oncology Biology Physics*, (8):2005–2010, 1982.
- [12] S. C. Davies, A. L. Hill, R. B. Holmes, M. Halliwell, and P. C. Jackson. Ultrasound quantitation of respiratory organ motion in the upper abdomen. *British Journal of Radiology*, 67:1096–1102, 1994.

-
- [13] M. A. Moerland. The influence of respiration induced motion of the kidneys on the accuracy of radiotherapy treatment planning, a magnetic resonance imaging study. *Radiotherapy and Oncology*, 30:150–154, 1994.
- [14] Christelle Gendrin, Hugo Furtado, Christoph Weber, Christoph Bloch, Michael Figl, Supriyanto Ardjo Pawiro, Helmar Bergmann, Markus Stock, Gabor Fichtinger, Dietmar Georg, and Wolfgang Birkfellner. Monitoring tumor motion by real time 2D/3D registration during radiotherapy. *Radiotherapy and Oncology*, 102:274–280, 2012.
- [15] Hugo Furtado, Elisabeth Steiner, Markus Stock, Dietmar Georg, and Wolfgang Birkfellner. Real-time 2D/3D registration using kV-MV image pairs for tumor motion tracking in image guided radiotherapy. *Acta oncologica (Stockholm, Sweden)*, 52:1464–71, 2013.
- [16] Jakob Spoerk, Christelle Gendrin, Christoph Weber, Michael Figl, Supriyanto Ardjo Pawiro, Hugo Furtado, Daniella Fabri, Christoph Bloch, Helmar Bergmann, Eduard Gröller, and Wolfgang Birkfellner. High-performance GPU-based rendering for real-time, rigid 2D/3D-image registration and motion prediction in radiation oncology. *Zeitschrift für Medizinische Physik*, 22:13–20, 2012.
- [17] Hiroshi Onishi, Kengo Kuriyama, Takafumi Komiyama, Shiho Tanaka, Naoki Sano, Yoshihito Aikawa, Yoshihito Tateda, Tsutomu Araki, Satoshi Ikenaga, and Minoru Uematsu. A new irradiation system for lung cancer combining linear accelerator, computed tomography, patient self-breath-holding, and patient-directed beam-control without respiratory monitoring devices. *International Journal of Radiation Oncology Biology Physics*, 56:14–20, 2003.
- [18] Martin J. Murphy, David Martin, Richard Whyte, Jenny Hai, Cihat Ozhasoglu, and Quynh Thu Le. The effectiveness of breath-holding to stabilize lung and pancreas tumors during radiosurgery. *International Journal of Radiation Oncology Biology Physics*, 53:475–482, 2002.
- [19] David Sarrut, Vlad Boldea, Myriam Ayadi, J. N. Badel, Chantal Ginestet, Sébastien Clippe, and Christian Carrie. Nonrigid registration method to assess reproducibility of breath-holding with ABC in lung cancer. *International Journal of Radiation Oncology Biology Physics*, 61:594–607, 2005.
- [20] Laura A. Dawson, Kristy K. Brock, Sahira Kazanjian, Dwight Fitch, Cornelius J. McGinn, Theodore S. Lawrence, Randall K. Ten Haken, and James Balter. The reproducibility of organ position using active breathing control (ABC) during liver radiotherapy. *International Journal of Radiation Oncology Biology Physics*, 51:1410–1421, 2001.

- [21] J. C. Roeske, J. D. Forman, C. F. Mesina, T. He, C. A. Pelizzari, E. Fontenla, S. Vijayakumar, and G. T Y Chen. Evaluation of changes in the size and location of the prostate, seminal vesicles, bladder, and rectum during a course of external beam radiation therapy. In *International Journal of Radiation Oncology Biology Physics*, volume 33, pages 1321–1329, 1995.
- [22] Laura A. Dawson, Katherine Mah, Edmee Franssen, and Gerard Morton. Target position variability throughout prostate radiotherapy. *International Journal of Radiation Oncology Biology Physics*, 42:1155–1161, 1998.
- [23] Ai Nagano, Shinichi Minohara, Shingo Kato, Hiroki Kiyohara, and Ken Ando. Adaptive radiotherapy based on the daily regression of a tumor in carbon-ion beam irradiation. *Physics in medicine and biology*, 57:8343–56, 2012.
- [24] Di Yan, John Wong, Frank Vicini, Jeff Michalski, Cheng Pan, Arthur Frazier, Eric Horwitz, and Alvaro Martinez. Adaptive modification of treatment planning to minimize the deleterious effects of treatment setup errors. *International Journal of Radiation Oncology Biology Physics*, 38:197–206, 1997.
- [25] Di Yan, David Lockman, Donald Brabbins, Laura Tyburski, and Alvaro Martinez. An off-line strategy for constructing a patient-specific planning target volume in adaptive treatment process for prostate cancer. *International Journal of Radiation Oncology Biology Physics*, 48:289–302, 2000.
- [26] Weiguo Lu, Mingli Chen, Quan Chen, Kenneth Ruchala, and Gustavo Olivera. Adaptive fractionation therapy: I. Basic concept and strategy. *Physics in medicine and biology*, 53:5495–5511, 2008.
- [27] Philip Chan, Robert Dinniwell, Masoom A. Haider, Young Bin Cho, David Jaffray, Gina Lockwood, Wilfred Levin, Lee Manchul, Anthony Fyles, and Michael Milosevic. Inter- and Intrafractional Tumor and Organ Movement in Patients With Cervical Cancer Undergoing Radiotherapy: A Cinematic-MRI Point-of-Interest Study. *International Journal of Radiation Oncology Biology Physics*, 70:1507–1515, 2008.
- [28] Neelam Tyagi, John H. Lewis, Catheryn M. Yashar, Daniel Vo, Steve B. Jiang, Arno J. Mundt, and Loren K. Mell. Daily online cone beam computed tomography to assess interfractional motion in patients with intact cervical cancer. *International Journal of Radiation Oncology Biology Physics*, 80:273–280, 2011.
- [29] Seung Jae Huh, Won Park, and Youngyih Han. Interfractional variation in position of the uterus during radical radiotherapy for cervical cancer. *Radiotherapy and Oncology*, 71:73–79, 2004.

- [30] Jeong Eun Lee, Youngyih Han, Seung Jae Huh, Won Park, Min Gyu Kang, Yong Chan Ahn, and Do Hoon Lim. Interfractional variation of uterine position during radical RT: Weekly CT evaluation. *Gynecologic Oncology*, 104:145–151, 2007.
- [31] Karen Lim, Valerie Kelly, James Stewart, Jason Xie, Young Bin Cho, Joanne Moseley, Kristy Brock, Anthony Fyles, Anna Lundin, Henrik Rehbinder, and Michael Milosevic. Pelvic Radiotherapy for Cancer of the Cervix: Is What You Plan Actually What You Deliver? *International Journal of Radiation Oncology Biology Physics*, 74:304–312, 2009.
- [32] Yvette Seppenwoolde, Petra Georg, Dietmar Georg, Katharina Moser, Kwei-Yuang Bauer, Richard Pötter, and Markus Stock. Organ shape variations influencing PTV concepts for cervix cancer ART.
- [33] James Stewart, Karen Lim, Valerie Kelly, Jason Xie, Kristy K. Brock, Joanne Moseley, Young Bin Cho, Anthony Fyles, Anna Lundin, Henrik Rehbinder, Johan Löf, David Jaffray, and Michael Milosevic. Automated weekly replanning for intensity-modulated radiotherapy of cervix cancer. *International Journal of Radiation Oncology Biology Physics*, 78:350–358, 2010.
- [34] Seungjong Oh, James Stewart, Joanne Moseley, Valerie Kelly, Karen Lim, Jason Xie, Anthony Fyles, Kristy K. Brock, Anna Lundin, Henrik Rehbinder, Michael Milosevic, David Jaffray, and Young Bin Cho. Hybrid adaptive radiotherapy with on-line MRI in cervix cancer IMRT. *Radiotherapy and Oncology*, 110:323–328, 2014.
- [35] Luiza Bondar, Mischa Hoogeman, Jan Willem Mens, Glenn Dhawtal, Ilse De Pree, Rozilawati Ahmad, Sandra Quint, and Ben Heijmen. Toward an individualized target motion management for IMRT of cervical cancer based on model-predicted cervix-uterus shape and position. *Radiotherapy and Oncology*, 99(2):240–245, May 2011.
- [36] Rozilawati Ahmad, Luiza Bondar, Peter Voet, Jan-Willem Mens, Sandra Quint, Glenn Dhawtal, Ben Heijmen, and Mischa Hoogeman. A margin-of-the-day online adaptive intensity-modulated radiotherapy strategy for cervical cancer provides superior treatment accuracy compared to clinically recommended margins: a dosimetric evaluation. *Acta oncologica (Stockholm, Sweden)*, 52:1430–6, 2013.
- [37] Sabrina T. Heijkoop, Thomas R. Langerak, Sandra Quint, Luiza Bondar, Jan Willem M Mens, Ben J M Heijmen, and Mischa S. Hoogeman. Clinical Implementation of an On-line Adaptive Plan-of-the-Day Protocol for Nonrigid Motion Management in Locally Advanced Cervical Cancer IMRT, 2014.
- [38] Q Jackie Wu, Danthai Thongphiew, Zhiheng Wang, Boonyanit Mathayomchan, Vira Chankong, Sua Yoo, W Robert Lee, and Fang-Fang Yin. On-line re-optimization of

- prostate IMRT plans for adaptive radiation therapy. *Physics in medicine and biology*, 53(3):673–691, 2008.
- [39] Floris Pos and Peter Remeijer. Adaptive Management of Bladder Cancer Radiotherapy, 2010.
- [40] G J Webster, J Stratford, J Rodgers, J E Livsey, D Macintosh, and A Choudhury. Comparison of adaptive radiotherapy techniques for the treatment of bladder cancer. *The British journal of radiology*, 86(1021):20120433, January 2013.
- [41] K Tanderup, D Georg, R Pötter, C Kirisits, C Grau, and J C Lindegaard. Adaptive management of cervical cancer radiotherapy. *Seminars in Radiation Oncology*, 20(2):121–129, 2010.
- [42] Luiza Bondar, Mischa S Hoogeman, Eliana M Vásquez Osorio, and Ben J M Heijmen. A symmetric nonrigid registration method to handle large organ deformations in cervical cancer patients. *Medical physics*, 37:3760–3772, 2010.
- [43] M. L. Bondar, M. S. Hoogeman, J. W. Mens, S. Quint, R. Ahmad, G. Dhawtal, and B. J. Heijmen. Individualized nonadaptive and online-adaptive intensity-modulated radiotherapy treatment strategies for cervical cancer patients based on pretreatment acquired variable bladder filling computed tomography scans. *International Journal of Radiation Oncology Biology Physics*, 83(5):1617–1623, 2012.
- [44] Christian Kirisits, Stefan Lang, Johannes Dimopoulos, Daniel Berger, Dietmar Georg, and Richard Pötter. The Vienna applicator for combined intracavitary and interstitial brachytherapy of cervical cancer: Design, application, treatment planning, and dosimetric results. *International Journal of Radiation Oncology Biology Physics*, 65(2):624–630, 2006.
- [45] Christian Kirisits, Richard Pötter, Stefan Lang, Johannes Dimopoulos, Natascha Wachter-Gerstner, and Dietmar Georg. Dose and volume parameters for MRI-based treatment planning in intracavitary brachytherapy for cervical cancer. *International journal of radiation oncology, biology, physics*, 62(3):901–11, July 2005.
- [46] Karen Lim, William Small, Lorraine Portelance, Carien Creutzberg, Ina M Jürgenliemk-Schulz, Arno Mundt, Loren K Mell, Nina Mayr, Akila Viswanathan, Anuja Jhingran, Beth Erickson, Jennifer De los Santos, David Gaffney, Catheryn Yashar, Sushil Beriwal, Aaron Wolfson, Alexandra Taylor, Walter Bosch, Issam El Naqa, and Anthony Fyles. Consensus guidelines for delineation of clinical target volume for intensity-modulated pelvic radiotherapy for the definitive treatment of cervix cancer. *International journal of radiation oncology, biology, physics*, 79(2):348–55, February 2011.

- [47] Hiram A. Gay, H. Joseph Barthold, Elizabeth O'Meara, Walter R. Bosch, Issam El Naqa, Rawan Al-Lozi, Seth A. Rosenthal, Colleen Lawton, W. Robert Lee, Howard Sandler, Anthony Zietman, Robert Myerson, Laura A. Dawson, Christopher Willett, Lisa A. Kachnic, Anuja Jhingran, Lorraine Portelance, Janice Ryu, William Small, David Gaffney, Akila N. Viswanathan, and Jeff M. Michalski. Pelvic normal tissue contouring guidelines for radiation therapy: A radiation therapy oncology group consensus panel atlas. *International Journal of Radiation Oncology Biology Physics*, 83, 2012.
- [48] Robert C Orth, Michael J Wallace, and Michael D Kuo. C-arm cone-beam CT: general principles and technical considerations for use in interventional radiology. *Journal of vascular and interventional radiology : JVIR*, 19:814–820, 2008.
- [49] Christoph Georg Baum. *Konzepte zur bildgestützten, adaptiven Bestrahlungsplanung und zur Simulation von Behandlungsverläufen bei fluenzmodulierter Strahlentherapie*. PhD thesis, Eberhard-Karls-Universität zu Tübingen, 2007.
- [50] Ning Wen, Huaqun Guan, Rabih Hammoud, Deepak Pradhan, T Nurushev, Shidong Li, and Benjamin Movsas. Dose delivered from Varian's CBCT to patients receiving IMRT for prostate cancer. *Physics in medicine and biology*, 52(8):2267–2276, 2007.
- [51] XVI Protocols (M15). Technical report, NKI-AVL The Netherlands, 2011.
- [52] Jeremy P. Crew, Catherine R. Jephcott, and John M. Reynard. Radiation-induced haemorrhagic cystitis, 2001.
- [53] Dirk Manski. *Urologielehrbuch.de*. Auflage 20 edition, 2008.
- [54] E K Yeoh and M Horowitz. Radiation enteritis. *Journal of surgery, gynecology and obstetrics*, 165(4):373–9, 1987.
- [55] B W Stewart and C P Wild. World Cancer Report 2014. Technical report, 2014.
- [56] Cancer Research UK.
- [57] Alex F Bielajew. *Fundamentals of the Monte Carlo method for neutral and charged particle transport*. 2001.
- [58] K. R. Kase and W. R. Nelson. Concepts of Radiation Dosimetry. *Pergamon Press, Oxford*, 1978.
- [59] J J Duderstadt and W R Martin. *Transport Theory*. 1979.
- [60] W Feller. *An Introduction to Probability Theory and Its Applications*, volume 2. 1968.

- [61] Elekta. *Monaco Training Guide Version 3.01*.
- [62] Wolfgang A Tomé and Jack F Fowler. On cold spots in tumor subvolumes. *Medical physics*, 29(7):1590–1598, 2002.
- [63] Andriy Myronenko and Xubo Song. Point set registration: Coherent point drifts. *IEEE Transactions on Pattern Analysis and Machine Intelligence*, 32:2262–2275, 2010.
- [64] S Li, A Boyer, Y Lu, and G T Chen. Analysis of the dose-surface histogram and dose-wall histogram for the rectum and bladder. *Medical physics*, 24:1107–1116, 1997.
- [65] Susan L. Tucker, Lei Dong, Rex Cheung, Jennifer Johnson, Radhe Mohan, Eugene H. Huang, H. Helen Liu, Howard D. Thames, and Deborah Kuban. Comparison of rectal dose-wall histogram versus dose-volume histogram for modeling the incidence of late rectal bleeding after radiotherapy. *International Journal of Radiation Oncology Biology Physics*, 60:1589–1601, 2004.
- [66] Liesbeth J. Boersma, Mandy Van Den Brink, Allison M. Bruce, Tarek Shouman, Luuk Gras, Annet Te Velde, and Joos V. Lebesque. Estimation of the incidence of late bladder and rectum complications after high-dose (70-78 Gy) conformal radiotherapy for prostate cancer, using dose-volume histograms. *International Journal of Radiation Oncology Biology Physics*, 41:83–92, 1998.
- [67] A Jackson, M Skwarchuk, M Zelefsky, D Cowen, E Venkatraman, S Levegrun, C Burman, G Kutcher, Z Fuks, and S Liebel. Late rectal bleeding after conformal radiotherapy of prostate cancer (II): volume effects and dose-volume histograms. *International Journal of Radiation Oncology Biology Physics*, 49:685–698, 2001.
- [68] Cesare Cozzarini, Claudio Fiorino, Giovanni Luca Ceresoli, Giovanni Mauro Cattaneo, Angelo Bolognesi, Riccardo Calandrino, and Eugenio Villa. Significant correlation between rectal DVH and late bleeding in patients treated after radical prostatectomy with conformal or conventional radiotherapy (66.6-70.2 Gy). *International Journal of Radiation Oncology Biology Physics*, 55:688–694, 2003.
- [69] John D. Fenwick, Vincent S. Khoo, Alan E. Nahum, Beatriz Sanchez-Nieto, and David P. Dearnaley. Correlations between dose-surface histograms and the incidence of long-term rectal bleeding following conformal or conventional radiotherapy treatment of prostate cancer. In *International Journal of Radiation Oncology Biology Physics*, volume 49, pages 473–480, 2001.

List of Abbreviations

3D-CRT	three dimensional conformal radiotherapy
ALARA	as low as reasonably achievable
ART	adaptive radiotherapy
CBCT	cone-beam computed tomography
CCF	composite cost function
CLT	central limit theorem
CPD	continuous point drift
CRUK	Cancer Research UK
CT	computed tomography
CTV	clinical target volume
CTVN	nodal clinical target volume
CTVP	primary clinical target volume
D_{max}	maximum dose
D_{mean}	mean dose
$D_{x\%}$	dose that x% of the structure receives
DIR	deformable image registration
DVH	dose volume histogram
EBRT	external beam radiotherapy
ED	electron density
EUD	equivalent uniform dose
FBCT	fan-beam computed tomography
FF	flattening filter
FFF	flattening filter free
FOV	field of view
FSPB	finite size pencil beam
GTV	gross tumor volume
HDR	high dose rate
HU	hounsfield units

ICRU	International Commission on Radiation Units and Measurements
ICRP	International Commission on Radiological Protection
IGABT	image guided adaptive brachytherapy
IGART	image guided adaptive radiotherapy
IMAT	intensity modulated arc therapy
IMRT	intensity modulated radiotherapy
ITV	internal target volume
IV	irradiated volume
Linac	linear accelerator
LUTS	lower urinary tract symptoms
MC	Monte Carlo
MLC	multileaf collimator
MRI	magnetic resonance imaging
MU	monitor unit
NTCP	normal tissue complication probability
OAR	organ at risk
OrCA	Organ Contour Adaptor
PotD	Plan of the Day
PTV	planning target volume
ROI	region of interest
RTOG	Radiation Therapy Oncology Group
TCP	tumor control probability
ToUM	Top-of-Uterus-Motion
TPS	treatment planning system
TV	treated volume
V_{xGy}	volume of the structure receiving x Gy
VMAT	volumetric arc therapy
XVI	X-ray volume imaging

List of Tables

2.1	Late adverse effects of radiotherapy: Classification after Radiation Therapy Oncology Group (RTOG)	30
2.2	Attribution of the several available imaging data sets of patient 21. Numbers stand for the treatment week. Therefore planning-CT and MR are symbolized by 0.	46
3.1	Planning PTV-coverages for patient 20 (P20) and patient 12 (P12).	53
3.2	Statistically significant mean DVH value discrepancies of all fractions for both non-mover patients.	54
3.3	Planning values of patient 21.	61
3.4	Statistically significant mean DVH value discrepancies of all imaging data sets (CBCT, FBCT and MR0) for patient 21.	61
3.5	Statistically significantly and insignificantly (grey) diverging mean DVH values of imaging data sets selected for empty and full stage planning strategy for P21, respectively.	62
3.6	Planning DVH values for all small margin plans of all three patients.	65
3.7	Significant mean DVH value discrepancies of all fractions of the patients.	66

List of Figures

1.1	Schematic structure of three different linac-designs. The straight-through beam design (top) allows the machine only to produce X rays with energies of 4-6 MV, the other two designs allow to produce megavoltage X rays as well as electrons.[6]	12
1.2	Schematic constellation of the components of a linac treatment head.[7] . .	13
1.3	Schematic illustration of IMRT: A pair of collimator leaves corresponding to x_a at different times and the produced intensity profile. t_1 and t_2 are depicted for the marked position x_a	15
1.4	Oncological volume concepts: The small CTV on the right could depict an involved lymph node. The PTV is not necessarily one combined volume as illustrated in this example but can also be decomposed in two or more PTVs. The ITV accounts for physiological movements of the CTV.	19
1.5	Planned dose distribution based on the planning-CT and changing uterus positions for different bladder filling stages during the treatment fractions. The yellow contour depicts the uterus while the green one shows the bladder. [courtesy by webpage of Christian Doppler Laboratory for Medical Radiation Research and Radiation Oncology ¹]	22
2.1	Principle of FBCT and CBCT in direct comparison.	27
2.2	Small, medium and large FOV and detector offset (left) and 360° rotation with medium FOV (right)[51].	28
2.3	Sagittal view of pelvic region of female anatomy. The pelvic space contains the bowel which is not depicted here.	29
2.4	Visualization of the staging criteria for cervical cancer [56]. A common complication of stage IIIB is an occlusion of an ureter.	32
2.5	Flow diagram showing the essential steps in the Monte-Carlo transport of photons (excluding electron-transport) [1][Part A, Chapter 5.3]	35
2.6	Possible photon history and particle transport in MC simulation. Dashed lines represent photon paths, while solid lines give the electron and positron paths.	36

2.7	Penaltycurves: cell sensitivities are shown for the values 0.1, 0.25 and 0.5 [61]	37
2.8	Serial penalty curves: k values are set to 8, 12 and 16 [61]	38
2.9	Parallel complication curves: k values are shown for 2, 3 and 4. The inflection point is marked. [61]	39
2.10	Effects of serial and parallel cost functions on a DVH: The length of the arrows represent the relative impact of the cost function on the various points of the DVH.	39
2.11	Structure layering of rectum and PTV or two different PTVs. [61]	40
2.12	DVH-concept: The listed dose and volume values, except for the D_{mean} , are exemplarily plotted.	41
2.13	Deformation of CTV and dislocation of top of uterus in a mover-patient caused by bladder filling variations [42]. Lowest correlated bladder volume on the left, maximum on the right.	42
2.14	CTVs constructed via a motion model [43].	42
2.15	Schematic diagram of the future clinical workflow for PotD based ART of cervix cancer.	43
2.16	Anatomical 3D-view of patient 21 and her contoured organs. The red line symbolizes the rotation of the gantry during treatment.	48
2.17	Monaco prescription of patient 21 (non-ART plan) showing the applied cost functions and their correlating parameters.	49
3.1	Point clouds of two input CTVP contours (red and blue) and interpolated middle CTVP contour (yellow). On the right its triangulated surface is shown.	52
3.2	User interface of OrCSmoothing. blue x = smoothed points, blue curve = fit function, green o = raw data points	52
3.3	DVH value boxplots of the CTV data for patient 12 (P12) and 20 (P20).	54
3.4	DVH value boxplots of the OAR data for patient 12 (P12) and 20 (P20).	55
3.5	DVH value boxplots for V_{40Gy} and V_{45Gy} of bowel of patient 20 (P20) and 12 (P12).	56
3.6	DVHs for motion robust and non-ART plan of both non-mover patients.	57
3.7	DVHs of some selected CTVs of various imaging data sets (CBCT, FBCT) for non-ART plans of both non-mover patients. Yellow lines depict the CTVPs, pink lines the CTVNs.	58
3.8	Comparison of the dose distributions of non-ART and motion robust plan of patient 12 in coronal, sagittal and transverse view.	59
3.9	Comparison of the dose distributions of non-ART and motion robust plan of patient 20 in coronal, sagittal and transverse view.	60
3.10	All obtained DVH values for CTVs and D_{2ccm} for OARs of patient 21.	61

3.11	Remaining obtained DVH values for OARs of P21.	62
3.12	DVH of patient 21 for the non-ART plan and empty and full stage plan of the OAR-constellation (top) and the PTVs (bottom) of the planning-CT. . .	63
3.13	DVH of all CTVPs of patient 21 for the non-ART plan and empty and full stage plans with the corresponding CTVPs.	64
3.14	Comparison of the dose distributions of the non-ART (top) and the empty stage (middle) and full stage (bottom) plan of patient 21 in coronal, sagittal and transverse view.	67
3.15	CTVP variations and dose distribution of the two stage-plans. Yellow lines represent the CTVP contours.	68
3.16	DVH of patient 12 and patient 20. Plotted PTVs all include big margin. big margin = motion robust plan with normal (big) margins (1cm CTVP, 0.5cm CTVN) small margin = motion robust plan with smaller margins (0.5cm CTVP, 0.2cm CTVN)	68
3.17	Influence of margin: DVH value boxplots of CTV data for patient 12 (P12) and 20 (P20).	68
3.18	Influence of margin: DVH value boxplots of OAR data for patient 12 (P12) and 20 (P20).	69
3.19	Influence of margin: DVH value boxplots of V_{40Gy} and V_{45Gy} of bowel of patient 12 (P12) and 20 (P20).	70
3.20	Influence of margin: DVH value boxplots for CTVs and D_{2ccm} of OARs for P21.	70
3.21	Influence of margin: DVH value boxplots of OARs for P21.	70
4.1	Volume changes of the lymph nodes (CTVN) [courtesy of Yvette Seppenwoolde].	75
4.2	3D-view of different CTVN / lymph node volumes of patient 12.	76